

**Fast numerical methods for mixed, singular Helmholtz
boundary value problems and Laplace eigenvalue
problems—with applications to antenna design,
sloshing, electromagnetic scattering and spectral
geometry**

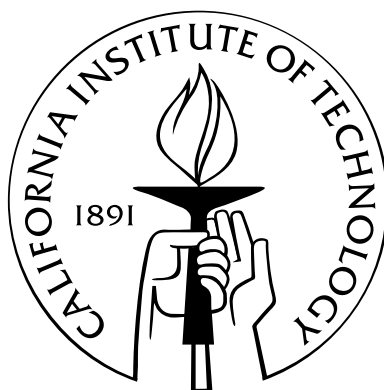
Thesis by

Eldar Akhmetgaliyev

In Partial Fulfillment of the Requirements

for the Degree of

Doctor of Philosophy



California Institute of Technology

Pasadena, California

2016

(Defended July 8, 2015)

Acknowledgments

I would like to start by expressing my sincere gratitude to my adviser professor Oscar Bruno for the support and guidance during the time I spent at Caltech. Solving challenging mathematical problems together is one of the most exciting experiences of my life, and I'm looking forward to the ongoing collaboration. A person whose support carried me throughout these years is my beloved wife Alma. You always encourage me to be a better person and for that I'm forever grateful.

Most of my research ideas originate from fruitful discussions with my colleagues and collaborators whom I thank deeply, especially professor Nilima Nigam at SFU and Carlos Perez-Arancibia at Caltech. I also thank professors James Beck, Dale Pullin and Barry Simon for participating in my defense and for valuable comments. Special thanks also goes to Carmen Sirois and Sydney Garstang - you made our office feel like home, and your willingness to help is greatly appreciated by me and all the members of our department.

In addition would like to thank all my friends for always being there for me: especially my friends back home - Daniyar Alshanabayev, Asker Alshanabayev, Dauren Auzhani, Alimzhan Zhubayev, Arman Bekembayev, Nurlybek Kassimov; my friends from Moscow, from Caltech, my friends in San Diego and all others across the world. This list also includes my feline friends Kisa and Misha who spent a lot of time near my computer to help me with research, or maybe just for the heat. An exciting part of my life during Caltech years was starting MOCAP Analytics with my friend Arian Forouhar, whom I thank deeply, as well as the entire team: Nurlybek Kassimov, Brandt Belson, Mat Kellogg and others. I'm looking forward to working together on exciting problems.

Lastly, my sincere gratitude goes towards my sister Darina and my parents Abdul and Aliya. Thank you for always being proud of me.

Contents

Abstract	5
1 Introduction	6
1.1 Overview	6
1.2 Historical Review I: Zaremba boundary value problems	8
1.3 Historical Review II: Laplace eigenvalue problems of Zaremba, Dirichlet, and Neumann type	10
1.4 Historical Review III: Steklov and sloshing eigenvalue problems	12
1.5 Overview of results	14
2 Integral equation solvers for the Zaremba boundary value problems on smooth domains	19
2.1 Preliminaries	19
2.2 Boundary integral equation formulation	21
2.3 Singularities of the solutions of equations (2.1) and (2.4)	27
2.3.1 Conformal mapping	30
2.3.2 Proof of theorem 2.3.2	31
2.3.3 Proof of theorem 2.3.3	39
2.4 Parametrized Integral Operators	42
2.5 Singularity resolution via Fourier Continuation	44
2.5.1 FC-based algorithm: Fourier Continuation	47
2.5.1.1 FC-based algorithm: Canonical kernel decomposition	48
2.5.1.2 FC-based algorithm: Numerical integration	50

2.6	Applications and numerical results	53
3	Integral equation solvers for the Zaremba boundary value problem on Lipschitz domains	62
3.1	Preliminaries	62
3.2	Singularities in solutions and integral equation densities	64
3.3	Graded-mesh algorithm	66
3.3.1	Graded-mesh algorithm: Polynomial change of variables	67
3.3.2	Graded-mesh algorithm: Discretization and quadratures	69
3.4	Applications and numerical results	71
4	Laplace-Zaremba eigenvalue problems and novel search method	76
4.1	Integral formulation of the eigenvalue problem	76
4.2	Discrete boundary integral operator	78
4.3	Eigenvalue search	80
4.3.1	Discussion	81
4.3.2	Eigenfunction normalization.	84
4.3.3	Sign changing procedure for the minimum singular value.	89
4.4	Eigenfunction evaluation	89
4.5	Numerical results	90
4.5.1	Convex polygonal domains	92
4.5.2	Convex smooth domains	93
4.5.3	Smooth, non-convex domains	95
4.5.4	Polygonal domains with obtuse Dirichlet-Neumann junctions	96
4.5.5	Comparison of FC-based and graded-mesh approaches	98
4.5.6	High-frequency wave numbers	99
4.5.7	Multiply connected domains	100
4.5.8	Pure Dirichlet and Pure Neumann eigenfunctions	102
5	Steklov eigenvalue solver	104
5.1	Preliminaries	104

5.2	Integral equation formulation	106
5.3	Nystrom method for Steklov eigenvalue problem on smooth domains	108
5.4	Graded-mesh algorithm for sloshing problem and Steklov problem on non-smooth domains	109
5.5	Numerical results	110
6	Conclusions and future work	115
6.1	Conclusions	115
6.2	Future work	116
6.2.1	Applications to antenna problems	116
6.2.2	Fully iterative solvers for eigenvalue problems.	118
6.2.3	Solution of Zaremba problems for electromagnetic Maxwell equations.	118
6.2.4	Transmission eigenvalues	118
6.2.5	Time explicit PDE solver using eigenfunction expansion and separation of variables.	121
A	Appendix: The Fourier Continuation method (FC)	125
B	Solution at interior resonances	128
C	Closed form expressions for integrals with a logarithmic kernel	131

Abstract

This thesis presents a novel class of algorithms for the solution of scattering and eigenvalue problems on general two-dimensional domains under a variety of boundary conditions, including non-smooth domains and certain “Zaremba” boundary conditions—for which Dirichlet and Neumann conditions are specified on various portions of the domain boundary. The theoretical basis of the methods for the Zaremba problems on smooth domains concern detailed information, which is put forth for the first time in this thesis, about the singularity structure of solutions of the Laplace operator under boundary conditions of Zaremba type. The new methods, which are based on use of Green functions and integral equations, incorporate a number of algorithmic innovations, including a fast and robust eigenvalue-search algorithm, use of the Fourier Continuation method for regularization of all smooth-domain Zaremba singularities, and newly derived quadrature rules which give rise to high-order convergence even around singular points for the Zaremba problem. The resulting algorithms enjoy high-order convergence, and they can tackle a variety of elliptic problems under general boundary conditions, including, for example, eigenvalue problems, scattering problems, and, in particular, eigenfunction expansion for time-domain problems in non-separable physical domains with mixed boundary conditions.

Chapter 1

Introduction

1.1 Overview

This thesis concerns a variety of problems in PDE theory (Partial Differential Equations) and computational science, with a focus on two closely related fields: electromagnetic scattering and spectral theory. In a broad sense, the term scattering refers to any situation in which a wave impinges on an obstacle and is thereby distorted, reflected, transmitted, or in some other way scattered. Computational analyses of scattered fields can provide information about the properties of an obstacle, can lead to improved designs for a wide variety of fields of engineering, including antenna design, stealth, and communications, and they can provide important insights into the phenomenology of scattering processes. Spectral theory, on the other hand, underlies a vast range of phenomena in science and engineering, including, for example, quantum mechanics, acoustics, and electromagnetism.

The contributions presented in this thesis include a tight characterization of the singular structure of a range of elliptic problems under Zaremba boundary conditions as well as a class of algorithms for the solution of scattering and eigenvalue problems on general domains under a variety of boundary conditions. A special focus of this thesis relates to singularities of solutions of elliptic problems at points at which either geometric singularities occur—such as corners or edges of a PDE domain—and at certain “Zaremba points” at which the boundary conditions *change type* from Dirichlet type to Neumann type. The theoretical basis of the methods for the smooth-domain Zaremba problems rely on detailed information, which is

put forth for the first time in this thesis, about the singularity structure of solutions of the Laplace operator and associated integral-equation densities at and around Zaremba points.

The remainder of this chapter presents a historical perspective on theory and computation for the types of problems under consideration (Sections 1.2—1.4) as well as an outline of some salient points in the theoretical ideas and computational methods proposed in this thesis (Section 1.5). Chapters 2 through 6 then present the main contents of this thesis: a theoretical discussion and a class of efficient high-order solvers for highly-singular scattering and eigenvalue problems in two-dimensional space. In detail, Chapter 2 analyses the singular character of PDE solutions and integral-equation densities for Zaremba problems on smooth domains; it describes the novel Fourier Continuation method (FC) for accurate Fourier expansion of non-periodic functions; it introduces an FC-based numerical algorithm for regularization of all smooth-domain Zaremba singularities; and it presents novel quadrature rules and an associated boundary-value solver which give rise to high-order convergence even around smooth-domain Zaremba points. Chapter 3 introduces a more general (albeit somewhat less efficient) boundary-value solver, which, based on use of graded meshes of the type considered in [79, 108], is applicable to both smooth and Lipschitz domains and to the various types of boundary conditions under consideration. Chapter 4 then presents a boundary integral algorithms for the numerical solution of the Zaremba, Dirichlet and Neumann eigenproblems, all of which include a certain regularization technique which gives rise to an efficient eigenvalue search method, and Chapter 5 introduces corresponding solvers for the Steklov eigenproblem for both smooth and Lipschitz domains. Chapter 6, finally, presents conclusions along with a description of ongoing and suggested future work.

1.2 Historical Review I: Zaremba boundary value problems

We consider the classical Helmholtz-Zaremba boundary value problem

$$\begin{aligned}\Delta u + K(x)u &= 0 & \text{in } \Omega, \\ u &= f & \text{on } \Gamma_D, \\ \partial_n u &= g & \text{on } \Gamma_N,\end{aligned}\tag{1.1}$$

($K(x) > 0$), where Ω is a 2-dimensional domain with boundary Γ consisting of two disjoint portions Γ_D and Γ_N . Such problems were first considered in Zaremba's 1910 contribution [130], which established existence and uniqueness of solution for the particular case $K(x) \equiv 0$ (Laplace-Zaremba problem). The Zaremba problem arises in a number of important areas, including elasticity theory (where it appears as a model in the contexts of contact mechanics [122] and crack theory [42]); homogenization theory (as it applies to problems of steady state diffusion through perforated membranes [42]), etc. One of the main motivations for our consideration of this problem concerns computational electromagnetics: the Zaremba problem serves as a valuable and virtually unavoidable stepping stone to the closely related but more complex problem of electromagnetic propagation and scattering at and around structures such as printed circuit-boards. (As in the Zaremba problem, where the boundary conditions change type at the Dirichlet-Neumann boundary, the boundary conditions for the Maxwell equations at and around circuit-boards change type—not from Dirichlet to Neumann but from dielectric transmission conditions to a perfect-conductor condition—at the edges of the perfectly conducting circuit elements.)

After the initial contribution by Zaremba, early works concerning the Zaremba boundary value problem include contributions by Signorini [112] (1916: solution of the Zaremba problem in the upper half plane using complex variable methods); Giraud [51] (1934: existence of solution of Zaremba problems for general elliptic operators); Fichera [44, 45] (1949, 1952: regularity studies at Zaremba points, Zaremba-type problem for the elasticity equations in two spatial dimensions); Magenes [94] (1955: proof of existence and uniqueness, single layer

potential representation); Lorenzi [90] (1975: Sobolev regularity around a corner which is also a Dirichlet-Neumann junction), and Wigley [125, 126] (1964, 1970: explicit asymptotic expansions around Dirichlet-Neumann junctions), amongst others. More recent contributions in this area include reference [122], which provides a valuable review in addition to a study of Zaremba singularities and computational approaches to the problem; reference [24], which considers the Zaremba problem for the biharmonic equation; references [37, 38], which study Zaremba boundary value problems for Helmholtz and Laplace-Beltrami equations; reference [26], which discusses the solvability of the Zaremba problem from the point of view of pseudo-differential calculus and Sobolev regularity theory; reference [64] which introduces a certain inverse preconditioning technique to reduce the number of linear algebra iterations for the iterative numerical solution of this problem and which gives rise to high-order convergence; and finally, reference [16], which successfully applies the method of difference potentials to the variable-coefficient Zaremba problem, with convergence order approximately equal to one.

Significant challenges arise in connection with Zaremba boundary value problems in view of the singular character of its solutions: as first shown by Fichera [45], Zaremba solutions are generally non-smooth even for infinitely differentiable boundary data f and g , and smoothness of solutions can only be ensured provided f and g obey certain stringent relations which generally are not satisfied in practice. As indicated above, Wigley [125, 126] provides a detailed description of the singularity structure around Zaremba points. In Section 2.3 it is shown, however, that a tighter result holds in the case the domain boundary is itself smooth. Building upon these results, further, Section 2.5 introduces a numerical algorithm that regularizes all Zaremba singularities and yields convergence of high order. For general, possibly non-smooth boundaries, in turn, a boundary-value solver, based on use of graded meshes of the type considered in [79, 108], is presented in Section 3. This approach is highly robust and accurate, and it can be applied to the various types of boundary conditions under consideration for both smooth and Lipschitz domains—although when applied to smooth domains this method is less efficient than the smooth-boundary algorithm mentioned above.

1.3 Historical Review II: Laplace eigenvalue problems of Zaremba, Dirichlet, and Neumann type

This thesis additionally considers Laplace eigenvalue problems of the form

$$\begin{aligned} -\Delta u_m &= \lambda_m u_m, & x \in \Omega \\ u_m &= 0, & x \in \Gamma_D \\ \frac{\partial u_m}{\partial n} &= 0, & x \in \Gamma_N. \end{aligned} \tag{1.2}$$

The eigenvalues λ_m and eigenfunctions u_m are called Laplace-Dirichlet, Laplace-Neumann, or Laplace-Zaremba depending on whether $\Gamma_N = \emptyset$, $\Gamma_D = \emptyset$ or both Γ_D and Γ_N are nonempty, respectively. Equation (1.2) famously arises as a model for vibrating of membranes; in such cases the eigenvalue λ_m corresponds to a principal frequency of vibration and the eigenfunctions u_m give the vibrational modes. Additionally, the Laplace-Dirichlet and Laplace-Neumann eigenproblems provide important building blocks in models of electromagnetic and acoustic wave propagation along waveguides. Laplace eigenfunctions under Zaremba boundary conditions can be used to model diffusion in domains containing apertures [36]. For all the eigenproblems considered in this thesis, for which the underlying domains are of Lipschitz type, the eigenvalues λ_m form a discrete set [50, Th. 8.37], but domains do exist for which the Laplace-Neumann spectrum is continuous; see [113].

Spectral theory for the Laplace operator has a significant impact in science and engineering. Laplace eigenvalue problem for simple shapes were considered by Poisson [105]; the 1896 contribution [106] contains Rayleigh’s conjecture that the first Laplace-Dirichlet eigenvalue is minimized by the spherical domain, a statement that was eventually proved independently by Faber [41] and Krahn [78]. Weyl’s contributions [100, 123, 124] concerning the asymptotic distribution of the eigenvalues λ_m as $m \rightarrow \infty$ initiated an active research area in the field of spectral theory. A pivotal contribution [70] by Kac, “Can one hear the shape of the drum”, epitomizes the important general area of inverse spectral problems. Laplace eigenvalue problems additionally impact on the fields of quantum chaos [8] and nuclear magnetic

resonance [57].

Numerical approaches for the Laplace eigenvalue problems fall into three main categories. The first class of approaches is based on use of Finite Element Methods (FEM); a useful review in these regards is provided by Boffi [14]). Finite element approximations provide several advantages, including generality, ease of implementation, and rigorous numerical bounds [89]; a useful numerical package for these problems (Deal.II) is described in [6]. Recent contributions based on use of FEM include a multiscale FEM approach [25]) as well as discontinuous Galerkin approaches for Laplace [5] and Maxwell [67] eigenvalue problems.

A second class of numerical approaches to Laplace eigenvalue problems is provided by the *Method of Particular Solutions* (MPS) [49]. That early contribution utilizes approximates eigenfunctions by means of Fourier-Bessel series and it performs eigenvalue searches via corresponding searches for zeros of a matrix determinant. Subsequently, [99] substituted this strategy by a search for zeros of minimum singular values—an idea which, with some variations, is incorporated as part of the algorithm proposed in this thesis as well. A modified version of the MPS, which was introduced in reference [11], alleviates some difficulties associated with the conditioning of the method.

Finally, a class of approaches based on use the use of boundary integral equations has been explored in a number of contributions, including methods based on collocation [29, 71] and Galerkin [114, 115] boundary element approaches for the Dirichlet and Neumann problems. Integral equation formulations for eigenvalue problems are advantageous as they 1) result in a reduction in the problem dimensionality, and, as shown in this thesis, they 2) greatly facilitate efficient treatment of the eigenfunction singularities that occur around corners and Dirichlet-Neumann transition points. The boundary element strategy for three-dimensional Dirichlet eigenproblems presented in [35, 114, 115], for example, yields errors that decrease cubically with the spatial mesh-sizes. As a counterpart, however, the integral form of the eigenvalue problem requires nonlinear searches (the eigenvalue appears as part of the integral kernel). Indeed, as mentioned in [114], “the convergence regions for the eigenvalues are still local” and “other techniques have to be considered and analyzed in order to increase the robustness”. Focusing on two-dimensional Laplace eigenvalue problems, in Chapter 4 we

present a Nyström algorithm that can achieve any user-prescribed order of convergence for smooth and non-smooth domains alike, as well as a novel, robust, search algorithm that yields fast eigenvalue convergence from nonlocal initial guesses. To the best of our knowledge, the Zaremba eigenvalue algorithm presented in this thesis is the first boundary-integral method for eigenvalue problems of Zaremba type.

1.4 Historical Review III: Steklov and sloshing eigenvalue problems

Here we consider a class of eigenvalue problems the prototypical example of which is the Steklov eigenvalue problem

$$\begin{aligned}\Delta u_m &= 0 & \text{in } \Omega, \\ \partial_n u_m &= \lambda u_m & \text{on } \Gamma.\end{aligned}\tag{1.3}$$

Here, $\Omega \subset \mathbb{R}^2$ is a bounded Lipschitz open set with boundary Γ . As is known, the eigenvalues form a discrete set, λ_m , $m = 1, \dots, \infty$. Further, the Steklov spectrum coincides with the spectrum of the Laplace Dirichlet-to-Neumann operator.

These problems were first considered by Steklov [116] in (1902). In 1954 Weinstock [121] proved that the disc maximizes the first non-trivial Steklov eigenvalue among all planar domains with a given measure. In 1974, Hersch, Payne, and Schiffer [66] proved a general isoperimetric inequality

$$\sup\{\lambda_n(\Omega) \cdot |\partial\Omega|\} \leq 2\pi n, \quad n \in \mathbb{N},\tag{1.4}$$

where the supremum is taken over bounded simply-connected domains $\Omega \subset \mathbb{R}^2$ with a smooth boundary, and where $|\partial\Omega|$ denotes the length of the boundary of Ω . In 2010, Girouard and Polterovich proved that this bound is sharp and attained by a sequence of domains degenerating into a disconnected union of n identical balls [52, 53]. For an overview of the recent work on Steklov eigenvalues and eigenfunctions we refer to the review papers [54]

and [84].

Particular interest has focused on the sloshing eigenvalue problem

$$\begin{aligned}\Delta u_m &= 0 \quad \text{in } \Omega, \\ \partial_n u_m &= 0 \quad \text{on } \Gamma_N \\ \partial_n u_m &= \lambda u_m \quad \text{on } \Gamma_S\end{aligned}\tag{1.5}$$

which, of course, is closely related to the Steklov eigenvalue problem. Studies of the sloshing problem (which originally arose as a model for small-amplitude motion of an inviscid, incompressible, and irrotational fluid within an open container) includes contributions by Euler [109] (1761), Poisson [104] (1828), Green [58, 59] (1838, 1848), Kelland [73] (1840), Airy [1] (1845), Stokes [117] (1846), Ostrogradsky [101] (1862), Rayleigh [107] (1876), Kirchhoff [75] (1879), Greenhill [61] (1887), Macdonald [92, 93] (1894,1896), Poincare [103] (1910), and Hadamard [62] (1910,1916), and it is treated in Lamb’s famous text “Hydrodynamics” [85] (1932). Aside from the hydrodynamic applications, Steklov eigenvalues relate closely to the Dirichlet-to-Neumann map which is the centerpiece of the electric impedance tomography problem [55, 110].

Recent contributions on Steklov and sloshing eigenvalue problems include [7] (extension of some classic eigenvalue inequalities to cases of mixed Steklov-Neumann and Steklov-Dirichlet eigenvalues), [81] (study of the fundamental sloshing mode of a liquid in a container and connection to hot spots conjecture), [77] (fundamental sloshing mode and the behaviour of its nodal line is characterized), [9] (study of the nodal sets of Steklov eigenfunctions: measure the length as the eigenvalue goes to infinity), [88] and [43] (approximate analytical solution for sloshing problem in containers of simple shapes), [72] (finite element modeling of sloshing in axisymmetric containers), and [4] (the result for the general case of elliptic equations with discontinuous coefficients in divergence form is proven).

The literature on numerical methods for Steklov problems in two dimensions include the contributions [12] (a multiscale FEM approach), [68] (which uses cubic order boundary element method), [87] (which utilises 3rd order finite element method), and [30] (where application of a 3rd order Nystrom method with subsequent Richardson acceleration is used

to solve the Steklov eigenvalue problem). To our knowledge, previous contributions do not incorporate spectrally convergent methods for smooth boundaries or high order convergent methods for non-smooth boundaries or for the sloshing eigenvalue problem. A set of efficient spectral/high-order algorithms for Steklov and sloshing eigenproblems are presented in Chapter 5.

1.5 Overview of results

This thesis concerns a variety of problems in PDE theory (Partial Differential Equations) and numerical analysis, with a focus on two closely related fields: electromagnetic scattering and spectral theory. The numerical algorithms presented in this thesis, which are based on use of Green functions and integral equations, incorporate a number of algorithmic innovations, including a fast and robust eigenvalue-search algorithm, use of the Fourier Continuation method for regularization of all smooth-domain Zaremba singularities, and newly derived quadrature rules which give rise to high-order convergence even around singular points for the Zaremba problem. The resulting algorithms, which enjoy high-order convergence for both smooth and Lipschitz domains, can tackle a variety of elliptic problems under general boundary conditions, including, for example, eigenvalue problems and scattering problems in smooth and non-smooth domains, as well as eigenfunction expansion for time-domain problems in non-separable physical domains under general boundary conditions.

The creation of these algorithms has required relevant studies of solution singularities for both boundary-value problems and eigenvalue problems. Prototypical boundary-value problems in our context relate to problems of scattering by obstacles, while the spectral problems we consider concern evaluation of eigenvalues and eigenfunctions for the Laplace operator. As discussed in previous sections, both scattering and eigenvalue problems have significant impact in a wide range of scientific and engineering applications, including acoustic, electromagnetic and quantum cavity resonators, vibrating membranes, modal analysis and design of waveguides and antennas, and solution of a variety of time-dependent problems, amongst many others.

Prototypical problems considered in this thesis concerns solution of the Helmholtz equation and solution of eigenvalue problems for the Laplace operator under Zaremba boundary conditions (where Dirichlet and Neumann boundary conditions are enforced on two disjoint portions of the domain boundary) on smooth and non-smooth domains. Previously existing algorithms for evaluation of solutions of the Helmholtz equation (for both scattering problems and Laplace eigenvalue problems) fall into two broad classes: volumetric/differential solvers on one hand, and boundary integral solvers on the other. The main representatives of the first class of methods rely on discretization of PDEs by means of finite elements or finite difference methods (FDM/FEM); boundary integral methods, on the other hand, are based on use of Green functions and discretization of domain boundaries.

The well known FDM/FEM solvers rely on discretizations of the volumetric computational domains, and thus they require use of suitable absorbing boundary conditions whenever infinite domains are considered. A significant advantage of such volumetric methods is that they generally lead to sparse linear systems. Unfortunately, however, solutions produced by means of these methods give rise to significant dispersion and dissipation errors, and treatment of singularities entails a variety of difficulties.

One of the main advantages of boundary integral methods, on the other hand, is dimensionality reduction: in such methods an integral equation on the $(d-1)$ -dimensional domain boundary needs to be solved instead of the full PDE in fully d -dimensional domain. Additionally, solutions produced by integral methods automatically satisfy the radiation condition at infinity, so that use of large computational domains and absorbing boundary conditions for exterior problems is unnecessary. Importantly, further, integral equation methods do not suffer from dispersion or dissipation errors. Unlike volumetric methods, however, boundary integral methods give rise to dense linear systems of equations. In view of the advent of fast solvers (see, e.g., [13, 18, 60]), this difficulty has been essentially eliminated, and boundary integral solvers, when applicable (i.e., for cases when Green functions can be used) can be highly competitive.

As suggested above, the development of integral equation solvers of high order of accuracy has required a study of the singularities in the solution of Helmholtz equation subject

to Zaremba boundary conditions. In particular, Chapter 2 shows that for smooth domain boundaries the singularity of Zaremba solution has an asymptotic form containing only powers of \sqrt{d} (without logarithmic terms included in previous solution asymptotics [125]), where d is the distance to the singular point. The solution of the integral equations (the integral density) is also singular in the presence of the Zaremba boundary conditions, and the singularity asymptotics are also derived in Chapter 2: as the PDE solution itself, the asymptotics of the integral density around singular points contains only powers of \sqrt{d} . As shown in Section 2.5, such singularity types can be successfully regularized and integrated with high-order accuracy via an application of the novel Fourier Continuation method [21, 91]. Certain associated integrals of products of the basic trigonometric functions and the logarithmic potential can then be evaluated explicitly on the basis of certain closed-form expressions presented in Appendix C. As desired, and as demonstrated in detailed Section 2.6, the resulting solvers yield highly accurate results.

An alternative approach, which does not rely on use of the FC method, is proposed in Chapter 3 for the numerical treatment of singularities in the integral densities arising at points of geometric singularities (corners). Based on use of graded meshes of the type considered in [79, 108], the algorithm is somewhat less efficient than the FC approach in applications to smooth domains, but it does give rise to high order accuracy even for challenging Lipschitz domains and under the various types of boundary conditions under consideration.

Our application of the proposed integral equation methods to eigenvalue problems is presented in Chapter 4, including eigensolvers based on the smooth-domain FC-based method and the graded-mesh method for Lipschitz domains. An important challenge we have found in the context of the eigenvalue problem concerns the algorithm for search of the values of wavenumber μ that make the relevant boundary integral operator singular and thus indicate the presence of a Laplace eigenvalue. Such values are obtained as zeroes of minimum singular value $\sigma_n(\mu)$ of the corresponding boundary integral operator. As shown in Section 4.3.1, direct use of a descent-based approach such as the Newton method fails in this context in view of the fact that the function $\sigma_n(\mu)$ is essentially constant away from its roots. A modified approach based on suitable normalization of the eigenfunction at a reduced set

of points is presented in Chapter 4 that successfully addresses this difficulty. The resulting eigensolver can tackle extremely challenging two-dimensional Dirichlet, Neumann, and Zaremba eigenproblems with high accuracies (see Section 4.5.6); in fact, we believe this is the first high-order eigensolver ever proposed for the Zaremba problem. An extension of our eigenvalue search method applicable to spectral problem on multiply-connected domains is introduced in Section 4.5.7: the generalized methodology can successfully eliminate spurious resonances that originate in bounded components of the domain complement as a result of the use of single-layer representations we use.

As discussed in previous sections, the evaluation of Laplace eigenvalues has numerous practical applications. In an ongoing collaboration with the Electrical Engineering department at Caltech (as well as recently started collaboration with National Radio Astronomy Observatory), for example, the integral-equation based methods are applied to the problem of modal analysis for the microwave-band antennas—specifically, evaluation of the Laplace spectrum for the cross sections of QRFH antennas. The resulting algorithm exhibits high accuracy and it significantly outperforms existing commercial EM software—in the accuracy of both eigenvalues and physical fields (eigenfunctions) even at and around boundaries; Section 6.2.1 presents some details in these regards.

The methodologies considered in this thesis can also be applied to other types of boundary value problems and eigenvalue problems, beyond the Zaremba, Dirichlet, and Neumann problems. Chapter 5, for example, introduces integral equation methodologies for Steklov and sloshing eigenvalue problems in general Lipschitz domains. In view of its close relation to the Dirichlet-to-Neumann map, the Steklov spectral problem has important applications in impedance tomography; the sloshing eigenvalue problem, in turn, has a significant impact on the classical sloshing problem in hydrodynamics. Our numerical approaches in these contexts are based on use of the single layer potential representation adjusted to avoid spurious frequencies. As demonstrated in Section 5.5) the resulting solvers achieve spectral accuracy on domains with smooth boundaries (including multiply-connected domains), and they are also highly accurate for Lipschitz domains.

Preliminary applications of the proposed eigensolvers to time-dependent problems based

on separation of the time variables are presented in Section 6.2.5. The desired algorithm can solve challenging time-dependent parabolic and hyperbolic problems with regular or singular boundaries and boundary conditions (e.g., Zaremba) while allowing for arbitrarily long-time integration without dissipation or dispersion errors.

This thesis thus presents a variety of solvers for boundary value problems and eigenvalue problems associated with the Laplace and Helmholtz operator, with applicability in a number of important fields of science and engineering. Plans for future research, which are presented in Chapter 6, include development of iterative eigensolvers for high frequency eigenfunctions (large eigenvalues) in two- and three-dimensional domains, application to transmission eigenvalue problems [23] (and, thus, potential application of such algorithm to the inverse scattering problems; see Section 6.2.4) and extension to full electromagnetic problems with mixed transmission/perfect-conductor boundary conditions.

Chapter 2

Integral equation solvers for the Zaremba boundary value problems on smooth domains

2.1 Preliminaries

We consider interior and exterior boundary value problems of the form

$$\begin{aligned}\Delta u(x) + k^2 u(x) &= 0 & x \in \Omega, \\ u(x) &= f(x) & x \in \Gamma_D, \\ \frac{\partial u(x)}{\partial n_x} &= g(x) & x \in \Gamma_N\end{aligned}\tag{2.1}$$

for $u \in H_{\text{loc}}^1(\Omega)$ (with a Sommerfeld radiation condition in case of exterior problems), where $\Omega \subset \mathbb{R}^2$ denotes either a bounded open simply-connected domain with a smooth boundary (which we will generically call an “*interior*” domain) or the complement of the closure of such a domain (an “*exterior*” domain), where the Dirichlet and Neumann boundary portions Γ_D and Γ_N ($\Gamma = \Gamma_D \cup \Gamma_N$) are disjoint relatively-open subsets of Γ of positive measure relative to Γ . Here $H_{\text{loc}}^1(\Omega)$ denotes the Sobolev space of functions u defined in the domain Ω such that $u \in H^1(\Omega \cap B_R)$ for any ball B_R of radius R and centered at the origin; of course $H_{\text{loc}}^1(\Omega) = H^1(\Omega)$ for bounded sets Ω . The Dirichlet and Neumann data f and g , in turn, are elements of certain Sobolev spaces (cf. Remark 2.1.1 item ii) which we define in what follows.

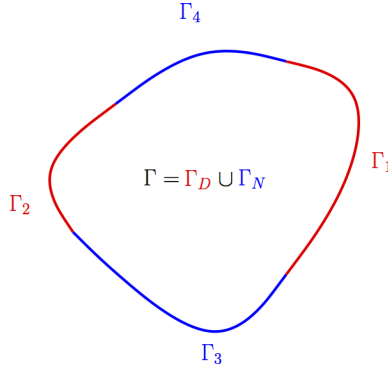


Figure 2.1: Domain Ω .

To do this we follow [97] and we first define, for a given relatively open subset $S \subseteq \Gamma$, the space

$$\tilde{H}^{1/2}(S) = \{u|_S : \text{supp } u \subseteq S, u \in H^{1/2}(\Gamma)\}.$$

The spaces associated with the Dirichlet and Neumann data f and g are then defined by

$$H^{1/2}(S) = \{u|_S : u \in H^{1/2}(\Gamma)\},$$

and, using the prime notation H' to denote the dual space of a given Hilbert space H ,

$$H^{-1/2}(S) = \left(\tilde{H}^{1/2}(S)\right)',$$

respectively.

Remark 2.1.1. *Throughout this thesis ...*

- (i) ... the term “smooth” is equated to “infinitely differentiable” and, as indicated above, it is assumed that the boundary of the domain Ω is smooth.
- (ii) ... it is assumed that the right hand sides in equation (2.1) satisfy $f \in H^{1/2}(\Gamma_D)$ and $g \in H^{-1/2}(\Gamma_N)$ so that certain existence and uniqueness results hold. Moreover, we assume the functions f and g are actually smooth.

The boundary Γ can be expressed in the form

$$\Gamma = \bigcup_{q=1}^{Q_D+Q_N} \Gamma_q, \quad (2.2)$$

where Q_D and Q_N denote the numbers of smooth *connected* Dirichlet and Neumann boundary portions, and where for $1 \leq q \leq Q_D$ (resp. $Q_D + 1 \leq q \leq Q_D + Q_N$) Γ_q denotes a Dirichlet (resp. Neumann) portion of the boundary curve Γ (see e.g. Figure 2.1). Clearly, letting

$$J_D = \{1, \dots, Q_D\} \quad \text{and} \quad J_N = \{Q_D + 1, \dots, Q_D + Q_N\}$$

we have that

$$\overline{\Gamma}_D = \bigcup_{q \in J_D} \Gamma_q \quad \text{and} \quad \overline{\Gamma}_N = \bigcup_{q \in J_N} \Gamma_q$$

are the subsets of Γ upon which Dirichlet and Neumann boundary conditions are enforced, respectively. Note that consecutive values of the index q do not necessarily correspond to consecutive boundary portions.

Remark 2.1.2. *In case Ω is an exterior domain, problem (2.1) admits unique solutions in $H_{\text{loc}}^1(\Omega)$. On the other hand, if Ω is an interior domain, this problem is not well posed for a discrete set of real values k_j , $j = 1, \dots, \infty$ —the squares of which are the Zaremba eigenvalues, that is to say, the eigenvalues of the Laplace operator under the corresponding homogeneous mixed Dirichlet-Neumann (Zaremba) boundary conditions (see [97, Th. 4.10], [2]).*

2.2 Boundary integral equation formulation

In what follows we seek solutions of problem (2.1) on the basis of the single-layer potential representation

$$u = \int_{\Gamma} G_k(x, y) \psi(y) ds_y, \quad (2.3)$$

where $G_k(x, y) = \frac{i}{4}H_0^1(k|x - y|)$ is the Helmholtz Green function in two-dimensional space. Taking into account well known expressions [34, p. 40] for the jump of the single layer potential and its normal derivative across Γ , the boundary conditions for the exterior (resp. interior) boundary value problem (2.1) give rise to the integral equations

$$\begin{aligned} \mathcal{A}_k^{(1)}[\psi](x) &:= \int_{\Gamma} G_k(x, y)\psi(y)ds_y = f(x) \quad x \in \Gamma_D, \\ \mathcal{A}_k^{(2)}[\psi](x) &:= \gamma \frac{\psi(x)}{2} + \int_{\Gamma} \frac{\partial G_k(x, y)}{\partial n_x} \psi(y)ds_y = g(x) \quad x \in \Gamma_N \end{aligned} \tag{2.4}$$

with $\gamma = -1$ (resp. $\gamma = 1$).

Important properties of *both the interior and exterior* integral equation problems (2.4) relate to existence of eigenvalues of certain *interior* problems for the Laplace operator under either Dirichlet or Zaremba boundary conditions. As shown in what follows, for example,

1. In case Ω is an exterior domain the integral equation system (2.4) admits unique solutions if and only if k^2 is not a Dirichlet eigenvalue of the Laplace operator in $\mathbb{R}^2 \setminus \Omega$.
2. For such an exterior domain Ω the PDE problem (2.1) admits unique solutions for any real value of k^2 in spite of the lack of uniqueness implied in point 1 for certain wavenumbers k . A procedure is presented in Section B which extends applicability of the proposed integral formulation to such values of k .
3. In case Ω is an interior domain, in turn, the integral equation system is uniquely solvable provided k^2 is not a Zaremba eigenvalue of the Laplace operator in Ω .
4. The PDE problem (2.1) in such an interior domain Ω does not admit unique solutions, of course, for values of k for which k^2 is a Zaremba eigenvalue in Ω . In this case the eigenfunctions of the Zaremba Laplace operator can be expressed in terms of the representation formula (2.3) for a certain density ψ which satisfies (2.4) with $f = 0$ and $g = 0$.

A detailed treatment concerning points 1, 3, and 4 above is presented in the remainder of this

section (Theorems 2.2.3, 2.2.4 and Definition 2.2.1). A corresponding discussion concerning point 2, in turn, is put forth in Section B.

Definition 2.2.1. *Given an interior (resp. exterior) domain Ω and a solution u of (2.1) in $H_{loc}^1(\Omega)$, a function $w \in H_{loc}^1(\mathbb{R}^2 \setminus \Omega)$ is said to be a solution “conjugate” to u if it satisfies*

$$\begin{aligned} \Delta w + k^2 w &= 0 & x \in \mathbb{R}^2 \setminus \Omega \\ w(x) &= u(x) & x \in \Gamma, \end{aligned} \tag{2.5}$$

as well as, in case $\mathbb{R}^2 \setminus \Omega$ is an exterior domain, Sommerfeld’s condition of radiation at infinity. Throughout this thesis the conjugate solution w in case $\mathbb{R}^2 \setminus \Omega$ is an exterior (resp. interior) domain will be denoted as $w = u_e$ (resp. $w = u_i$).

Lemma 2.2.2. *The conjugate solutions mentioned in Definition 2.2.1 exist and are uniquely determined in each one of the following two cases:*

1. $\mathbb{R}^2 \setminus \Omega$ is an exterior domain; and
2. $\mathbb{R}^2 \setminus \Omega$ is an interior domain and k^2 is not a Dirichlet eigenvalue of the Laplace operator in $\mathbb{R}^2 \setminus \Omega$.

Proof. For both point 1 and point 2 we rely on the fact that the solution u of the problem (2.1) is in $H_{loc}^1(\Omega)$ (see Remark 2.1.2), and, therefore, by the trace theorem (e.g., [97, Th 3.37]), its boundary values lie in $H^{1/2}(\Gamma)$. For point 1 we then invoke [97, Th 9.11] to conclude that a uniquely determined conjugate solution $w \in H_{loc}^1(\mathbb{R}^2 \setminus \Omega)$ exists, as needed. Point 2 follows similarly using [97, Th 4.10] under the assumption that k^2 is not a Dirichlet eigenvalue in the interior domain $\mathbb{R}^2 \setminus \Omega$. □

Theorem 2.2.3. *Let Ω be an exterior domain, and let $k \in \mathbb{R}$ be such that k^2 is not a Dirichlet eigenvalue of the Laplace operator in the interior domain $\mathbb{R}^2 \setminus \Omega$. Then the exterior integral equation system (2.4) ($\gamma = -1$, see also Remark 2.1.1 item ii) admits a unique solution given by*

$$\psi = \frac{\partial u_i}{\partial n} - \frac{\partial u}{\partial n}, \tag{2.6}$$

where u is the solution of the exterior mixed problem (2.1), and where u_i is the (uniquely determined) corresponding conjugate solution (Definition 2.2.1 and Lemma 2.2.2).

Proof. Since k^2 is not a Dirichlet eigenvalue for the Laplacian in $\mathbb{R}^2 \setminus \Omega$, the conjugate solution u_i is uniquely defined by the boundary values of the solution u . To obtain the expression (2.6) we first consider the Green representation formula for the functions u_i and u

$$\begin{aligned} u_i(x) &= \int_{\Gamma} \left(G_k(x, y) \frac{\partial u_i}{\partial n_y} - u_i \frac{\partial G_k(x, y)}{\partial n_y} \right) ds_y, \quad x \in \mathbb{R}^2 \setminus \Omega, \\ u(x) &= \int_{\Gamma} \left(u \frac{\partial G_k(x, y)}{\partial n_y} - G_k(x, y) \frac{\partial u}{\partial n_y} \right) ds_y, \quad x \in \Omega \end{aligned} \quad (2.7)$$

which, in view of the jump relations for the single and double layer potential operators, in the limit $x \rightarrow \Gamma$ leads to the relations

$$\begin{aligned} \frac{u_i(x)}{2} &= \int_{\Gamma} \left(G_k(x, y) \frac{\partial u_i}{\partial n_y} - u_i \frac{\partial G_k(x, y)}{\partial n_y} \right) ds_y, \quad x \in \Gamma \\ \frac{u(x)}{2} &= \int_{\Gamma} \left(u \frac{\partial G_k(x, y)}{\partial n_y} - G_k(x, y) \frac{\partial u}{\partial n_y} \right) ds_y, \quad x \in \Gamma. \end{aligned} \quad (2.8)$$

Since for $x \in \Gamma_D$ we have $u(x) = u_i(x) = f(x)$, the sum of the two equations in (2.8) yields

$$f(x) = \int_{\Gamma} G_k(x, y) \left(\frac{\partial u_i}{\partial n_y} - \frac{\partial u}{\partial n_y} \right) ds_y, \quad x \in \Gamma_D, \quad (2.9)$$

and, thus, in view of (2.6),

$$f(x) = \int_{\Gamma} G_k(x, y) \psi(y) ds_y, \quad x \in \Gamma_D. \quad (2.10)$$

Similarly, in the limit $x \rightarrow \Gamma$ the normal derivatives of the integrals in (2.7) give rise to the relations

$$\begin{aligned} \frac{1}{2} \frac{\partial u_i}{\partial n_x} &= \frac{\partial}{\partial n_x} \int_{\Gamma} \left(G_k(x, y) \frac{\partial u_i}{\partial n_y} - u_i \frac{\partial G_k(x, y)}{\partial n_y} \right) ds_y, \quad x \in \Gamma \\ \frac{1}{2} \frac{\partial u}{\partial n_x} &= \frac{\partial}{\partial n_x} \int_{\Gamma} \left(u \frac{\partial G_k(x, y)}{\partial n_y} - G_k(x, y) \frac{\partial u}{\partial n_y} \right) ds_y, \quad x \in \Gamma. \end{aligned} \quad (2.11)$$

The sum of the equations in (2.11) results in the identity

$$\frac{1}{2} \frac{\partial u_i}{\partial n_x} + \frac{1}{2} \frac{\partial u}{\partial n_x} = \int_{\Gamma} \frac{\partial G_k(x, y)}{\partial n_x} \left(\frac{\partial u_i}{\partial n_y} - \frac{\partial u}{\partial n_y} \right) ds_y \quad x \in \Gamma, \quad (2.12)$$

or, equivalently,

$$\frac{\partial u}{\partial n_x} = -\frac{1}{2} \left(\frac{\partial u_i}{\partial n_x} - \frac{\partial u}{\partial n_x} \right) + \int_{\Gamma} \frac{\partial G_k(x, y)}{\partial n_x} \left(\frac{\partial u_i}{\partial n_y} - \frac{\partial u}{\partial n_y} \right) ds_y \quad x \in \Gamma. \quad (2.13)$$

But for $x \in \Gamma_N$ we have $\frac{\partial u}{\partial n_x} = g(x)$, and, thus, equation (2.13) can be made to read

$$g(x) = -\frac{\psi(x)}{2} + \int_{\Gamma} \frac{\partial G_k(x, y)}{\partial n_x} \psi(y) ds_y, \quad x \in \Gamma_N. \quad (2.14)$$

Equations (2.10) and (2.14) tell us that the density ψ is a solution of the exterior integral equation system (2.4), as claimed.

In order to establish the solution uniqueness let ξ be a solution of equation (2.4) with $f = 0$ and $g = 0$. Since as mentioned above the exterior mixed problem is uniquely solvable, the corresponding single layer potential

$$v = \int_{\Gamma} G_k(x, y) \xi(y) ds_y \quad (2.15)$$

is equal to zero everywhere in Ω . It then follows from the continuity of the single layer potential that v satisfies the Dirichlet problem in the interior domain $\mathbb{R}^2 \setminus \Omega$ with zero boundary values. Since by assumption k^2 is not a Dirichlet eigenvalue of the Laplacian in $\mathbb{R}^2 \setminus \Omega$ it follows that $v = 0$ in that region as well. Thus, both the interior and exterior normal derivatives vanish, and therefore so does their difference ξ . The proof is complete. \square

Theorem 2.2.4. *Let Ω be an interior domain. Then we have:*

1. *If k^2 is not a Zaremba eigenvalue (see Remark 2.1.2), then the interior integral equation system (2.4) ($\gamma=1$, see also Remark 2.1.1 item ii) admits a unique solution, which is*

given by

$$\psi = \frac{\partial u}{\partial n} - \frac{\partial u_e}{\partial n}. \quad (2.16)$$

Here u is the solution of the interior mixed problem (2.1), and u_e is the solution conjugate to u (Definition 2.2.1 and Lemma 2.2.2).

2. If k^2 is a Zaremba eigenvalue, in turn, any eigenfunction u satisfying (2.1) with $f = 0$ and $g = 0$ can be expressed by means of a single-layer representation

$$u(x) = \int_{\Gamma} G_k(x, y) \left(\frac{\partial u}{\partial n_y} - \frac{\partial u_e}{\partial n_y} \right) ds_y, \quad x \in \Omega \cup \Gamma, \quad (2.17)$$

where u_e denotes the conjugate solution corresponding to the eigenfunction u (Definition 2.2.1 and Lemma 2.2.2).

Proof. We first consider properties that are common to Zaremba solutions and eigenfunctions, and which therefore relate to both points 1 and 2 in the statement of the theorem. For any given solution u of the interior mixed problem (2.1) (u can be either the unique solution of the interior mixed problem in the case k^2 is not an eigenvalue, or any eigenfunction satisfying (2.1) with $f = 0$ and $g = 0$) the conjugate solution u_e is uniquely defined (see Lemma 2.2.2), and so is the density ψ given by (2.16). Letting

$$w(x) = \int_{\Gamma} G_k(x, y) \left(\frac{\partial u}{\partial n_y} - \frac{\partial u_e}{\partial n_y} \right) ds_y, \quad (2.18)$$

using the Green representation formula for u and u_e ,

$$\begin{aligned} u(x) &= \int_{\Gamma} \left(G_k(x, y) \frac{\partial u}{\partial n_y} - u \frac{\partial G_k(x, y)}{\partial n_y} \right) ds_y, \quad x \in \Omega, \\ u_e(x) &= \int_{\Gamma} \left(u_e \frac{\partial G_k(x, y)}{\partial n_y} - G_k(x, y) \frac{\partial u_e}{\partial n_y} \right) ds_y, \quad x \in \mathbb{R}^2 \setminus \Omega, \end{aligned} \quad (2.19)$$

and taking into account the jump relations for the double layer potential as well as the fact that $u_e(x) = u(x)$ for $x \in \Gamma$ we obtain

$$u(x) = \int_{\Gamma} G_k(x, y) \left(\frac{\partial u}{\partial n_y} - \frac{\partial u_e}{\partial n_y} \right) ds_y = w(x), \quad x \in \Gamma. \quad (2.20)$$

Similarly, taking normal derivatives of both sides of each equation in (2.19) at a point $x \in \Gamma$ we obtain the equations

$$\begin{aligned} \frac{1}{2} \frac{\partial u}{\partial n_x} &= \frac{\partial}{\partial n_x} \int_{\Gamma} \left(G_k(x, y) \frac{\partial u}{\partial n_y} - u \frac{\partial G_k(x, y)}{\partial n_y} \right) ds_y, & x \in \Gamma, \\ \frac{1}{2} \frac{\partial u_e}{\partial n_x} &= \frac{\partial}{\partial n_x} \int_{\Gamma} \left(u_e \frac{\partial G_k(x, y)}{\partial n_y} - G_k(x, y) \frac{\partial u_e}{\partial n_y} \right) ds_y, & x \in \Gamma, \end{aligned} \quad (2.21)$$

whose sum yields

$$\frac{\partial u}{\partial n_x} = -\frac{1}{2} \left(\frac{\partial u}{\partial n_x} - \frac{\partial u_e}{\partial n_x} \right) + \int_{\Gamma} \frac{\partial G_k(x, y)}{\partial n_x} \left(\frac{\partial u}{\partial n_y} - \frac{\partial u_e}{\partial n_y} \right) ds_y = \frac{\partial w}{\partial n_x} \quad x \in \Gamma. \quad (2.22)$$

We now conclude the proof by applying these concepts to points 1 and 2 in the statement of the theorem.

1. In case k^2 is not an eigenvalue for the Laplace-Zaremba problem (2.1), equations (2.20) and (2.22) evaluated for $x \in \Gamma_D$ and $x \in \Gamma_N$, respectively, show that the density ψ given by (2.16) satisfies the integral equation system (2.4) with $\gamma = 1$.
2. In case k^2 is an eigenvalue for the Laplace-Zaremba problem (2.1), in turn, let u denote a corresponding eigenfunction. Equations (2.20) and (2.22) along with the Green representation formula show that $u(x) = w(x)$ for any $x \in \Omega$, that is to say, equation (2.17) is satisfied.

The proof is now complete. □

2.3 Singularities of the solutions of equations (2.1) and (2.4)

With reference to equation (2.2), let $y^0 = (y_1^0, y_2^0) \in \Gamma$ be a point which separates Dirichlet and Neumann regions Γ_{q_1} and Γ_{q_2} ($q_1 \in J_D$ and $q_2 \in J_N$) within Γ . In order to express the singular character around y^0 of both the solution $u(y)$ of problem (2.1) ($y = (y_1, y_2) \in \Omega$) and the corresponding integral equation density $\psi(y)$ in equation (2.4) ($y = (y_1, y_2) \in \Gamma$) we

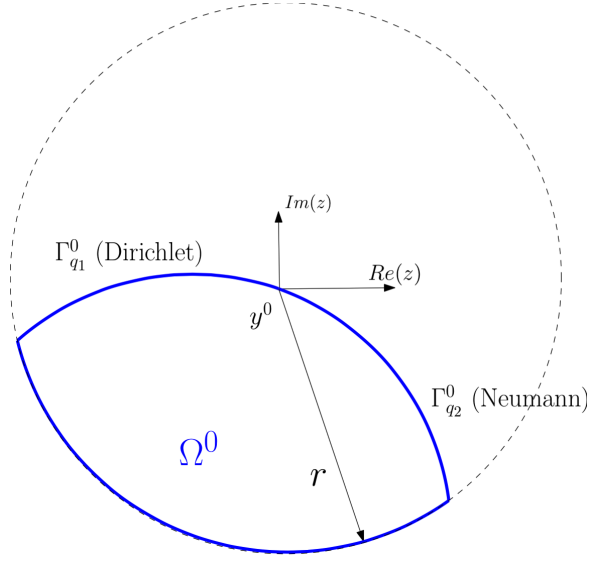


Figure 2.2: Singular point y^0 .

consider the neighborhoods

$$\Omega^0 = \overline{\Omega \cap B(y^0, r)}, \quad \Gamma_{q_1}^0 = \overline{\Gamma_{q_1} \cap B(y^0, r)} \quad \text{and} \quad \Gamma_{q_2}^0 = \overline{\Gamma_{q_2} \cap B(y^0, r)} \quad (2.23)$$

of the singular point y^0 relative to Ω , Γ_{q_1} and Γ_{q_2} , respectively. Here for a set $A \subset \mathbb{R}^2$, \overline{A} denotes the topological closure of A in \mathbb{R}^2 , $B(y^0, r)$ denotes the circle centered at y^0 of radius r , and $r > 0$ is sufficiently small that $B(y^0, r)$ only has nonempty intersections with $\overline{\Gamma_q}$ for the Dirichlet index $q = q_1$ and the Neumann index $q = q_2$. Additionally, we use certain functions $\widehat{u}_{y^0} = \widehat{u}_{y^0}(z)$, $\widehat{\psi}_{y^0}^1 = \widehat{\psi}_{y^0}^1(d)$ and $\widehat{\psi}_{y^0}^2 = \widehat{\psi}_{y^0}^2(d)$ where the Dirichlet (resp. Neumann) function $\widehat{\psi}_{y^0}^1$ (resp $\widehat{\psi}_{y^0}^2$) is the density as a function of the distance d to the point y^0 in $\Gamma_{q_1}^0$ (resp. $\Gamma_{q_2}^0$), and where $z = (y_1 - y_1^0) + i(y_2 - y_2^0)$ is a complex variable (see Figure 2.2). The functions \widehat{u}_{y^0} , $\widehat{\psi}_{y^0}^1$ and $\widehat{\psi}_{y^0}^2$ are given by

$$\begin{aligned} \widehat{u}_{y^0}(z) &= u(y), \\ \psi(y) &= \widehat{\psi}_{y^0}^1(d(y)) \quad y \in \Gamma_{q_1}^0, \\ \psi(y) &= \widehat{\psi}_{y^0}^2(d(y)) \quad y \in \Gamma_{q_2}^0, \end{aligned} \quad (2.24)$$

where, as mentioned above

$$z = (y_1 - y_1^0) + i(y_2 - y_2^0) \quad ; \quad d(y) = \sqrt{(y_1 - y_1^0)^2 + (y_2 - y_2^0)^2}. \quad (2.25)$$

It is known [125, 126] that, under our assumption that the curve Γ is piecewise smooth, for any given integer \mathcal{N} the function $\widehat{u}_{y^0}(z)$ can be expressed in the form

$$\widehat{u}_{y^0}(z) = \log(z)P_{y^0}^{1,\mathcal{N}} + \log(\bar{z})P_{y^0}^{2,\mathcal{N}} + P_{y^0}^{3,\mathcal{N}} + o(z^\mathcal{N}) \quad (2.26)$$

for all z in a neighborhood of the point, where $P_{y^0}^{1,\mathcal{N}}, P_{y^0}^{2,\mathcal{N}}$ and $P_{y^0}^{3,\mathcal{N}}$ are \mathcal{N} -dependent polynomial functions of $z, \bar{z}, z^{1/(2\alpha)}, \bar{z}^{1/(2\alpha)}, z \log(z), \bar{z}^q \log(\bar{z})$.

Remark 2.3.1. *In the asymptotic expansion (2.26), and, indeed, in all similar asymptotic expansions in this thesis, it is assumed that none of the right hand side polynomials contain terms that, multiplied by the relevant factors, could be included in the error term.*

Under our standing assumption of smoothness of the domain boundary the following two theorems provide 1) Finer details on the asymptotics (2.26) as well as 2) A corresponding asymptotic expression around y^0 for the solutions $\widehat{\psi}_{y^0}^1(d)$ and $\widehat{\psi}_{y^0}^2(d)$ of the integral-equation system (2.4).

Theorem 2.3.2. *Let y^0 be a Dirichlet-Neumann point as described above in this section. Then, given an arbitrary integer \mathcal{N} , the function $\widehat{u}_{y^0}(z)$ can be expressed in the form*

$$\widehat{u}_{y^0}(z) = P_{y^0}^\mathcal{N}(z^{1/2}, \bar{z}^{1/2}) + o(z^\mathcal{N}) \quad (2.27)$$

around y^0 , where $P_{y^0}^\mathcal{N}$ is an \mathcal{N} -dependent polynomial function of its arguments; see Remark 2.3.1.

Theorem 2.3.3. *Let y^0 be a Dirichlet-Neumann point. Then given an arbitrary integer \mathcal{N} the functions $\widehat{\psi}_{y^0}^1(d)$ and $\widehat{\psi}_{y^0}^2(d)$ can be expressed in the forms*

$$\begin{aligned} \widehat{\psi}_{y^0}^1(d) &= d^{-1/2}Q_{y^0}^{1,\mathcal{N}}(d^{1/2}) + o(d^{\mathcal{N}-1}) \quad \text{and} \\ \widehat{\psi}_{y^0}^2(d) &= d^{-1/2}Q_{y^0}^{2,\mathcal{N}}(d^{1/2}) + o(d^{\mathcal{N}-1}) \end{aligned} \quad (2.28)$$

around $d = 0$, where $Q_{y_0}^{1,\mathcal{N}}$ and $Q_{y_0}^{2,\mathcal{N}}$ are \mathcal{N} -dependent polynomial functions of their arguments; see Remark 2.3.1.

Note in particular that Theorem 2.3.2 shows that, under our assumptions of boundary smoothness, all logarithmic terms in equation (2.26) actually drop out. The proofs of these theorems (which are given in Sections 2.3.2 and 2.3.3, respectively) utilize a certain conformal map introduced in Section 2.3.1 that transforms Ω^0 into a semi-circular region.

2.3.1 Conformal mapping

Following [125], in order to establish Theorem 2.3.2 we identify \mathbb{R}^2 with the complex plane \mathbb{C} via the aforementioned relationship $z = (y_1 - y_1^0) + i(y_2 - y_2^0) \leftrightarrow (y_1 - y_1^0, y_2 - y_2^0)$, and we utilize a conformal map $z = w(\xi)$ which maps the semi-circular region $D_A = \{\xi \in \mathbb{C} : |\xi| \leq A \text{ and } \text{Im}(\xi) \leq 0\}$ in the complex ξ -plane (Figure 2.3) onto the domain Ω^0 (equation (2.23)) in the complex z -plane. We assume, as we may, that w maps the origin to itself and that the intervals $\{\text{Im}(\xi) = 0, 0 \leq \text{Re}(\xi) \leq A\}$ and $\{\text{Im}(\xi) = 0, -A \leq \text{Re}(\xi) \leq 0\}$ are mapped onto the boundary portions $\Gamma_{q_1}^0$ and $\Gamma_{q_2}^0$, respectively.

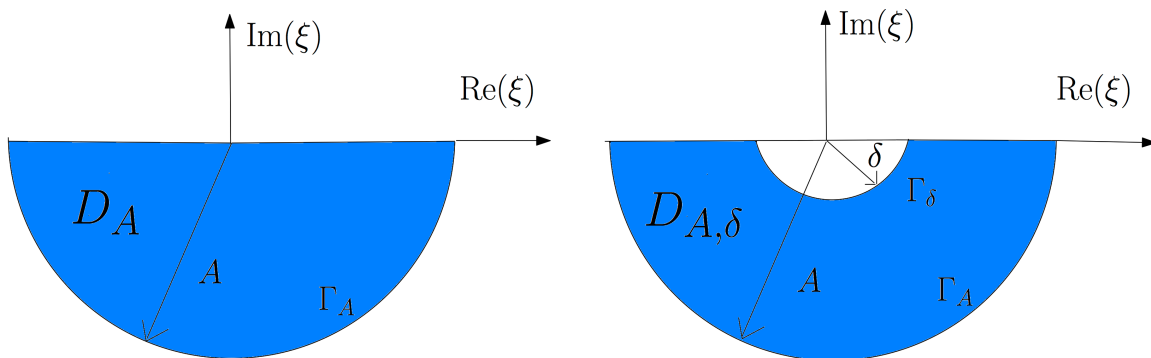


Figure 2.3: Semi-circular and semi-annular Green-identity regions.

Letting

$$U(\xi) = \widehat{u}_{y^0}(w(\xi)) \tag{2.29}$$

we note that, in view of the relation $\Delta_\xi U(\xi) = \Delta_z \widehat{u}_{y^0}(w(\xi)) \cdot |w'(\xi)|^2$ satisfied by a complex

analytic function w (see [46, eq. 5.4.17]), U satisfies the second order elliptic equation

$$\Delta U + K(\xi)U = 0 \quad \text{for } \xi \in \text{int}(D_A), \quad (2.30)$$

$$U(\xi) = F(\xi) \quad \text{for } \text{Im}(\xi) = 0, \text{Re}(\xi) > 0, \quad (2.31)$$

$$\frac{\partial U(\xi)}{\partial n} = G(\xi) \quad \text{for } \text{Im}(\xi) = 0, \text{Re}(\xi) \leq 0, \quad \text{and} \quad (2.32)$$

$$U(\xi) = M(\xi) \quad \text{for } |\xi| = A. \quad (2.33)$$

Here $F(\xi) = f(w(\xi))$, $G(\xi) = g(w(\xi))$ and $M(\xi) = u(w(\xi))$. (The function M is thus obtained from the restriction of the solution u to the set $\partial\Omega^0 \setminus (\Gamma_{q_1}^0 \cup \Gamma_{q_2}^0)$; see equation (2.23) and Figure 2.2).

2.3.2 Proof of theorem 2.3.2

The proof of this theorem, which, under the present scope of smooth-domain problems establishes a result stronger than [125, Th. 3.2], does incorporate some of the lines of the proof provided in that reference. In what follows we use the Laplace-Zaremba Green function

$$H(t, \xi) = -\frac{1}{2\pi} \left\{ \log |t - \xi| + \log |t - \bar{\xi}| - 2 \log \left| \sqrt{t} + \sqrt{\xi} \right| - 2 \log \left| \sqrt{t} - \sqrt{\bar{\xi}} \right| \right\} \quad (2.34)$$

for the lower half plane with homogeneous Dirichlet (resp. Neumann) boundary conditions on the positive (resp. negative) real axis in terms of the complex variables $t = t_1 + it_2 = (t_1, t_2)$ and $\xi = \xi_1 + i\xi_2 = (\xi_1, \xi_2)$. The branches of the square roots in (2.34) are given by $\sqrt{t} = \sqrt{\rho_t e^{i\theta_t}} = \sqrt{\rho_t} e^{i\theta_t/2}$ and $\sqrt{\bar{\xi}} = \sqrt{\rho_\xi e^{i\theta_\xi}} = \sqrt{\rho_\xi} e^{i\theta_\xi/2}$, where (ρ_t, θ_t) and (ρ_ξ, θ_ξ) denote polar coordinates in the complex t - and ξ -plane respectively ($-\pi \leq \theta_t, \theta_\xi < \pi$). Note that, with these conventions the domain D_A in the t variables is given by $\rho_t \leq A$ and $-\pi \leq \theta_t \leq 0$. The following Lemma establishes certain important properties of the aforementioned Green function.

Lemma 2.3.4. *The function $H = H(t, \xi)$ (equation (2.34)) is indeed a Laplace-Zaremba Green function for the lower half plane with a Dirichlet-Neumann junction at the origin,*

that is we have $\Delta_t H(t, \xi) = -\delta(t - \xi)$ and H satisfies

$$H(t, \xi) = 0 \quad \text{for } \theta_t = 0 \quad \text{and} \quad \frac{\partial H}{\partial n_t}(t, \xi) = 0 \quad \text{for } \theta_t = -\pi. \quad (2.35)$$

In addition, for a certain constant C we have

$$\int_0^A \left| \frac{\partial}{\partial n_t} (H(t, \xi)) \right| dt \leq C \quad (2.36)$$

for all $\xi \in \mathbb{C}$.

Proof. The function $H(t, \xi)$ can be re-expressed in the form

$$H(t, \xi) = -\frac{1}{2\pi} \log \frac{|\sqrt{t} - \sqrt{\xi}| |\sqrt{t} + \sqrt{\bar{\xi}}|}{|\sqrt{t} + \sqrt{\xi}| |\sqrt{t} - \sqrt{\bar{\xi}}|}. \quad (2.37)$$

The first statement in equation (2.35) follows from the relations $|\sqrt{t} - \sqrt{\xi}| = |\sqrt{t} - \sqrt{\bar{\xi}}|$ and $|\sqrt{t} + \sqrt{\bar{\xi}}| = |\sqrt{t} + \sqrt{\xi}|$, which hold for $\theta_t = 0$ ($t > 0$) since, in view of our selection of branch cuts we have

$$\sqrt{\bar{\xi}} = \overline{\sqrt{\xi}}. \quad (2.38)$$

In order to establish the second statement in (2.35) and equation (2.36) we consider the relations

$$\begin{aligned} \frac{\partial}{\partial t_2} \log |\sqrt{t} - (z_1 + iz_2)| &= \frac{z_1}{2\sqrt{-t_1} (z_1^2 + (\sqrt{-t_1} + z_2)^2)} \quad \text{for } \theta_t = -\pi, \quad \text{and} \\ \frac{\partial}{\partial t_2} \log |\sqrt{t} - (z_1 + iz_2)| &= -\frac{z_2}{2\sqrt{t_1} ((z_1 - \sqrt{t_1})^2 + z_2^2)} \quad \text{for } \theta_t = 0, \end{aligned} \quad (2.39)$$

which are valid for all complex numbers $z = z_1 + iz_2$, and since on the axis $t_2 = 0$ we have $\frac{\partial}{\partial n_t} = \frac{\partial}{\partial t_2}$, the second statement in (2.35) follows from (2.38). In order to establish a bound of the form (2.36), finally, we use (2.39) to obtain the expression

$$\left| \frac{\partial}{\partial n_t} (H(t, \xi)) \right| = \frac{|\text{Im}(\sqrt{\xi})|}{2\pi\sqrt{t}} \left(\frac{1}{(\sqrt{t} + \text{Re}(\sqrt{\xi}))^2 + \text{Im}(\sqrt{\xi})^2} + \frac{1}{(\sqrt{t} - \text{Re}(\sqrt{\xi}))^2 + \text{Im}(\sqrt{\xi})^2} \right) \quad (2.40)$$

for the absolute value of the derivative of (2.37) with respect to t_2 . It is then easy to check that

$$\int_0^A \left| \frac{\partial}{\partial n_t} (H(t, \xi)) \right| dt = \frac{|\operatorname{Im}(\sqrt{\xi})|}{\pi \operatorname{Im}(\sqrt{\xi})} \left(\arctan \frac{\sqrt{A} - \operatorname{Re}(\sqrt{\xi})}{\operatorname{Im}(\sqrt{\xi})} + \arctan \frac{\sqrt{A} + \operatorname{Re}(\sqrt{\xi})}{\operatorname{Im}(\sqrt{\xi})} \right) \quad (2.41)$$

for all $\xi \in \mathbb{C} \setminus [0; A]$. Since the right-hand side of equation (2.41) is uniformly bounded for $\xi \in \mathbb{C} \setminus [0; A]$ and since for $\xi \in [0; A]$ the integrand in (2.36) vanishes (in view of the second expression in (2.39)), we see that there exists a constant C such that equation (2.36) holds for all $\xi \in \mathbb{C}$, as needed, and the proof is thus complete. \square

The proof of the theorem 2.3.2 is based on a bootstrapping argument which is initiated by the simple but suboptimal asymptotic relation put forth in the following lemma following lemma.

Lemma 2.3.5. *The solution U of the problem (2.30)–(2.33) satisfies the asymptotic relation*

$$U(\xi) = o(\xi^\mu) \quad (2.42)$$

for all $-\frac{1}{2} < \mu < 0$.

Proof. To establish this relation we consider the Green formula

$$U(\xi) = \int \int_{D_A} H(t, \xi) \Delta U(t) dx_t dy_t + \int_{\partial D_A} \left\{ U(t) \frac{\partial}{\partial n_t} H(t, \xi) - H(t, \xi) \frac{\partial}{\partial n_t} U(t) \right\} ds_t. \quad (2.43)$$

Since H satisfies (2.35) as it befits a Green function for (2.30)–(2.33), denoting by Γ_A the radius- A part of ∂D_A it follows that

$$\begin{aligned} |U(\xi)| \leq & \left| \int \int_{D_A} H(t, \xi) K(t) U(t) dx_t dy_t \right| + \left| \int_0^A F(x) \frac{\partial}{\partial n_t} H(t, \xi) dt \right| \\ & + \left| \int_0^A G(-t) H(-t, \xi) dt \right| + \left| \int_{\Gamma_A} \left\{ U(t) \frac{\partial}{\partial n_t} H(t, \xi) - H(t, \xi) \frac{\partial}{\partial n_t} U(t) \right\} ds_t \right|. \end{aligned} \quad (2.44)$$

For the integral over the outer arc Γ_A in (2.44) we have

$$\left| \int_{\Gamma_A} \left\{ U(t) \frac{\partial}{\partial n_t} H(t, \xi) - H(t, \xi) \frac{\partial}{\partial n_t} U(t) \right\} ds_t \right| \leq C, \quad \text{for } |\xi| < A/2, \quad (2.45)$$

as it can be checked easily in view of the boundedness of the integrands for ξ near the origin. Taking into account that $u \in H_{\text{loc}}^1(\Omega)$ (see Remark 2.1.2), on the other hand, it easily follows that $U \in H^1(D_A)$, and thus, bounding the absolute value of the first integral in (2.44) by means of the Cauchy-Schwarz inequality, for ξ near 0 we obtain the uniform estimate

$$\left| \int \int_{D_A} H(t, \xi) K(t) U(t) dx_t dy_t \right| \leq \|H\|_{L^2} \|U\|_{L^2} \max(K). \quad (2.46)$$

The second and third integrals in equation (2.44), finally, may be estimated on the basis of Remark 2.1.1, which implies that the functions F and G (defined in Section 2.3.1) are smooth. Indeed H is clearly absolutely integrable, and the absolute integrability of $\partial H / \partial n_t$ follows from Lemma 2.3.4. The boundedness of F and G thereby implies the uniform boundedness of the function U near the origin. The relation (2.42) thus follows for all $-\frac{1}{2} < \mu < 0$ and the proof is complete. \square

Corollary 2.3.6. *The derivatives of the solution U of the problem (2.30)–(2.33) satisfy the asymptotic relation*

$$D^h U = o(\xi^{\mu-h}) \quad (2.47)$$

for all $-\frac{1}{2} < \mu < 0$.

Proof. See [125, Section 4] \square

A key element in the bootstrapping algorithm mentioned at the beginning of this section is a representation formula for the function U that is presented in the following Lemma.

Lemma 2.3.7. *The solution U of equation (2.30)–(2.33) satisfies the representation*

$$\begin{aligned}
U(\xi) = & -\frac{1}{2\pi} \{ \Lambda_1(-K(t)U(t), \xi, 1) + \Lambda_1(-K(t)U(t), \bar{\xi}, 1) - 2\Lambda_1(-K(t)U(t), \xi, 2) \\
& - 2\Lambda_1(-K(t)U(t), \bar{\xi}, 2) - \Lambda_3(F(t), \xi, 1) - \Lambda_3(F(t), \bar{\xi}, 1) + 2\Lambda_3(F(t), \xi, 2) \\
& + 2\Lambda_3(F(t), \bar{\xi}, 2) - \Lambda_2(G(-t), -\xi, 1) - \Lambda_2(G(-t), -\bar{\xi}, 1) + 2\Lambda_2(G(-t), -\xi, 2) \\
& + 2\Lambda_2(G(-t), -\bar{\xi}, 2) \} + p_1(\sqrt{\xi}) + p_2(\sqrt{\bar{\xi}}),
\end{aligned} \tag{2.48}$$

where

$$\begin{aligned}
\Lambda_1(q(t), \xi, \mu) &:= \int_{-\pi}^0 \int_0^A q(t) \log \left| t^{\frac{1}{\mu}} - \xi^{\frac{1}{\mu}} \right| \rho_t d\rho_t d\theta_t, \\
\Lambda_2(q(t), \xi, \mu) &:= \int_0^A q(t) \log \left| t^{\frac{1}{\mu}} - \xi^{\frac{1}{\mu}} \right| dt, \\
\Lambda_3(q(t), \xi, \mu) &:= \int_0^A q(t) \frac{1}{t} \frac{\partial}{\partial \theta_t} \log \left| t^{\frac{1}{\mu}} - \xi^{\frac{1}{\mu}} \right| dt,
\end{aligned} \tag{2.49}$$

and where p_1 and p_2 denote power series with positive radii of convergence.

Proof. Applying Green formula on the set

$$D_{A,\delta} = \{ \xi \in \mathbb{C} : \delta \leq |\xi| \leq A \text{ and } \text{Im}(\xi) \leq 0 \} \tag{2.50}$$

(right portion of Figure 2.3) we obtain the expression

$$U(\xi) = \int \int_{D_{A,\delta}} H(t, \xi) \Delta U(t) dx_t dy_t + \int_{\partial D_{A,\delta}} \left\{ U(t) \frac{\partial}{\partial n_t} H(t, \xi) - H(t, \xi) \frac{\partial}{\partial n_t} U(t) \right\} ds_t. \tag{2.51}$$

Further, for fixed $\xi \neq 0$ we have

$$H(t, \xi) = \mathcal{O}(\sqrt{t}) \text{ as } t \rightarrow 0, \tag{2.52}$$

and therefore, in view of (2.42) and (2.47),

$$\begin{aligned} U(t)H(t, \xi) &= o(t^\mu), \\ U(t)\frac{\partial}{\partial \rho_t}H(t, \xi) - H(t, \xi)\frac{\partial}{\partial \rho_t}U(t) &= o\left(t^{\mu-\frac{1}{2}}\right). \end{aligned} \tag{2.53}$$

Letting Γ_δ denote the radius- δ arc within the boundary $\partial D_{A,\delta}$ of $D_{A,\delta}$ (Figure 2.3), and noting that for $t \in \Gamma_\delta$ we have $\frac{\partial}{\partial \rho_t} = \frac{\partial}{\partial n_t}$, in view of (2.53) we obtain

$$\int_{\Gamma_\delta} \left\{ U(t)\frac{\partial}{\partial n_t}H(t, \xi) - H(t, \xi)\frac{\partial}{\partial n_t}U(t) \right\} ds_t \rightarrow 0 \text{ as } \delta \rightarrow 0. \tag{2.54}$$

Further, exploiting the fact that the Green function (2.34) is a jointly analytic function of $\sqrt{\xi}$ and $\sqrt{\bar{\xi}}$ for $t \in \Gamma_A$ and ξ around $\xi = 0$, we obtain

$$\int_{\Gamma_A} \left\{ U(t)\frac{\partial}{\partial n_t}H(t, \xi) - H(t, \xi)\frac{\partial}{\partial n_t}U(t) \right\} ds_t = p_1\left(\sqrt{\xi}\right) + p_2\left(\sqrt{\bar{\xi}}\right), \tag{2.55}$$

where p_1 and p_2 denote power series with positive radii of convergence.

Letting $\delta \rightarrow 0$ in (2.51) and (2.54) and using (2.55) we finally obtain

$$\begin{aligned} U(\xi) &= \int_{-\pi}^0 \int_0^A H(t, \xi)(-K(t)U(t))\rho_t d\rho_t d\theta_t - \int_0^A F(x)\frac{1}{t}\frac{\partial}{\partial \theta_t}H(t, \xi)dt \\ &\quad - \int_0^A G(-t)H(-t, \xi)dt + p_1\left(\sqrt{\xi}\right) + p_2\left(\sqrt{\bar{\xi}}\right). \end{aligned} \tag{2.56}$$

Using the definitions (2.49) for the functions Λ_1 , Λ_2 , and Λ_3 , equation (2.56) is equivalent to equation (2.48) and the proof is complete. \square

In order to determine the singular character of $U(\xi)$ around $\xi = 0$ (and therefore that of $\widehat{u}_{y^0}(z)$ around $z = 0$) we study the corresponding asymptotic behavior of each one of the Λ -terms in equation (2.48). An important part of this discussion is the following Lemma, which presents certain regularity properties of the operators Λ_1 , Λ_2 , and Λ_3 .

Lemma 2.3.8. *Let $\alpha \geq 0$, $\beta > -1$ and $\gamma > -1$, and let $\mu = 1$ or $\mu = 2$. Then*

$$\Lambda_1(t^{\beta}\bar{t}^{\gamma}, \xi, \mu) = C_1\xi^{\beta+\gamma+2} + C_2\bar{\xi}^{\beta+\gamma+2} + C_3\xi^{\beta+1}\bar{\xi}^{\gamma+1} + p_1\left(\xi^{\frac{1}{\mu}}\right) + p_2\left(\bar{\xi}^{\frac{1}{\mu}}\right), \quad (2.57)$$

$$\Lambda_2(t^{\beta}, \xi, \mu) = C_4\xi^{\beta+1} + C_5\bar{\xi}^{\beta+1} + p_3(\xi^{1/\mu}) + p_4(\bar{\xi}^{1/\mu}) \quad \text{and} \quad (2.58)$$

$$\Lambda_3(t^{\alpha}, \xi, \mu) = C_6\xi^{\alpha} + C_7\bar{\xi}^{\alpha} + p_5(\xi^{1/\mu}) + p_6(\bar{\xi}^{1/\mu}). \quad (2.59)$$

For general functions $g(t) \in C^{\ell}(D_A)$ and $h(t) \in C^{\ell}((0, A])$ satisfying $g(t) = o(t^{\gamma})$ and $h(t) = o(t^{\alpha})$ as $t \rightarrow 0$, further, we have

$$\Lambda_1(g(t), \xi, \mu) = q_1\left(\xi^{\frac{1}{\mu}}\right) + q_2\left(\bar{\xi}^{\frac{1}{\mu}}\right) + o(\xi^{\gamma+2}), \quad (2.60)$$

$$\Lambda_2(g(t), \xi, \mu) = q_3\left(\xi^{\frac{1}{\mu}}\right) + q_4\left(\bar{\xi}^{\frac{1}{\mu}}\right) + o(\xi^{\gamma+1}) \quad \text{and} \quad (2.61)$$

$$\Lambda_3(h(t), \xi, \mu) = q_5\left(\xi^{\frac{1}{\mu}}\right) + q_6\left(\bar{\xi}^{\frac{1}{\mu}}\right) + o(\xi^{\alpha}), \quad (2.62)$$

(see Remark 2.3.1). Here p_i (resp. q_i), $i = 1, \dots, 6$, are power series with positive radii of convergence (resp. polynomials), C_i , $i = 1 \dots 7$ are complex constants, and the expansions are ℓ -times differentiable as $\xi \rightarrow 0$ —in the sense of Wigley: the derivatives of the left hand sides in (2.60) through (2.62) are equal to the corresponding derivatives of the first two term of the right hand sides, with error terms given by the “formal” derivatives of the corresponding error terms—e.g. $d/d\xi(o(\xi^{\alpha})) = o(\xi^{\alpha-1})$.

Proof of Lemma 2.3.8. The proof follows by specializing the proofs of Lemmas 7.1 – 7.2 and 8.1 – 8.6 in [125]. □

We are now ready to provide the main proof of this section.

Proof of Theorem 2.3.2. Since the solutions \widehat{u}_{y^0} and U are related by equation (2.29), using the classical result [120, Th. IV] (which establishes, in particular, that the conformal mapping w is smooth up to and including the boundary for any smooth portion of the domain boundary; see also [119]) and expanding $w(\xi)$ in Taylor series around $\xi = 0$, we see that it

suffices to prove that for an arbitrary integer \mathcal{M} we have the asymptotic relation

$$U(\xi) = \mathcal{Q}^{\mathcal{M}}(\xi^{1/2}, \bar{\xi}^{1/2}) + o(\xi^{\mathcal{M}}) \quad (2.63)$$

for the solution $U(\xi)$ of the problem (2.30)–(2.33), where $\mathcal{Q}^{\mathcal{M}} = \mathcal{Q}^{\mathcal{M}}(r, s)$ is a polynomial function of the independent variables r and s .

The proof now proceeds inductively. The induction basis is provided by the asymptotics (2.42) of the function U . To complete the proof we thus need to establish that *provided that* for some integer \mathcal{L} the function U can be expressed in the form

$$U(\xi) = \mathcal{P}^{\mathcal{L}}(\xi^{1/2}, \bar{\xi}^{1/2}) + o(\xi^{\mathcal{L}-\lambda}) \quad \text{as } \xi \rightarrow 0, \quad (2.64)$$

for some $0 < \lambda < 1$, where $\mathcal{P}^{\mathcal{L}} = \mathcal{P}^{\mathcal{L}}(r, s)$ is a polynomial function of the independent variables r and s , *then* a similar relation holds for U with an error of order $o(\xi^{\mathcal{L}+1-\lambda})$ and for a certain polynomial $\mathcal{P}^{\mathcal{L}+1}(\xi^{1/2}, \bar{\xi}^{1/2})$:

$$U(\xi) = \mathcal{P}^{\mathcal{L}+1}(\xi^{1/2}, \bar{\xi}^{1/2}) + o(\xi^{\mathcal{L}+1-\lambda}). \quad (2.65)$$

To do this we apply Lemma (2.3.8) to each term on the right hand side of equation (2.48). For the terms including the operator Λ_1 , for example, such an asymptotic representation with error of the order $o(\xi^{\mathcal{L}+1-\lambda})$ can be obtained by using the assumption (2.64) and the \mathcal{L} -th order Taylor expansion of the smooth function $K(t)$ around $t = 0$, and by applying equations (2.57) with $\beta = 0, 1/2, 1, \dots, \mathcal{L}$, $\gamma = 0, 1/2, 1, \dots, \mathcal{L}$ and equation (2.60) with $\gamma = \mathcal{L} - \lambda$ to the resulting polynomial and error terms for the product $K(t)U(t)$. The terms that contain the operators Λ_2 and Λ_3 can be treated similarly on the basis of Taylor expansions of the functions $F(t)$ and $G(t)$ around $t = 0$ and application of equations (2.58), (2.59) with $\beta = 1, \dots, \mathcal{L}$, $\alpha = 1, \dots, \mathcal{L}$, and equations (2.61), (2.62) with $\gamma = \mathcal{L} - \lambda, \alpha = \mathcal{L} - \lambda + 1$. The inductive step and therefore the proof of Theorem 2.3.2 are thus complete. \square

2.3.3 Proof of theorem 2.3.3

The relationship between the density ψ and the PDE solution u is given by equation (2.6) if Ω is an exterior domain and by equation (2.16) if Ω is an interior domain. Throughout this section we assume that Ω is an interior domain, and, thus, that ψ is given by equation (2.16); the proof for exterior domains (equation (2.6)) is analogous.

In order to establish the singular character of the density ψ we first seek an asymptotic expression for the conjugate solution u_e near $z = 0$ (see Definition 2.2.1). Using a conformal mapping approach for u_e similar to the one used in Section 2.3.1 for the solution u of the problem (2.1), in this case we employ a conformal map $z = v(\xi)$ which maps the semi-circular region D_A depicted in Figure 2.3 in the complex ξ -plane onto the domain $\overline{B(y^0, r)} \setminus \Omega^0$ in the complex z -plane (see Figure 2.2). We assume, as we may, that v maps the origin to itself and that the intervals $\{\text{Im}(\xi) = 0, 0 \leq \text{Re}(\xi) \leq A\}$ and $\{\text{Im}(\xi) = 0, -A \leq \text{Re}(\xi) \leq 0\}$ are mapped onto the boundary portions $\Gamma_{q_1}^0$ and $\Gamma_{q_2}^0$, respectively (see equation (2.23)). Following Section 2.3.1 in this case we introduce the function $V(\xi) = u_e(v(\xi))$ and we note that V satisfies the second order elliptic problem (cf. [46, eq. 5.4.17])

$$\Delta V + K_1(\xi)V = 0 \quad \text{for } \xi \in \text{int}(D_A), \quad (2.66)$$

$$V(\xi) = u_e(v(\xi)) \quad \text{for } \text{Im}(\xi) = 0, \quad \text{and} \quad (2.67)$$

$$V(\xi) = M_1(\xi) \quad \text{for } |\xi| = A, \quad (2.68)$$

where M_1 is given by $M_1(\xi) = u_e(v(\xi))$.

The following Lemma parallels Lemma 2.3.5.

Lemma 2.3.9. *The solution V of the problem (2.66)–(2.68) satisfies the asymptotic relation*

$$V(\xi) = o(\xi^\mu) \quad (2.69)$$

for all $-\frac{1}{2} < \mu < 0$.

Proof. Employing the Laplace Green function

$$G_1(t, \xi) = -\frac{1}{2\pi} \{ \log |t - \xi| - \log |t - \bar{\xi}| \} \quad (2.70)$$

for the Dirichlet problem (2.66)–(2.68) and applying the Green formula to the functions V and G_1 on the domain D_A we obtain

$$V(\xi) = \int \int_{D_A} G_1(t, \xi) \Delta V(t) dx_t dy_t + \int_{\partial D_A} \left\{ V(t) \frac{\partial}{\partial n_t} G_1(t, \xi) - G_1(t, \xi) \frac{\partial}{\partial n_t} V(t) \right\} ds_t. \quad (2.71)$$

Since $G_1(t, \xi) = 0$ for $\text{Im}(\xi) = 0$ and since $\partial D_A = [-A, A] \cup \Gamma_A$, the triangle inequality yields

$$\begin{aligned} |V(\xi)| &\leq \left| \int \int_{D_A} G_1(t, \xi) K_1(t) V(t) dx_t dy_t \right| + \left| \int_{-A}^A V(t) \frac{\partial}{\partial n_t} G_1(t, \xi) dt \right| \\ &\quad + \left| \int_{\Gamma_A} \left\{ V(t) \frac{\partial}{\partial n_t} G_1(t, \xi) - G_1(t, \xi) \frac{\partial}{\partial n_t} V(t) \right\} ds_t \right|. \end{aligned} \quad (2.72)$$

For the integral over the outer arc Γ_A in (2.72) we have

$$\left| \int_{\Gamma_A} \left\{ V(t) \frac{\partial}{\partial n_t} G_1(t, \xi) - G_1(t, \xi) \frac{\partial}{\partial n_t} V(t) \right\} ds_t \right| \leq C_1 \quad \text{for } |\xi| < A/2 \quad (2.73)$$

where C_1 is a nonnegative constant, as it can be checked easily in view of the boundedness of the integrands for ξ near the origin. From Lemma 2.2.2, further, it easily follows that $V \in H^1(D_A)$, and thus, bounding the absolute value of the first integral in equation (2.72) by means of the Cauchy-Schwarz inequality we obtain the bound

$$\left| \int \int_{D_A} G_1(t, \xi) K_1(t) V(t) dx_t dy_t \right| \leq \|G_1\|_{L^2(D_A)} \|V\|_{L^2(D_A)} \max_{t \in D_A} (K_1(t)) \quad (2.74)$$

for all $\xi \in D_A$. As is well known, finally, double layer potentials for bounded densities are uniformly bounded in all of space (see e.g. [47, Lemma 3.20]). It follows that the second integral in equation (2.72) is uniformly bounded for $\xi \in \mathbb{R}^2$ since, in view of (2.67), Definition 2.2.1, and Theorem 2.3.2, V is a bounded function for $t_2 = \text{Im}(t) = 0$. The relation (2.69) thus follows for all $-\frac{1}{2} < \mu < 0$ and the proof is complete. \square

Corollary 2.3.10. *The derivatives of the solution V of the problem (2.66)–(2.68) satisfy the asymptotic relation*

$$D^h V = o(\xi^{\mu-h}) \quad (2.75)$$

for all $-\frac{1}{2} < \mu < 0$.

Proof. See [125, Section 4] □

We now proceed with the main proof of this section, which is based on an inductive argument similar to the one used in the proof of Theorem 2.3.2.

Proof of Theorem 2.3.3. Applying the Green formula on the set $D_{A,\delta}$ (equation (2.50)) and letting $\delta \rightarrow 0$ we obtain

$$V(\xi) = \int \int_{D_A} (-K_1(t)V(t)) G_1(t, \xi) dt - \int_{-A}^A V(t) \frac{\partial}{\partial n_t} G_1(t, \xi) dt + p_1(\xi) + p_2(\bar{\xi}), \quad (2.76)$$

where p_1 and p_2 denote power series with positive radii of convergence. In view of equation (2.67), Definition 2.2.1 and Theorem 2.3.2, on the other hand, we see that, for any given integer \mathcal{L} , the boundary values of V at $\xi_2 = 0$ satisfy

$$V(\xi_1, 0) = V(\xi) = u_e(\xi) = \mathcal{P}_{y_0}^{\mathcal{L}}(\xi^{1/2}, \bar{\xi}^{1/2}) + o(\xi^{\mathcal{L}}) \quad \text{for } \xi_2 = \text{Im}(\xi) = 0 \quad (2.77)$$

(see (2.27)). Relying on equations (2.76) and (2.77) as well as Lemma 2.3.8, an inductive argument similar to the one used in the proof of Theorem 2.3.2 shows that for any integer \mathcal{N} the function V satisfies an asymptotic relation of the form

$$V(\xi) = \mathcal{P}^{\mathcal{N}}(\xi^{1/2}, \bar{\xi}^{1/2}) + o(\xi^{\mathcal{N}}) \quad \text{as } \xi \rightarrow 0, \quad (2.78)$$

where $\mathcal{P}^{\mathcal{N}}$ is an \mathcal{N} -dependent polynomial. In view of corollaries 2.3.6 and 2.3.10, substitution of the normal derivatives of equations (2.78) and (2.27) for $\text{Im}(\xi) = 0$ into equation (2.16) yields

$$\psi(\xi) = \xi^{-1/2} \mathcal{Q}_1^{\mathcal{N}}(\xi^{1/2}, \bar{\xi}^{1/2}) + \bar{\xi}^{-1/2} \mathcal{Q}_2^{\mathcal{N}}(\xi^{1/2}, \bar{\xi}^{1/2}) + o(\xi^{\mathcal{N}-1}) \quad \text{for } \xi_2 = \text{Im}(\xi) = 0, \quad (2.79)$$

where $Q_i^{\mathcal{N}}$ are \mathcal{N} -dependent polynomials. The desired asymptotic relations (2.28) now follow by re-expressing (2.79) in terms of the distance function d , and the proof is thus complete. \square

2.4 Parametrized Integral Operators

In view of the notations in Section 1, the operators (2.4) applied to a density ψ and evaluated at a given point $x \in \Gamma$ can be expressed in the form

$$\begin{aligned} \mathcal{A}_k^{(1)}[\psi](x) &= \sum_{q=1}^{Q_D+Q_N} \int_{\Gamma_q} G_k(x, y) \psi(y) ds_y \quad \text{for } x \in \Gamma_D, \\ \mathcal{A}_k^{(2)}[\psi](x) &= -\frac{\psi(x)}{2} + \sum_{q=1}^{Q_D+Q_N} \int_{\Gamma_q} \frac{\partial}{\partial n_x} G_k(x, y) \psi(y) ds_y \quad \text{for } x \in \Gamma_N. \end{aligned} \tag{2.80}$$

We seek expressions of these operators in terms of parametrizations of the underlying integration curves. Without loss of generality, we assume the boundary curve Γ is parametrized by a single smooth vector function $y = z(\tau) = (z_1(\tau), z_2(\tau))$ ($a \leq \tau < b$) satisfying $(z_1')^2 + (z_2')^2 > \delta$ for some scalar $\delta > 0$ at each point where z is differentiable; the parametrization we use for integration on each one of the (smooth) Dirichlet and Neumann segments Γ_q is then taken to equal the relevant restriction of the function z to a certain interval $[a_q, b_q]$, $a_q \leq b_q$. Clearly, $[a, b] = \cup_{q=1}^{Q_D+Q_N} [a_q, b_q]$ where the intersection of any subintervals in this union is either the empty set or a set containing a single point.

To evaluate each one of the integrals in (2.80) for a point $x \in \Gamma$ we rely on the decomposition

$$H_\nu^{(1)}(\zeta) = F_\nu^{(0)}(\zeta) \log(\zeta) + F_\nu^{(1)}(\zeta)$$

for the Hankel function H_ν^1 ($\nu \in \mathbb{R}$), where $F_\nu^{(0)}$ and $F_\nu^{(1)}$ are analytic functions (cf. [32, p. 68]). For each $q_2 \in J_D \cup J_N$ two integrals over Γ_{q_2} appear in equation (2.80). Using the substitutions $x = z(t)$ and $y = z(\tau)$ and assuming $x = z(t) \in \Gamma_{q_1}$ for a certain $q_1 \in J_D \cup J_N$ ($t \in [a_{q_1}, b_{q_1}]$), we express each one of the aforementioned integrals over Γ_{q_2} in terms of the

operator

$$\tilde{\mathcal{I}}_{q_1, q_2}[\tilde{\varphi}](t) = \int_{a_{q_2}}^{b_{q_2}} \left\{ \tilde{K}^1(t, \tau) \log R^2(t, \tau) + \tilde{K}^2(t, \tau) \right\} \tilde{\varphi}(\tau) d\tau, \quad (2.81)$$

where

$$R(t, \tau) := |x - y| = |z(t) - z(\tau)| \quad , \quad \tilde{\varphi}(\tau) = \psi(z(\tau)). \quad (2.82)$$

Here the kernels $\tilde{K}^1(t, \tau)$ and $\tilde{K}^2(t, \tau)$ denote functions that depend on the integral under consideration. For the integrals included in the operator $\mathcal{A}_k^{(1)}[\psi]$ these kernels are given by the products of the arc-length $\sqrt{|z'(t)|^2}$ and the factors $F_\nu^{(0)}$ and $F_\nu^{(1)}$ for $\zeta = kR(t, \tau)$ and $\nu = 0$. For the integrals included in the operator $\mathcal{A}_k^{(2)}[\psi]$, on the other hand, an additional smooth factor is included, and the value $\nu = 1$ is used; see [32, p. 68] for details. In particular, for each $t \in [a, b]$, $\tilde{K}^1(t, \tau)$ and $\tilde{K}^2(t, \tau)$ are smooth (resp. analytic) functions of τ for all $\tau \in [a_{q_2}, b_{q_2}]$ provided $y(\tau)$ is itself smooth (resp. analytic). (The notations \tilde{K}^1 , \tilde{K}^2 , and $\tilde{\varphi}$ are used in connection with the basic parametrization z ; corresponding kernels K^1 , K^2 , and density φ , which include additional “smoothing” reparametrizations, are utilized in Sections 2.5 and 3.3 below.)

Remark 2.4.1. *Clearly the kernel in the integral operator (2.81) (the quantity in curly brackets in this equation) is singular, smooth, or nearly singular depending, respectively, on whether 1) $q_1 = q_2 = q$ (that is, $t, \tau \in [a_q, b_q]$); 2) $q_1 \neq q_2$ and t is “far” from $[a_{q_2}, b_{q_2}]$, or 3) $q_1 \neq q_2$ and t is “close” to $[a_{q_2}, b_{q_2}]$. The significance of the terms “far” and “close” and corresponding selections of algorithmic thresholds is taken up in Remark 2.4.2.*

Remark 2.4.2. *In the case $q_1 \neq q_2$ point t is considered to be “far” from the interval $[a_{q_2}, b_{q_2}]$ (case 2 in Remark 2.4.1) provided*

$$\min(|z_{q_1}(t) - z_{q_2}(a_{q_2})|, |z_{q_1}(t) - z_{q_2}(b_{q_2})|) > h_1, \quad (2.83)$$

that is, provided the minimum Euclidean distance between $z_{q_1}(t)$ and the interval endpoints larger than h_1 , where h_1 is a given (user-provided) parameter which is to be selected so as to maximize overall accuracy. Otherwise the point t is considered to be “close” to the interval $[a_{q_2}, b_{q_2}]$ (case 3 in Remark 2.4.1).

Remark 2.4.3. *In view of (2.3.3) the asymptotic behavior of $\tilde{\varphi}$ near $\tau = a_{q_2}$ and near $\tau = b_{q_2}$ is given, respectively, by the relations*

$$\begin{aligned}\tilde{\varphi}(\tau) &= (\tau - a_{q_2})^{-1/2} P_3((\tau - a_{q_2})^{1/2}) + \mathcal{O}((\tau - a_{q_2})^{\mathcal{N}-1-\varepsilon}), \\ \tilde{\varphi}(\tau) &= (\tau - b_{q_2})^{-1/2} P_4((\tau - b_{q_2})^{1/2}) + \mathcal{O}((\tau - b_{q_2})^{\mathcal{N}-1-\varepsilon}),\end{aligned}\tag{2.84}$$

where, once again, for any given integer \mathcal{N} , P_3 and P_4 are polynomials that depend on q_2 and \mathcal{N} .

We now turn to the design of high-order accurate quadrature rules for integrals of the type (2.81) which, by necessity, must take into account the singular character of the integrand—including the explicit logarithmic singularities and near singularities mentioned above as well as the singularities that the (unknown) density function $\tilde{\varphi}$ possesses at Dirichlet-Neumann junctions and corner points (Remarks 2.4.1 and 2.4.3).

2.5 Singularity resolution via Fourier Continuation

Theorem 2.3.2 tells us that the solutions of Zaremba problem (2.1) possess a very specific singularity structure near the Dirichlet-Neumann junctions—which, as shown in Theorem 2.3.3, are inherited by the solutions of the corresponding integral equation system (2.4). In particular, equation (2.28) shows that the integral equation solutions can be expressed as a product of the function $1/\sqrt{d}$ and a smooth function of \sqrt{d} , where d denotes the distance to the Dirichlet-Neumann junction.

The question thus arises as to how to incorporate the singular characteristics of the integral equation solutions in order to design a numerical integration method of high order of accuracy for the numerical discretization of the integral equation system (2.4). A relevant reference in these regards is provided by the contribution [19] (see also [129]), which provides a high-order solver for the problem of scattering by open arcs. As is known, the open-arc integral equation solutions possess singularities around the end-points: they can be expressed as a product of the function $1/\sqrt{d}$ and a smooth function of d —or, in other words, the asymptotics of the integral solutions are functions which *only contain powers of \sqrt{d} with*

exponents equal to $(2n - 1)$ for $n \geq 0$. As shown in [19] a change of variables of the form $t = \cos s$, $0 \leq s \leq \pi$ in parameter space completely regularizes the problem, and it thus gives rise to spectrally accurate numerical approximations of the form

$$\psi \sim \sum_{j=0}^n C_j \cos(js) \quad 0 \leq s \leq \pi \quad (2.85)$$

for the integral-equation solutions ψ .

As shown in Theorem (2.3.3), on the other hand, the asymptotic expansions of the integral-equation solutions ψ considered in this thesis contain *all integer powers of \sqrt{d}* , and therefore, as established in [2], a cosine change of variables such as the one considered above leads to a full Fourier series—containing all 2π -periodic cosines and sines,

$$\psi \sim \sum_{j=0}^n C_j \cos(js) + D_j \sin(js) \quad 0 \leq s \leq \pi, \quad (2.86)$$

even though values for ψ can only be determined for $0 \leq s \leq \pi$. The key element that allows such expansions in the extended interval $[0, 2\pi]$ is the Fourier Continuation (FC) method introduced in [3, 21] and first suitably generalized to the present context in [2]. This leads to a Fourier series that converges with high-order accuracy m to the integral density ψ in the interval $[0, \pi]$; as in reference [2], the numerical examples in the present thesis are based on use of the value $m = 5$.

As mentioned above, all singularities must be taken into account in order to obtain an overall high-order accurate solver. In what follows we describe an approach that simultaneously eliminates the density singularities and accounts for both the logarithmically singular kernel $\widetilde{K}^1 \cdot \log R^2$ and smooth kernel \widetilde{K}^2 in (2.81) and thereby results in a high-order accurate method for evaluation of this integral operator. To do this we proceed by introducing a cosine transformation for the integral in a segment Γ_{q_2} —after a necessary scaling to the interval $[-1, 1]$.

In detail we first map each parameter interval $[a_{q_2}, b_{q_2}]$ to the interval $[-1, 1]$ by means

of the linear transformations

$$\tau = \xi_{q_2}(\rho) := \frac{(b_{q_2} - a_{q_2})\rho + (a_{q_2} + b_{q_2})}{2}. \quad (2.87)$$

Clearly, values of t within $[a_{q_1}, b_{q_1}]$ are given by $t = \xi_{q_1}(r)$ for some $r \in [-1, 1]$. Denote

$$\tilde{K}_{q_1, q_2}(r, \rho) = \tilde{K}^1(\xi_{q_1}(r), \xi_{q_2}(\rho)) \log R^2(\xi_{q_1}(r), \xi_{q_2}(\rho)) + \tilde{K}^2(\xi_{q_1}(r), \xi_{q_2}(\rho)).$$

After application of this transformation, the integral (2.81) becomes

$$\tilde{\mathcal{I}}_{q_1, q_2}[\tilde{\varphi}](r) = \frac{b_{q_2} - a_{q_2}}{2} \int_{-1}^1 \tilde{K}_{q_1, q_2}(r, \rho) \tilde{\varphi}(\xi_{q_2}(\rho)) d\rho. \quad (2.88)$$

Introducing the sinusoidal change of variables

$$r = \cos(s) \quad \text{and} \quad \rho = \cos(\sigma), \quad (2.89)$$

and letting

$$\varphi_{q_2}(\sigma) = \tilde{\varphi}(\xi_{q_2}(\cos(\sigma))) \quad (2.90)$$

and

$$K_{q_1, q_2}(s, \sigma) = \tilde{K}_{q_1, q_2}(\cos(s), \cos(\sigma)), \quad (2.91)$$

equation (2.88) becomes

$$\mathcal{I}_{q_1, q_2}[\varphi_{q_2}](s) = \frac{b_{q_2} - a_{q_2}}{2} \int_0^\pi K_{q_1, q_2}(s, \sigma) \varphi_{q_2}(\sigma) \sin(\sigma) d\sigma. \quad (2.92)$$

Lemma 2.5.1. *The product $\varphi_{q_2}(\sigma) \sin(\sigma)$ is a smooth function of σ for $\sigma \in [0, \pi]$.*

Proof. Clearly, for any integer $\ell \geq -1$ for τ near a_{q_2} (which corresponds to ρ near -1 and σ near π), up to multiplicative constants we have

$$(\tau - a_{q_2})^{\ell/2} \sin(\sigma) \sim (\rho + 1)^{\ell/2} \sin(\sigma) \sim \sin(\sigma)^{\ell+1}.$$

Similarly for τ near b_{q_2} (which corresponds to ρ near 1, to σ near zero), once again up to multiplicative constants there holds

$$(\tau - b_{q_2})^{\ell/2} \sin(\sigma) \sim (\rho - 1)^{\ell/2} \sin(\sigma) \sim \sin(\sigma)^{\ell+1}.$$

It then follows from Theorem 2.3.3 that $\varphi_{q_2}(\sigma) \sin(\sigma)$ is a smooth function of σ and the proof is complete. \square

2.5.1 FC-based algorithm: Fourier Continuation

We seek to produce high order quadrature rules for evaluation of the integral operator $\mathcal{I}_{q_1, q_2}[\varphi](r)$ in equation (2.92) by exploiting existing explicit formulae for evaluation of integrals of the form

$$\int_0^\pi \log |r - \cos(\sigma)| \cos(n\sigma) d\sigma \quad \text{and} \quad \int_0^\pi \log |r - \cos(\sigma)| \sin(n\sigma) d\sigma \quad (2.93)$$

for all real values of r

Remark 2.5.2. *Explicit expressions for the integrals (2.93) in the case of cosine integrands and $|r| \leq 1$ can be found in [17, 96, 129]. Corresponding expressions for the sine integrands and for the case $|r| > 1$, which are derived in Appendix C, in turn, are reproduced in equations (2.107)-(2.108) below. Note that values $|r| \leq 1$ give rise to weakly singular logarithmic integration, while values $|r| > 1$ result in smooth integrands which, however, are nearly singular for values of r close to 1 and -1 .*

In order to take advantage of the expressions (2.93) we need to express the integrand in equation (2.92) in terms of the functions $\cos(n\sigma)$ and $\sin(n\sigma)$; we do this by relying on a certain Fourier Continuation method [3, 21, 91], which we discuss in what follows.

To demonstrate the Fourier Continuation procedure as it applies in the present context we consider the function $\tilde{f}(\rho) = \arccos(\rho)$ whose asymptotic expansions around $\rho = 1$ and $\rho = -1$, just like those for the function $\tilde{\varphi}(\xi_{q_2}(\rho))$, contain the singular powers $(\rho - 1)^{n/2}$ and $(\rho + 1)^{n/2}$, respectively, for all positive odd values of the integer n . (Note in passing that

the function $\tilde{\varphi}(\xi_{q_2}(\rho))$ contains, additionally, the smooth terms $(\rho - 1)^{n/2}$ and $(\rho + 1)^{n/2}$ that result for *even* values of n ; this, however, is of no significance in the present example.) The left portion of Figure 2.4 displays the function \tilde{f} on the interval $[-1, 1]$. Under the cosine change of variables used earlier in this section in the definition of the function $\tilde{\varphi}(\xi_{q_2}(\rho))$, this function becomes $f(\sigma) = \tilde{f}(\cos(\sigma)) = \sigma$ on the interval $[0, \pi]$. The expansion sought above for the function \tilde{f} , would, in this simplified example, require representation of the function $f(\sigma) = \sigma$ in a rapidly convergent series in $\cos(n\sigma)$ and $\sin(n\sigma)$. This objective could be achieved by means of an adequate globally smooth and 2π -periodic continuation of the function f . Although theoretically this does not present difficulties, a fast and stable numerical algorithm for evaluation of such a Fourier series has been provided only recently—this is the Fourier Continuation (FC) method mentioned above [3, 21, 91]. A brief overview in these regards is presented in appendix A. The result of an application of the FC approach to the function $f(\sigma)$ discussed above is given in Figure 2.4: the desired globally smooth periodic function, which is given as a rapidly convergent Fourier expansion in terms of the functions $\cos(n\sigma)$ and $\sin(n\sigma)$, is depicted on the right portion of this figure.

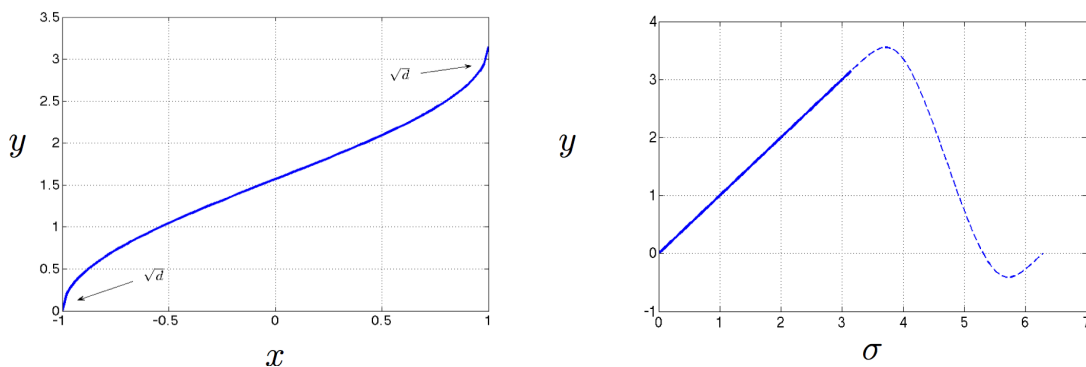


Figure 2.4: A cosine change of variables on the (singular) curve displayed in the left image produces the $y = x$ curve between 0 and π in the right image. An application of the Fourier Continuation method then gives rise to the dashed-line continuation to a fully 2π -periodic globally-smooth function shown on the right image.

2.5.1.1 FC-based algorithm: Canonical kernel decomposition

This section provides canonical decompositions for the integral kernels in equation (2.92) in terms of smooth factors and factors that explicitly display logarithmic singularities and

near-singularities. We consider three cases that parallel those in Remark 2.4.1; in each case the decomposition depends on the singular character of the kernel $K_{q_1, q_2}(s, \sigma)$:

1) **Case $q_1 \neq q_2$ and t is “far” from $[a_{q_2}, b_{q_2}]$**

The kernel $K_{q_1, q_2}(s, \sigma)$ is a smooth function of σ in this case (Remark 2.4.1).

2) **Case $q_1 = q_2 = q$**

Introducing the kernels

$$\begin{aligned} K_{q,q}^1(s, \sigma) &= 2\widetilde{K}^1(\xi_q(\cos(s)), \xi_q(\cos(\sigma))), \\ K_{q,q}^2(s, \sigma) &= \widetilde{K}^2(\xi_q(\cos(s)), \xi_q(\cos(\sigma))) + \frac{K_{q,q}^1(s, \sigma)}{2} \log \left(\frac{R^2(\xi_q(\cos(s)), \xi_q(\cos(\sigma)))}{|\cos(s) - \cos(\sigma)|^2} \right), \end{aligned} \quad (2.94)$$

(where, for $s = \sigma$, an appropriate limit as $\sigma \rightarrow s$ is taken for the fraction in the argument of the logarithm in equations (2.94) and where the quantity $K_{q,q}^1$ used in the second equation is defined in the first equation), the required decomposition is

$$K_{q,q}(s, \sigma) = K_{q,q}^1(s, \sigma) \log |\cos(s) - \cos(\sigma)| + K_{q,q}^2(s, \sigma). \quad (2.95)$$

3) **Case $q_1 \neq q_2$ and t is “close” to $[a_{q_2}, b_{q_2}]$**

As mentioned in Remark 2.4.1, in this case the kernel is nearly singular. A specialized procedure is described in what follows which, using equation (2.87) beyond its domain of definition—for values of ρ and τ for which $|\tau| > 1$ —gives rise to a useful decomposition in the present case. In detail, taking advantage of the smoothness of the curve Γ (which is assumed throughout this section) we use the changes of variables (2.87) and (2.89) that relate τ to σ to also express t as a function of s . We thus define a function $r^{\text{out}}(s)$ by means of the relation

$$t = \xi_{q_2}(r^{\text{out}}(s)) = \xi_{q_1}(\cos(s)); \quad (2.96)$$

it is easy to check that, for a given $s \in [0, \pi]$, $r = r^{\text{out}}(s)$ lies in the interval

$$\left[\frac{2a_{q_1} - a_{q_2} - b_{q_2}}{b_{q_2} - a_{q_2}}, \frac{2b_{q_1} - a_{q_2} - b_{q_2}}{b_{q_2} - a_{q_2}} \right], \quad (2.97)$$

and, in particular, $r^{\text{out}}(s)$ is *outside* the interval $[-1, 1]$. Owing to the continuity of the boundary parametrization $z(t)$, further, $r^{\text{out}}(s)$ is close to either 1 or -1 for values of s near 0 or π .

On the basis of the sinusoidal change of variables $\rho = \cos(\sigma)$ (cf. (2.89)) and the reparametrization $r = r^{\text{out}}(s)$ we can now produce the desired decomposition for the kernel (2.91): letting

$$\begin{aligned} K_{q_1, q_2}^1(s, \sigma) &= 2\widetilde{K}^1(\xi_{q_1}(r^{\text{out}}(s)), \xi_{q_2}(\cos(\sigma))), \\ K_{q_1, q_2}^2(s, \sigma) &= \widetilde{K}^2(\xi_{q_1}(r^{\text{out}}(s)), \xi_{q_2}(\cos(\sigma))) + \\ &\quad \frac{K_{q_1, q_2}^1(s, \sigma)}{2} \log \left(\frac{R^2(\xi_{q_1}(r^{\text{out}}(s)), \xi_{q_2}(\cos(\sigma)))}{|r^{\text{out}}(s) - \cos(\sigma)|^2} \right), \end{aligned} \quad (2.98)$$

(where the quantity K_{q_1, q_2}^1 used in the second equation is defined in the first equation) we obtain

$$K_{q_1, q_2}(s, \sigma) = K_{q_1, q_2}^1(s, \sigma) \log |r^{\text{out}}(s) - \cos(\sigma)| + K_{q_1, q_2}^2(s, \sigma). \quad (2.99)$$

2.5.1.2 FC-based algorithm: Numerical integration

This section describes numerical methods for evaluation of the integrals \mathcal{I}_{q_1, q_2} (equation (2.92)) for the three cases considered in Section 2.5.1.1. In each case 2π -periodic Fourier continuation approximations of the form

$$\phi_{q_1, q_2}^j(s, \sigma) \sim \sum_{\ell=0}^n \alpha_\ell^j \cos(\ell\sigma) + \beta_\ell^j \sin(\ell\sigma) \quad j = 1, 2 \quad (2.100)$$

(that is, partial Fourier continuation expansions in the variable σ with coefficients $\alpha_\ell^j = \alpha_\ell^j(s)$ and $\beta_\ell^j = \beta_\ell^j(s)$) are used, where $\phi_{q_1, q_2}^j = \phi_{q_1, q_2}^j(s, \sigma)$ are certain smooth functions of s and

σ for $0 \leq s, \sigma \leq \pi$. With reference to equation (2.92), Lemma 2.5.1 and equations (2.95) and (2.99) (and as detailed in what follows), in all three cases ϕ_{q_1, q_2}^j denotes the product of $\varphi_{q_2}(\sigma) \sin(\sigma)$ and the relevant smooth function that multiplies a singular log (which we may call the “log prefactor”) for $j = 1$, and the product of $\varphi_{q_2}(\sigma) \sin(\sigma)$ and the smooth remainder term for $j = 2$. Note that in case 1 of section 2.5.1.1 the log prefactor vanishes.

The numerical quadrature methods for each of the three cases considered in Section 2.5.1.1 are given in what follows.

1) **Case $q_1 \neq q_2$ and t is “far” from $[a_{q_2}, b_{q_2}]$**

From point 1) in Section 2.5.1.1, in this case we set

$$\phi_{q_1, q_2}^1(s, \sigma) = 0 \quad , \quad \phi_{q_1, q_2}^2(s, \sigma) = K_{q_1, q_2}(s, \sigma) \varphi_{q_2}(\sigma) \sin(\sigma). \quad (2.101)$$

The desired quadrature rule for (2.92) results from use of (2.100) and explicit evaluation of the integrals of sines and cosines in the resulting approximate expression

$$\mathcal{I}_{q_1, q_2}[\varphi_{q_2}](s) \sim \frac{b_{q_2} - a_{q_2}}{2} \sum_{\ell=0}^n \int_0^\pi [\alpha_\ell^2(s) \cos(\ell\sigma) + \beta_\ell^2(s) \sin(\ell\sigma)] d\sigma. \quad (2.102)$$

2) **Case $q_1 = q_2 = q$**

Using the kernel decomposition (2.95) we set

$$\phi_{q, q}^1(s, \sigma) = K_{q, q}^1(s, \sigma) \varphi_q(\sigma) \sin(\sigma) \quad \text{and} \quad \phi_{q, q}^2(s, \sigma) = K_{q, q}^2(s, \sigma) \varphi_q(\sigma) \sin(\sigma), \quad (2.103)$$

so that in view of (2.100) we have

$$\begin{aligned} \mathcal{I}^{(q, q)}[\varphi_q](s) &\sim \frac{b_q - a_q}{2} \sum_{\ell=0}^n \int_0^\pi \log |\cos(s) - \cos(\sigma)| [\alpha_\ell^1(s) \cos(\ell\sigma) + \beta_\ell^1(s) \sin(\ell\sigma)] d\sigma \\ &\quad + \frac{b_q - a_q}{2} \sum_{\ell=0}^n \int_0^\pi [\alpha_\ell^2(s) \cos(\ell\sigma) + \beta_\ell^2(s) \sin(\ell\sigma)] d\sigma. \end{aligned} \quad (2.104)$$

Our quadrature rule for (2.92) in the present case thus results from explicit evaluation

of integrals of sines and cosines as well as integrals of the form (2.93) with $r = \cos s$ (equations (2.107) and (2.108) below).

3) **Case $q_1 \neq q_2$ and t is “close” to $[a_{q_2}, b_{q_2}]$**

Using the decomposition (2.99) and setting

$$\phi_{q_1, q_2}^1(s, \sigma) = K_{q_1, q_2}^1(s, \sigma) \varphi_{q_2}(\sigma) \sin(\sigma) \quad \text{and} \quad \phi_{q_1, q_2}^2(s, \sigma) = K_{q_1, q_2}^2(s, \sigma) \varphi_{q_2}(\sigma) \sin(\sigma), \quad (2.105)$$

from (2.100) we have

$$\begin{aligned} \mathcal{I}_{q_1, q_2}[\varphi_{q_2}](s) &\sim \frac{b_{q_2} - a_{q_2}}{2} \sum_{\ell=0}^n \int_0^\pi \log |r^{\text{out}}(s) - \cos(\sigma)| [\alpha_\ell^1(s) \cos(\ell\sigma) + \beta_\ell^1(s) \sin(\ell\sigma)] d\sigma \\ &\quad + \frac{b_{q_2} - a_{q_2}}{2} \sum_{\ell=0}^n \int_0^\pi [\alpha_\ell^2(s) \cos(\ell\sigma) + \beta_\ell^2(s) \sin(\ell\sigma)] d\sigma. \end{aligned} \quad (2.106)$$

A quadrature rule for (2.92) now results from explicit evaluation of integrals of sines and cosines as well as integrals of the form (2.93) with $r = r^{\text{out}}(s)$ (equations (2.107) and (2.108) below).

The integrals (2.93) can be produced in closed form for all real values of r (cf. Remark 2.5.2).

The well known expressions for the log-cosine integrals (Symms operator) [96]

$$\begin{aligned} \int_0^\pi \log |r - \cos(\sigma)| \cos(n\sigma) d\sigma &= \frac{1}{2n} \cos(n \arccos(r)) \quad \text{for } n \neq 0, \\ \int_0^\pi \log |r - \cos(\sigma)| d\sigma &= \frac{\log(2)}{2} \quad \text{for } n = 0 \end{aligned} \quad (2.107)$$

are valid provided $|r| \leq 1$. The recently derived expression (see Appendix C)

$$\begin{aligned} \int_0^\pi \log(r - \cos(\sigma)) e^{in\sigma} d\sigma &= (-i) \left[-\frac{1 - \omega_1^n}{n} \log|1 - \omega_1| + \frac{(-1)^n - \omega_1^n}{n} \log|1 + \omega_1| \right. \\ &\quad \left. + \frac{1}{n} \sum_{j=0}^{n-1} (\omega_1^j + \omega_2^j) \frac{(1 - (-1)^{n-j})}{n-j} - \frac{1 - \omega_2^n}{n} \log|1 - \omega_2| \right. \\ &\quad \left. + \frac{(-1)^n - \omega_2^n}{n} \log|1 + \omega_2| - i\pi \frac{\omega_2^n}{n} - \frac{1}{n^2} [1 - (-1)^n] + \log(2) \frac{1 - (-1)^n}{n} \right], \end{aligned} \quad (2.108)$$

where ω_1 and ω_2 are the roots of the polynomial

$$2\omega r - \omega^2 - 1 = -(\omega - \omega_1)(\omega - \omega_2), \quad (2.109)$$

holds for all real values of r ; the real and imaginary parts of this expression provide the necessary log-cosine and log-sine integrals.

In view of the high-order convergence of the FC method (cf. Section 4.5 and Appendix A), a high-order accurate algorithm for evaluation of $\mathcal{I}_{q_1, q_2}[\varphi]$ (and thus $\tilde{\mathcal{I}}_{q_1, q_2}[\tilde{\varphi}]$) on the sole basis of a uniform σ mesh results through application of equations (2.107) and (2.108) in conjunction with equations (2.102), (2.104), and (2.106).

Remark 2.5.3. *In the following chapter we propose an algorithm that is applicable in the case Γ is a non-smooth but piecewise smooth curve Γ . While the methods of that chapter can also be used for smooth curves Γ , the FC-based methods introduced in the present section are generally significantly more efficient for a given prescribed error and more accurate for a given discretization size. The improvements that result from use of the FC-based approach are demonstrated in Section 2.6 and a comparison with more general Lipschitz-boundary algorithm is carried out in Section 4.5.5 in the context of Zaremba eigenvalue problems.*

2.6 Applications and numerical results

The present section presents results of applications of the new solvers to problems of scattering of Zaremba type by smooth obstacles. This entails solution of the problem (2.1) for

exterior domains Ω and for which the right hand sides f and g are given by

$$\begin{aligned} f &= e^{ik\alpha \cdot x} = e^{ik(\cos(\alpha)x_1 + \sin(\alpha)x_2)} \\ g &= n_x \cdot e^{ik\alpha \cdot x} \end{aligned} \tag{2.110}$$

(where α is the angle of incidence). Note, however, that as mentioned in Theorem 2.2.3 the integral equation system (2.4) is not uniquely solvable for a discrete set of values that correspond to Dirichlet eigenvalues of the complement $\mathbb{R}^2 \setminus \Omega$; the numerical approach we use to eliminate this difficulty is discussed in Appendix B.

In our first experiment we apply our scattering solver to the kite-shaped scatterer that is presented in Figure 2.6, whose smooth boundary is given by the parametrization

$$x_1 = \cos(t) + 0.65 \cos(2t) - 0.65 \quad \text{and} \quad x_2 = 1.5 \sin(t), \tag{2.111}$$

and we assume Neumann and Dirichlet boundary conditions in the interval $t \in [\pi/2; 3\pi/2]$ and its complement, respectively. In this figure and throughout this thesis Dirichlet and Neumann boundary segments Γ_D and Γ_N are color-coded in red and blue, respectively. Figure 2.8 demonstrates the high-order convergence results for the value of the scattered field $u(x_0)$ at the particular point $x_0 = (1, 2)$, which lies in the exterior of the domain. Figures 2.6 and 2.7 depict the scattering pattern for the incident wave coming at an angle $\alpha = \pi/8$ with wavenumber $k = 40$. Figure 2.5 displays the unknown current ψ (see equation (2.3)) obtained in the course of the present experiment. Note the indication of the $d^{-1/2}$ behavior of the integral density near the Dirichlet-Neumann junction. The character of the Dirichlet-Neumann singularity demonstrated in this image is consistent with the results of Theorem 2.3.3, but it suggests that densities on the Neumann segments may in fact be smoother than implied by that theorem.

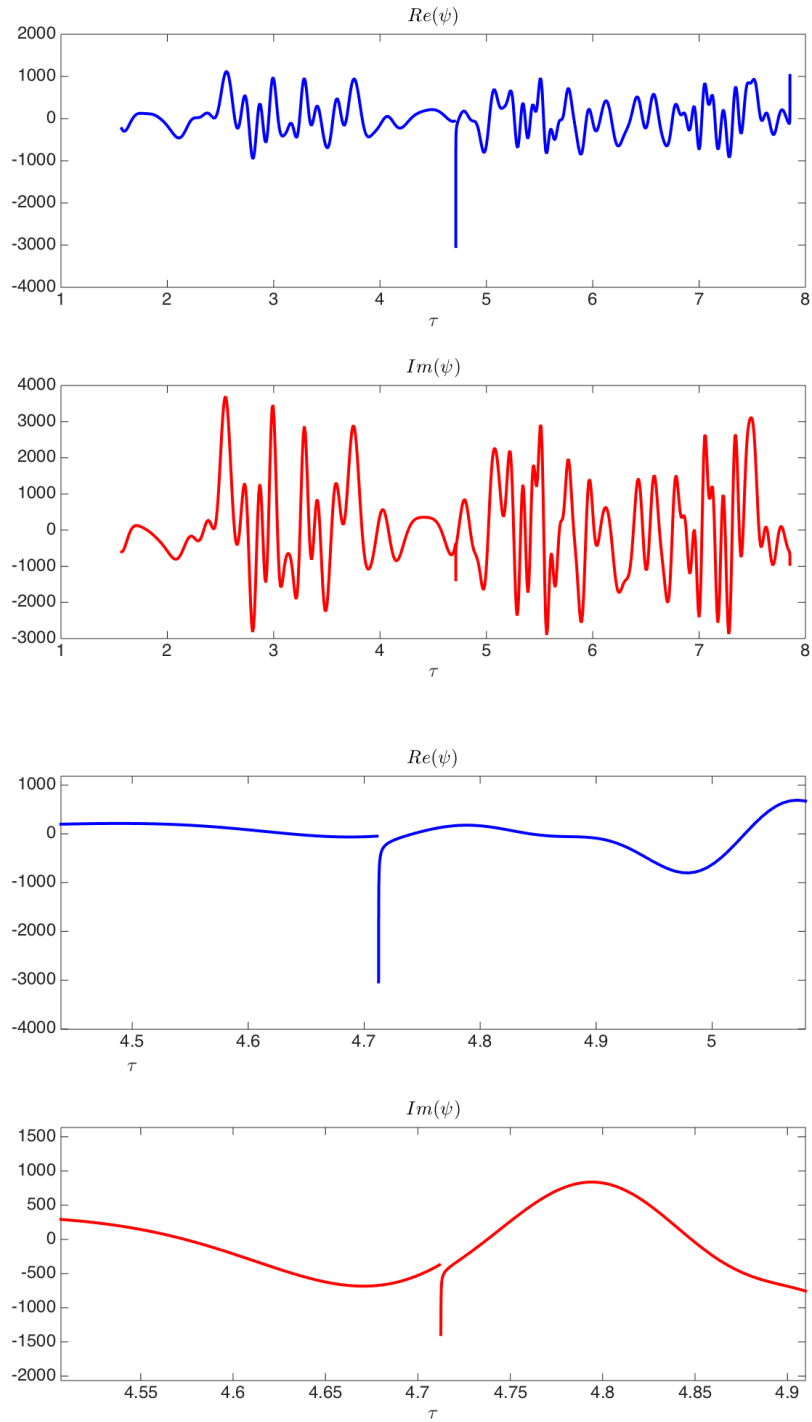


Figure 2.5: Integral density along the entire boundary (top) and zoomed near the Dirichlet-Neumann junction (bottom). The character of the singularity at the Dirichlet-Neumann junction is consistent with the results of Theorem 2.3.3, but it suggests that densities on the Neumann segments may in fact be smoother than implied by that theorem.

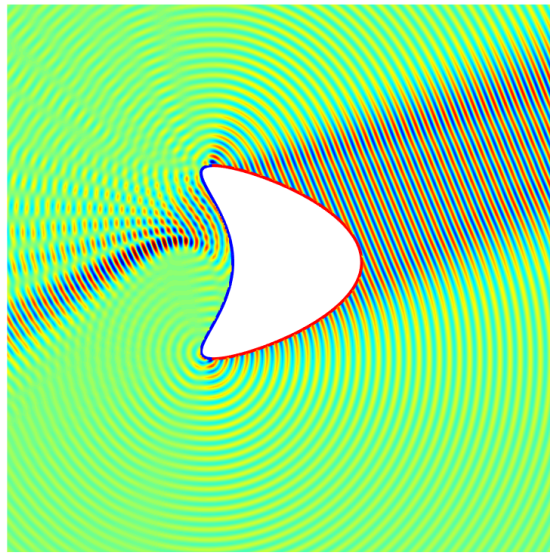
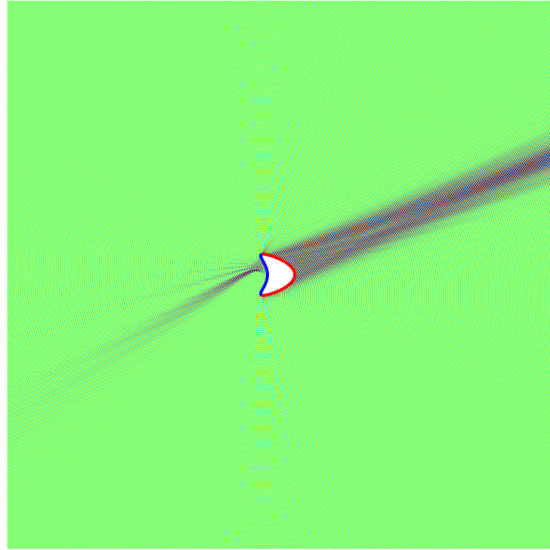


Figure 2.6: Scattering from a kite-shaped domain under Zaremba boundary conditions. Scattered field. In this figure and throughout this thesis Dirichlet and Neumann boundary segments Γ_D and Γ_N are color-coded in red and blue, respectively.

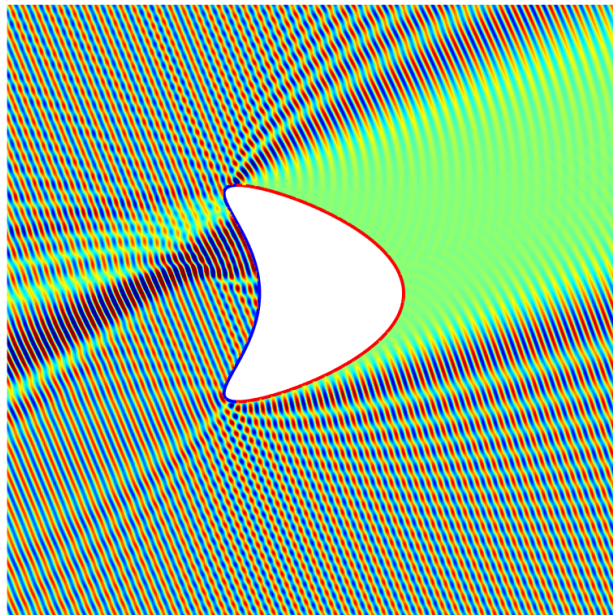
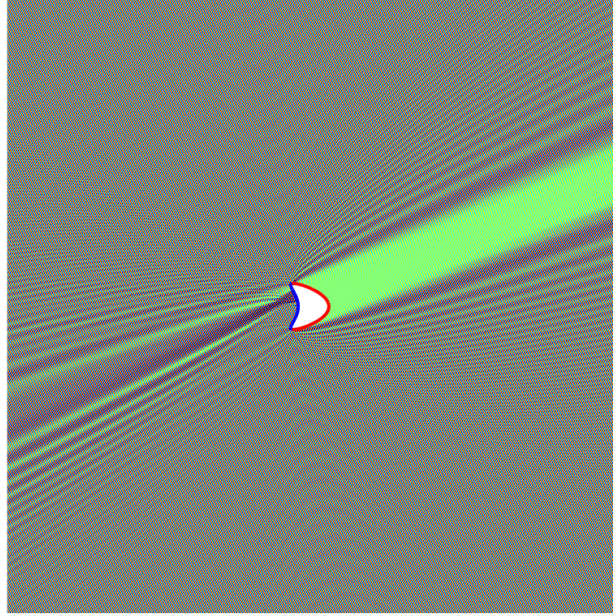


Figure 2.7: Scattering from a kite-shaped domain under Zaremba boundary conditions. Total field.

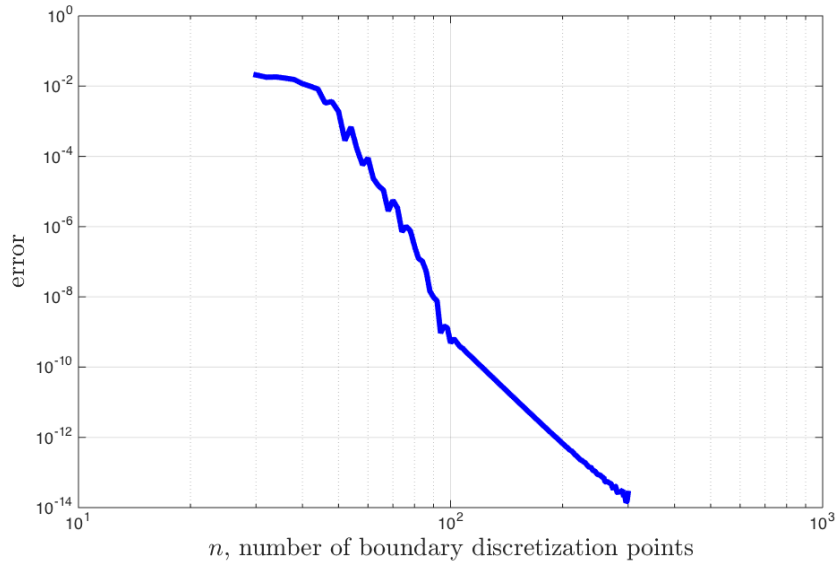


Figure 2.8: Convergence of the value $u(x_0)$ for a kite shaped domain with $k = 10$.

The following experiment concerns the unit disc (where Dirichlet and Neumann boundary conditions are prescribed on the left and right halves of the disc boundary). Figures 2.9 and 2.10 demonstrate the diffraction pattern for a total field solved in the domain exterior to the disc (incident wave angle $\alpha = \pi/8$ and wavenumber $k = 50$). Note the expected asymmetry in the scattered field, as well as the wave patterns near both transition points.

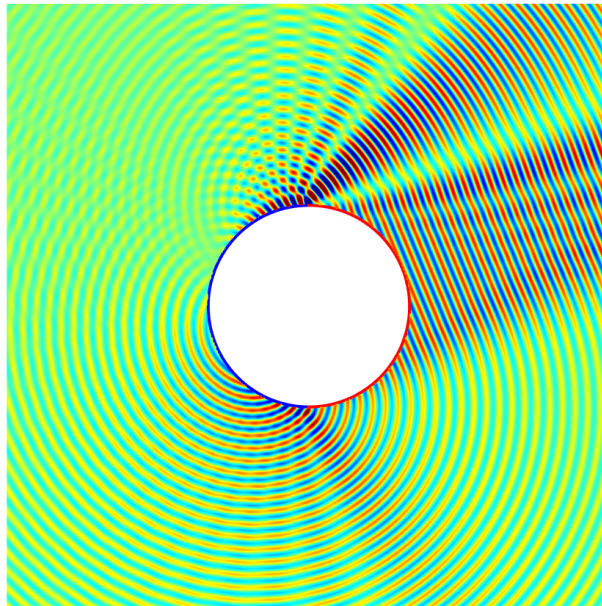
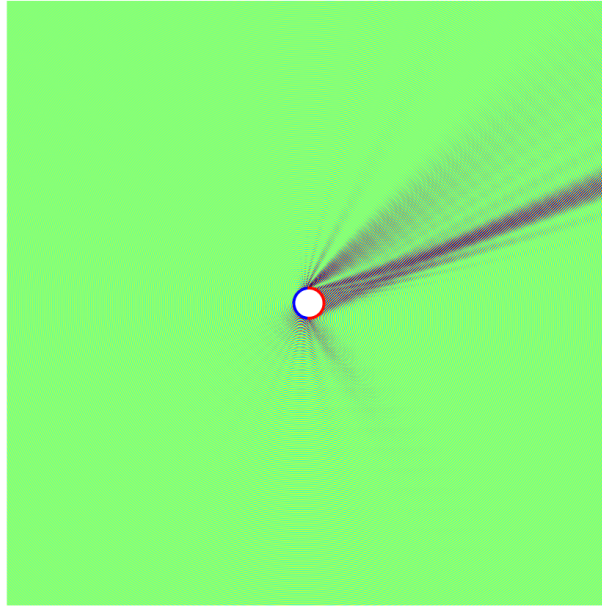


Figure 2.9: Scattering from a disc under Zaremba boundary conditions. Scattered field.

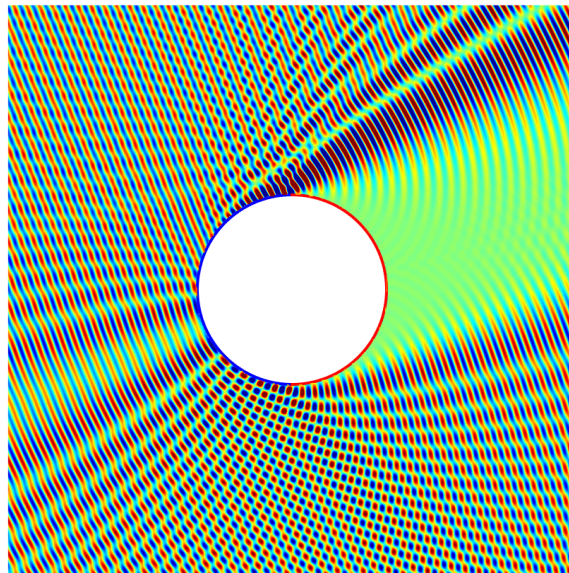
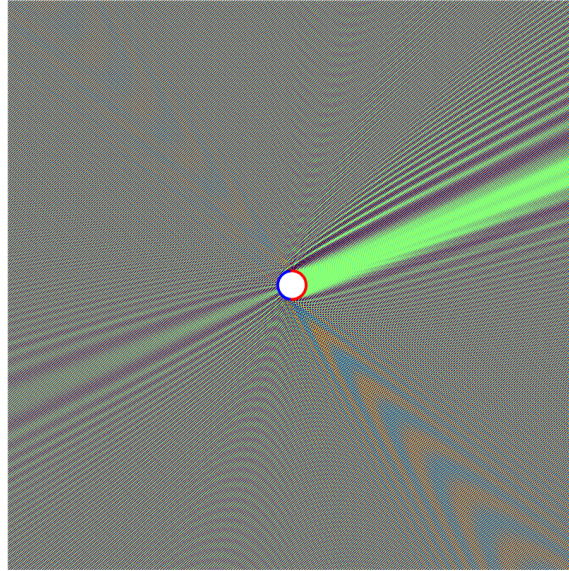


Figure 2.10: Scattering from a disc under Zaremba boundary conditions. Total field.

To conclude this section we present a brief comparison of the proposed solvers with one of the most efficient Zaremba solvers previously available [64]. The method introduced in reference [64] is based on iterative inverse preconditioning that solves Zaremba problems for

the Laplace and elasticity equation. This method, which applies to a variety of singular problems, is described in detail with examples in [65], and it has been implemented in a numerical MATLAB package which is freely available (<http://www.maths.lth.se/na/staff/helsing/Tutor/index.html>). Zaremba boundary conditions are not implemented in the package, but even for the simpler Dirichlet problem the execution time required by this algorithm is not as favorable as those required by the solvers proposed in this thesis: a computing time of 0.46 seconds is required for the Dirichlet problem for Helmholtz equation, while with the FC-based solver presented in this thesis executes in 0.06 seconds for the significantly more challenging Zaremba problem for Helmholtz equation on the same domain (unit disc), with the same incident wave frequency $k = 2$ and for the same relative error 10^{-13} in the solution. (All the numerical results presented in this thesis were obtained on a single core of a 2.4 GHz Intel E5-2665 processor.) Such time differences, a factor of eight in this case, can be very significant in practice, in contexts where thousands or even tens of thousands of solutions are necessary, as is the case in inverse problems as well as in our own solution of high-frequency eigenvalue problems, etc. The main reason for the difference in execution times is that even though the iterative solver requires a limited number of iterations, iteration-dependent matrix entries occur (in view of corresponding iteration dependent discretization points), which require large number of evaluations of expensive Hankel functions at each iteration, and, thus, a significantly increased computing cost.

Additional results demonstrating the high-order convergence of the FC-solver when it is applied to solve challenging eigenvalue problems are presented in Section 4.5.

Chapter 3

Integral equation solvers for the Zaremba boundary value problem on Lipschitz domains

3.1 Preliminaries

We consider interior and exterior boundary value problems of the form

$$\begin{aligned}\Delta u(x) + k^2 u(x) &= 0 & x \in \Omega, \\ u(x) &= f(x) & x \in \Gamma_D, \\ \frac{\partial u(x)}{\partial n_x} &= g(x) & x \in \Gamma_N\end{aligned}\tag{3.1}$$

for $u \in H_{\text{loc}}^1(\Omega)$ (with a Sommerfeld radiation condition in case of exterior problems). Throughout this chapter $\Omega \subset \mathbb{R}^2$ denotes a bounded simply-connected domain with a Lipschitz boundary $\Gamma = \partial\Omega$ and the Dirichlet and Neumann boundary portions Γ_D and Γ_N are disjoint subsets of Γ .

Let the piecewise-smooth boundary Γ be expressed in the form

$$\Gamma = \bigcup_{q=1}^{Q_N+Q_D} \Gamma_q,\tag{3.2}$$

where Q_D and Q_N denote the numbers of smooth Dirichlet and Neumann boundary portions, and where for $1 \leq q \leq Q_D$ (resp. $Q_D + 1 \leq q \leq Q_D + Q_N$) Γ_q denotes a *smooth* Dirichlet

(resp. Neumann) segment of the boundary curve Γ . Clearly, letting

$$J_D = \{1, \dots, Q_D\} \quad \text{and} \quad J_N = \{Q_D + 1, \dots, Q_D + Q_N\}$$

we have that

$$\overline{\Gamma}_D = \bigcup_{q \in J_D} \Gamma_q \quad \text{and} \quad \overline{\Gamma}_N = \bigcup_{q \in J_N} \Gamma_q$$

are the (piecewise smooth) portions of Γ upon which Dirichlet and Neumann boundary conditions are enforced, respectively. Note that in view of the assumption above both Dirichlet-Neumann junctions and non-smooth points in Γ necessarily occur at a common endpoint of two segments $\Gamma_{q_1}, \Gamma_{q_2}$ ($1 \leq q_1, q_2 \leq Q_D + Q_N$). Note, additionally, that consecutive values of the index q do not necessarily correspond to consecutive boundary segments (see, e.g., Figure 3.1).

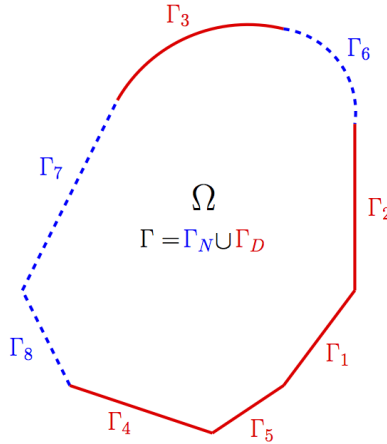


Figure 3.1: Boundary decomposition illustration. Dashed line: Neumann boundary. Solid line: Dirichlet boundary.

Remark 3.1.1. *Throughout this chapter the decomposition of the curve Γ is taken in such a way that no Dirichlet-Dirichlet or Neumann-Neumann junctions occur at a point at which the curve Γ is smooth. In other words, every endpoint of Γ_q is either a Dirichlet-Neumann junction or a non-smooth point of Γ . Clearly this is not a restriction: two Dirichlet (resp. Neumann) segments Γ_{q_1} and Γ_{q_2} that meet at a point at which Γ is smooth can be combined into a single Dirichlet (resp. Neumann) segment.*

We employ the integral equation approach described in detail in Section 2.4 and write here the integral equation system (2.4) for the problem 3.1:

$$\begin{aligned} \int_{\Gamma} G_k(x, y)\psi(y)ds_y &= f(x) \quad x \in \Gamma_D, \\ \gamma \frac{\psi(x)}{2} + \int_{\Gamma} \frac{\partial G_k(x, y)}{\partial n_x} \psi(y)ds_y &= g(x) \quad x \in \Gamma_N. \end{aligned} \tag{3.3}$$

3.2 Singularities in solutions and integral equation densities

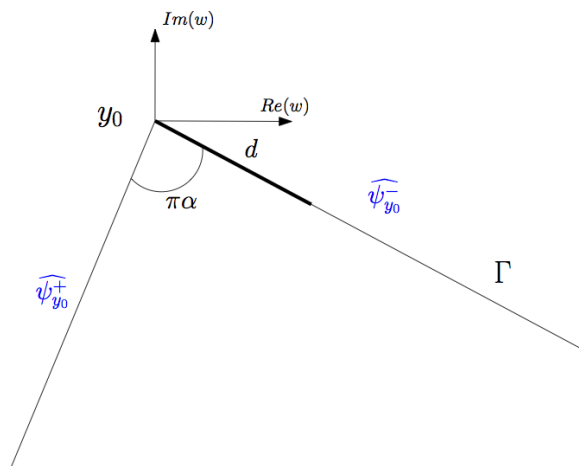


Figure 3.2: Point y_0 of singularity of the density function ψ . For $\alpha = 1$ y_0 may or may not be a point at which Γ is smooth (infinitely differentiable); cf. Remark 3.1.1.

This section collects known results about the smoothness properties and singularities of the solutions of equation (3.1) and the corresponding integral densities in equation (3.3). The singular character of these functions is incorporated as part of the discretization strategies we introduce in Section 3.3.

Let $y_0 = (y_1^0, y_2^0) \in \Gamma$ be either a corner point (with associated corner angle $\alpha\pi$) at which a Dirichlet-Neumann junction may or may not occur, or a point around which the curve Γ is smooth ($\alpha = 1$) and which separates Dirichlet and Neumann regions within Γ . In either case y_0 is a singular point for the problem. Following [126] in order to express the singular character of the solutions $u(y)$ ($y = (y_1, y_2) \in \Omega$) and corresponding integral

equation densities $\psi(y)$ ($y = (y_1, y_2) \in \Gamma$) around y_0 we use certain functions $\widehat{u}_{y_0} = \widehat{u}_{y_0}(w)$, $\widehat{\psi}_{y_0}^+ = \widehat{\psi}_{y_0}^+(d)$ and $\widehat{\psi}_{y_0}^- = \widehat{\psi}_{y_0}^-(d)$. Here the left (resp. right) function $\widehat{\psi}_{y_0}^-$ (resp $\widehat{\psi}_{y_0}^+$) is the density as a function of the distance d to the point y_0 in a small one-sided neighborhood immediately before (resp. immediately after) the point y_0 as the curve is traversed in the counterclockwise direction, and $w = (y_1 - y_1^0) + i(y_2 - y_2^0)$ is a complex variable (see Figure 3.2). The functions \widehat{u}_{y_0} , $\widehat{\psi}_{y_0}^+$ and $\widehat{\psi}_{y_0}^-$ are given by

$$\begin{aligned}\widehat{u}_{y_0}(w) &= u(y), \\ \psi(y) &= \widehat{\psi}_{y_0}^+(d(y)) \quad y \in \Gamma_{q1}, \\ \psi(y) &= \widehat{\psi}_{y_0}^-(d(y)) \quad y \in \Gamma_{q2},\end{aligned}\tag{3.4}$$

where, as mentioned above

$$w = (y_1 - y_1^0) + i(y_2 - y_2^0) \quad ; \quad d(y) = \sqrt{(y_1 - y_1^0)^2 + (y_2 - y_2^0)^2}.\tag{3.5}$$

It is known [125, 126] that, under our assumption that the curve Γ is piecewise smooth, for any given integer \mathcal{N} and any given positive number ε the eigenfunctions in equation (4.1) can be expressed in the form

$$\widehat{u}_{y_0} = \log(w)P_{y_0}^1 + \log(\bar{w})P_{y_0}^2 + P_{y_0}^3 + \mathcal{O}(w^{\mathcal{N}-\varepsilon})\tag{3.6}$$

for all w in a neighborhood of the point, where $P_{y_0}^1, P_{y_0}^2$ and $P_{y_0}^3$ are polynomials in $w, \bar{w}, w^{1/(2\alpha)}, \bar{w}^{1/(2\alpha)}$ if α is irrational; $P_{y_0}^1, P_{y_0}^2$ and $P_{y_0}^3$ are polynomials in $w, \bar{w}, w^{1/(2\alpha)}, \bar{w}^{1/(2\alpha)}, w^q \log(w), \bar{w}^q \log(\bar{w})$ if $\alpha = p/q$ for certain relatively prime integers p and q where q is odd, and $P_{y_0}^1, P_{y_0}^2$, and $P_{y_0}^3$ are polynomials in $w, \bar{w}, w^{1/(2\alpha)}, \bar{w}^{1/(2\alpha)}, w^{q/2} \log(w), \bar{w}^{q/2} \log(\bar{w})$ if $\alpha = p/q$ for relatively prime integers p and q where q is even. (In fact, for Dirichlet-Dirichlet and Neumann-Neumann corners some of the coefficients in the asymptotic expressions above vanish and weaker singularities—polynomials in powers of $1/\alpha$ instead of $1/(2\alpha)$ in equation (3.6)—thus result; see [125] for details. This point is not of any practical significance in the context of this thesis, however.)

The singular character of the density ψ plays a fundamental role in our proposed numerical strategy for discretization of the system of integral equations (3.3). To determine the singularities of the function ψ we assume without loss of generality that Ω is an interior domain and we let u_e denote the conjugate solution of an auxiliary Dirichlet problem outside Ω with Dirichlet boundary values given by the boundary values of the solution u (see Definition 2.2.1). In view of Theorem 2.2.4, which shows that the solution ψ of the integral equation system (3.3) is given by

$$\psi = \frac{\partial u_e}{\partial n} \Big|_{\Gamma} - \frac{\partial u}{\partial n} \Big|_{\Gamma}, \quad (3.7)$$

it can then be shown that around the point (y_1^0, y_2^0) the functions $\widehat{\psi}_{y_0}^+$ and $\widehat{\psi}_{y_0}^-$ of equation (3.4) are given in terms of the distance function (3.5) by

$$\begin{aligned} \widehat{\psi}_{y_0}^+(d) &= d^{1/(2\alpha)-1} Q_{y_0}^1(d, d^{1/(2\alpha)}, \log(d)) + \mathcal{O}(d^{\mathcal{N}-1-\varepsilon}), \\ \widehat{\psi}_{y_0}^-(d) &= d^{1/(2\alpha)-1} Q_{y_0}^2(d, d^{1/(2\alpha)}, \log(d)) + \mathcal{O}(d^{\mathcal{N}-1-\varepsilon}) \end{aligned} \quad (3.8)$$

for all $\mathcal{N} \in \mathbb{N}$. For the sake of conciseness we do not present a proof of this result here, and we merely point out that the proof is entirely analogous to the one presented in Section 2.3.3 in a slightly different context. (Note that, while correct, the boundary expressions (3.8) are less detailed than the corresponding volumetric expression (3.6). In our context the additional detail provided by equation (3.6), which shows that the logarithmic terms are always accompanied by a w^r factor for an integer r equal to either q or $q/2$, do not carry any particular significance.)

3.3 Graded-mesh algorithm

As can be seen by consideration of equations (3.8), the presence of corners in the domain boundary affects significantly the singular character of the Zaremba integral density. In order to accurately approximate our integral operators for domains with corners we utilize a quadrature method [34, 79, 83, 95, 108] which, based on changes of variables that induce

graded meshes and vanishingly small Jacobians, regularize the associated integrands at corners and thus enable high order integration even in presence of density singularities. To describe the proposed graded mesh algorithm, here we re-express the boundary integrals in the system (3.3) in terms of the operators

$$\tilde{\mathcal{I}}_{q_1, q_2}[\tilde{\varphi}](t) = \int_{a_{q_2}}^{b_{q_2}} \left\{ \tilde{K}^1(t, \tau) \log R^2(t, \tau) + \tilde{K}^2(t, \tau) \right\} \tilde{\varphi}(\tau) d\tau; \quad (3.9)$$

cf. Section 2.4

3.3.1 Graded-mesh algorithm: Polynomial change of variables

A set of quadrature weights similar to those given in [34, p. 75] are incorporated in the present context to account accurately for the logarithmic singularity of the kernel and the singularities of the integral density at corners. As in [34] a graded mesh on each of the intervals $[a_q, b_q]$, $q = 1, \dots, Q_D + Q_N$ is induced by means of a polynomial change of variables of the form $\tau = w_q(\sigma)$, where

$$\begin{aligned} w_q(\sigma) &= a_q + (b_q - a_q) \frac{[v(\sigma)]^p}{[v(\sigma)]^p + [v(2\pi - \sigma)]^p}, \quad 0 \leq \sigma \leq 2\pi, \\ v(\sigma) &= \left(\frac{1}{p} - \frac{1}{2} \right) \left(\frac{\pi - \sigma}{\pi} \right)^3 + \frac{1}{p} \frac{\sigma - \pi}{\pi} + \frac{1}{2}, \end{aligned} \quad (3.10)$$

and where $p \geq 2$ is an integer. Each function w_q is smooth and increasing in the interval $[0, 2\pi]$, and their k -th derivatives satisfy $w_q^{(k)}(0) = w_q^{(k)}(2\pi) = 0$ for $1 \leq k \leq p - 1$.

Remark 3.3.1. *In addition to change of variables (3.10) and associated graded meshes, the method [34] for domain with corners (which is only applicable to the Dirichlet problem) relies on a certain subtraction of values of the integral density at corner points times a Gauss integral to provide additional regularization of the integration process. The algorithms in this thesis, which can be used to treat all three, the Dirichlet, Neumann, and Zaremba boundary value problems, do not incorporate any such subtraction; however, see Remark 3.3.3 for a brief discussion in these regards.)*

In detail, the integrand in equation (3.9) contains singularities of various types, namely

1. Singularities that result solely from corresponding singularities in the density $\tilde{\varphi}$ —in the term $\widetilde{K}^1(t, \tau) \log R^2(t, \tau) \tilde{\varphi}(\tau)$ for $q_2 \neq q_1$ and in the term $\widetilde{K}^2(t, \tau) \tilde{\varphi}(\tau)$ for both $q_2 \neq q_1$ and $q_2 = q_1$; and
2. Combined singularities induced by the density and the logarithmic factor—in the term $\widetilde{K}^1(t, \tau) \log R^2(t, \tau) \tilde{\varphi}(\tau)$ for $q_1 = q_2$.

Remark 3.3.2. *Concerning point 1 above note that, although for $q_1 \neq q_2$ the factor $\log R^2(t, \tau)$ is smooth, this term does give rise to a logarithmic near-singularity for t close to either a_{q_2} or b_{q_2} . It is easy to check, however, that the approach provided below for treatment of the singular character of $\tilde{\varphi}$ suffices to account with high-order accuracy for the near-logarithmic singularity as well.*

Using the change of variables (3.10) for both integration and observation variables, that is, setting $t = w_{q_1}(s)$ and $\tau = w_{q_2}(\sigma)$, the integral (3.9) can be re-expressed in the form

$$\begin{aligned} \mathcal{I}_{q_1, q_2}[\varphi](s) = & \int_0^{2\pi} \widetilde{K}^1(w_{q_1}(s), w_{q_2}(\sigma)) \log R^2(w_{q_1}(s), w_{q_2}(\sigma)) \varphi_{q_2}(\sigma) w'_{q_2}(\sigma) d\sigma + \\ & \int_0^{2\pi} \widetilde{K}^2(w_{q_1}(s), w_{q_2}(\sigma)) \varphi_{q_2}(\sigma) w'_{q_2}(\sigma) d\sigma, \end{aligned} \quad (3.11)$$

where $\varphi_{q_2}(\sigma) = \tilde{\varphi}(w_{q_2}(\sigma))$. This procedure effectively treats the density singularities mentioned in point 1 above. Indeed, since values $p \geq 2$ are used for the parameter p in equation (3.10) and given the singular character (3.8) of the density $\tilde{\varphi}$, the product $\varphi(\sigma) w'_{q_2}(\sigma)$ is smoother than $\tilde{\varphi}$: this product can be made to achieve any finite order of differentiability by selecting p large enough.

To deal with the singularities mentioned in point 2 above, on the other hand, we utilize the following notations: for $q_1 = q_2 = q$, we let

$$\begin{aligned} K_{q,q}^1(s, \sigma) &= \widetilde{K}^1(w_q(s), w_q(\sigma)), \\ K_{q,q}^2(s, \sigma) &= \widetilde{K}^1(w_q(s), w_q(\sigma)) \log \left(\frac{R^2(w_q(s), w_q(\sigma))}{4 \sin^2 \frac{s-\sigma}{2}} \right) + \widetilde{K}^2(w_q(s), w_q(\sigma)). \end{aligned} \quad (3.12)$$

Note that the “diagonal term” that occurs in the kernel $K_{q,q}^2$ for $s = \sigma$ is given by $K_{q,q}^2(s, s) =$

$2\widetilde{K}^1(w_q(s), w_q(s)) \log(w'_q(s)|z'(w_q(s))|) + \widetilde{K}^2(w_q(s), w_q(s))$. Using these transformations the integrals (3.11) for $q_1 = q_2 = q$ can be re-expressed in the form

$$\mathcal{I}_{q,q}[\varphi_q](s) = \int_0^{2\pi} K_{q,q}^1(s, \sigma) \log\left(4 \sin^2 \frac{s-\sigma}{2}\right) \varphi_q(\sigma) w'_q(\sigma) d\sigma + \int_0^{2\pi} K_{q,q}^2(s, \sigma) \varphi_q(\sigma) w'_q(\sigma) d\sigma. \quad (3.13)$$

3.3.2 Graded-mesh algorithm: Discretization and quadratures

In view of the discussion presented in Section 3.3.1 our overall numerical algorithm for evaluation of the integrals (3.11) (and thus (3.9)) proceeds through separate consideration of the cases $q_1 = q_2 = q$ and $q_1 \neq q_2$. In the case $q_1 = q_2 = q$ we utilize the expression (3.13): the first (resp. second) integral in this equation is evaluated by means of the logarithmic quadrature (3.14) below (resp. the spectrally accurate trapezoidal rule (3.15) below). For the case $q_1 \neq q_2$, on the other hand, we use the expression (3.11) directly: we combine both integrals into one which is then evaluated by means of the trapezoidal rule (3.15). The logarithmic and trapezoidal rules mentioned above proceed as follows:

- Logarithmic quadrature ($q_1 = q_2 = q$).

We consider integrals whose integrand, like the one in the first integral in equation (3.13), consists of a product of a smooth 2π -periodic function f times the logarithmic factor $\log\left(4 \sin^2 \frac{s-\sigma}{2}\right)$. Such integrals are produced with spectral accuracy by means of the rule

$$\int_0^{2\pi} f(\sigma) \log\left(4 \sin^2 \frac{s-\sigma}{2}\right) d\sigma \sim \sum_{j=1}^{2n} R_j^{(n)}(s) f(\sigma_j), \quad (3.14)$$

where $\sigma_j = (j-1)\pi/n$, $n \in \mathbb{N}$ and where the quadrature weights $R_j(s)$ are given by [32, p. 70]

$$R_j(s) = -\frac{2\pi}{n} \sum_{m=1}^{n-1} \frac{1}{n} \cos m(s - \sigma_j) - \frac{\pi}{n^2} \cos n(s - \sigma_j).$$

Following [19] we note that, letting

$$R_k = -\frac{2\pi}{n} \sum_{m=1}^{n-1} \frac{1}{n} \cos \frac{mk\pi}{n} - \frac{(-1)^k \pi}{n^2}$$

we have $R_j(\sigma_i) = R_{|i-j|}$ —so that the weights $R_j(\sigma_i)$ can be evaluated rapidly by means of Fast Fourier Transforms.

- Trapezoidal rule.

As is well known, spectrally accurate integrals of smooth 2π -periodic functions f can be obtained by means of the trapezoidal rule

$$\int_0^{2\pi} f(\sigma) d\sigma \sim \frac{\pi}{n} \sum_{j=1}^{2n} f(\sigma_j), \quad (3.15)$$

where again $\sigma_j = (j-1)\pi/n$.

Remark 3.3.3. *With reference to Remark 3.3.1, subtraction of a certain multiple of a Gauss integral can be used in the case of the Dirichlet problem to somewhat mollify corner singularities and thereby enhance the convergence of the numerical integration method. Considering the expressions (3.8) for the singularities in the density functions, even without the subtraction the method described above in this section is easily checked to be consistent with the system (3.3) of integral equations for sufficiently large value of p . Although a proof of the stability of the method is left for future work, the numerical results in this thesis strongly suggest that stability results from this approach. As the value of α grows, however, the minimum required value of p grows as well, thereby increasing the condition number of the system. This difficulty can alternatively be addressed by means of a singularity resolution methodology introduced in [22]—a full development of which is beyond the scope of this thesis and which is thus left for future work.*

3.4 Applications and numerical results

In this section we present a few results on solution of scattering problems (2.110) for the cases

- 1) Ω is a trapezoid with corners $(0,0)$, $(1,1)$, $(2,1)$, and $(2,0)$ (Neumann data is prescribed along one side of length $\sqrt{2}$, and Dirichlet data is prescribed along the other sides) and
- 2) Ω is an isosceles triangle with corners $(0,0)$, $(0,1)$, and $(1,0)$ (Neumann data is prescribed along one side of unit length, and Dirichlet data is prescribed along the other two sides).

Figures 3.3, 3.4, 3.5, and 3.6 depict the scattering pattern for the incident wave coming at an angle $\alpha = \pi/8$ and frequency $k = 200$.

Additional results demonstrating the high-order convergence of the graded-mesh algorithm when it is applied to solve challenging eigenvalue problems are presented in Section 4.5.

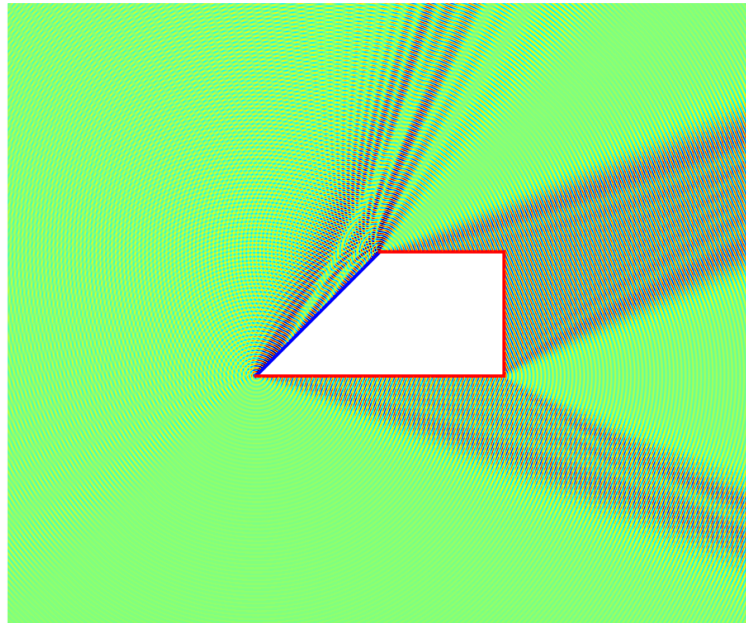
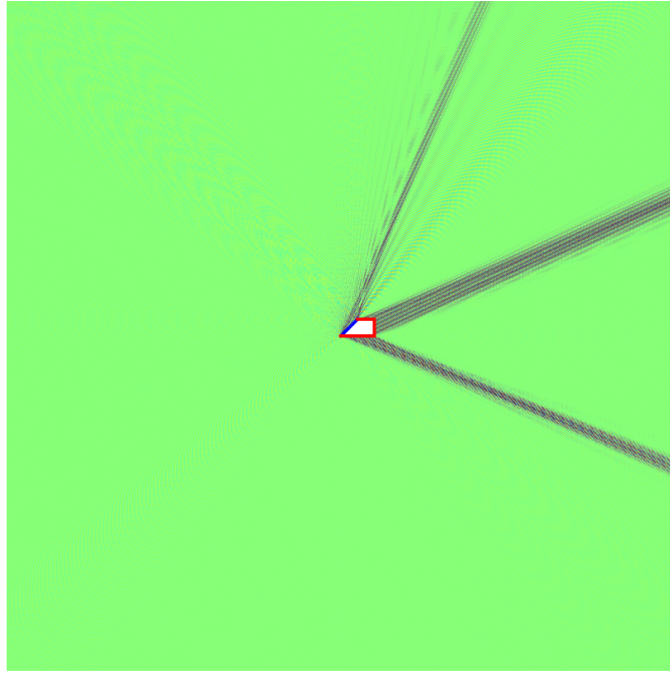


Figure 3.3: Scattering from a trapezoidal domain under Zaremba boundary conditions. Scattered field.

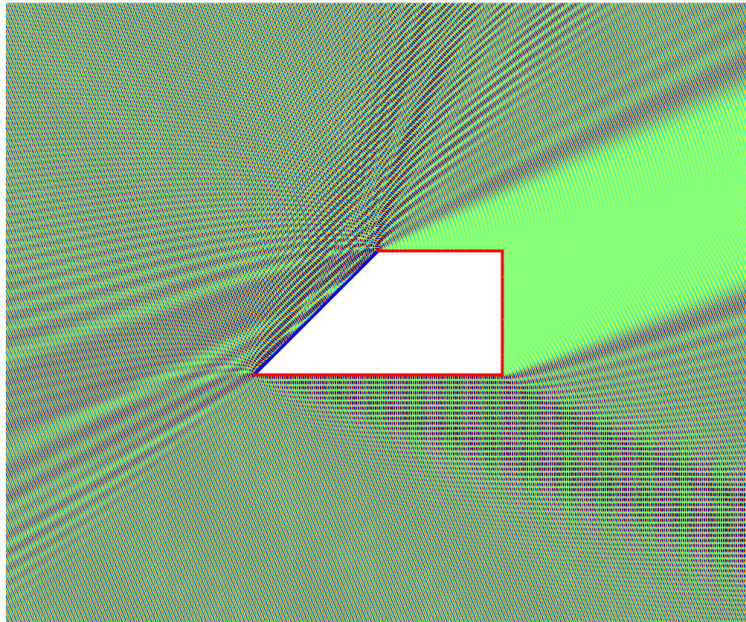
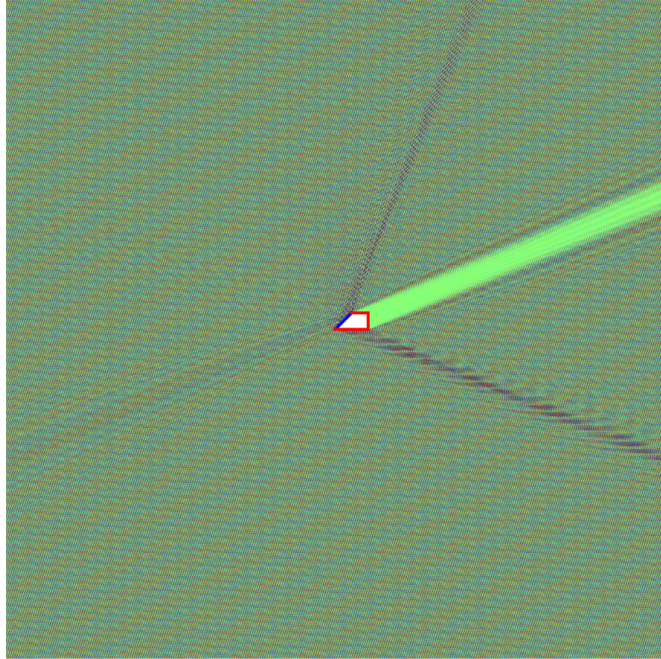


Figure 3.4: Scattering from a trapezoidal domain under Zaremba boundary conditions. Total field.

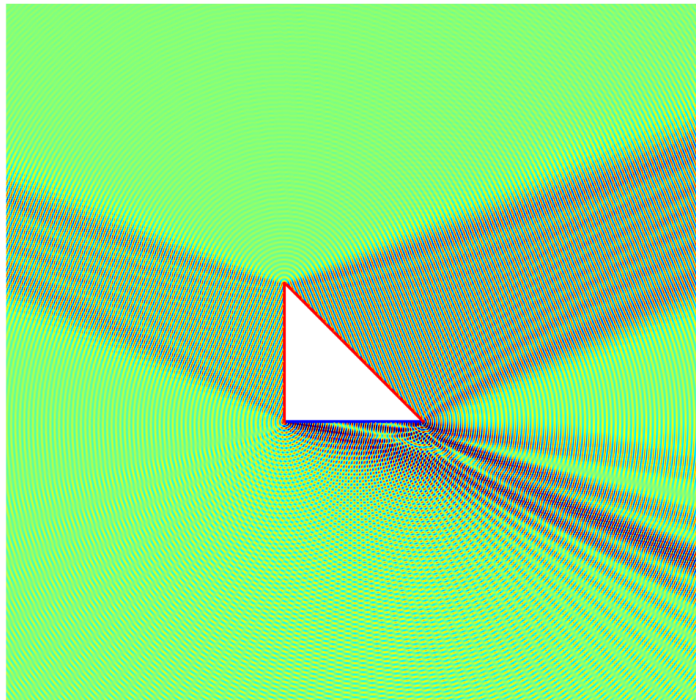
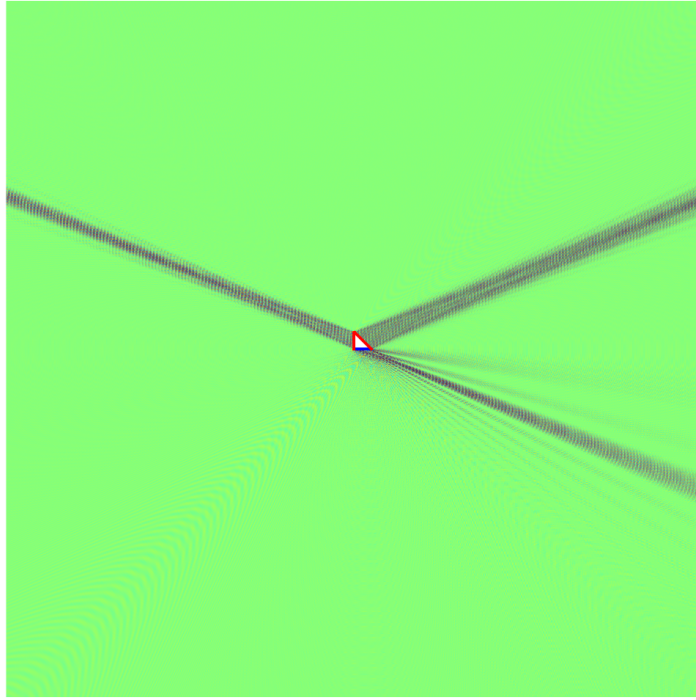


Figure 3.5: Scattering from a triangular domain under Zaremba boundary conditions. Scattered field.

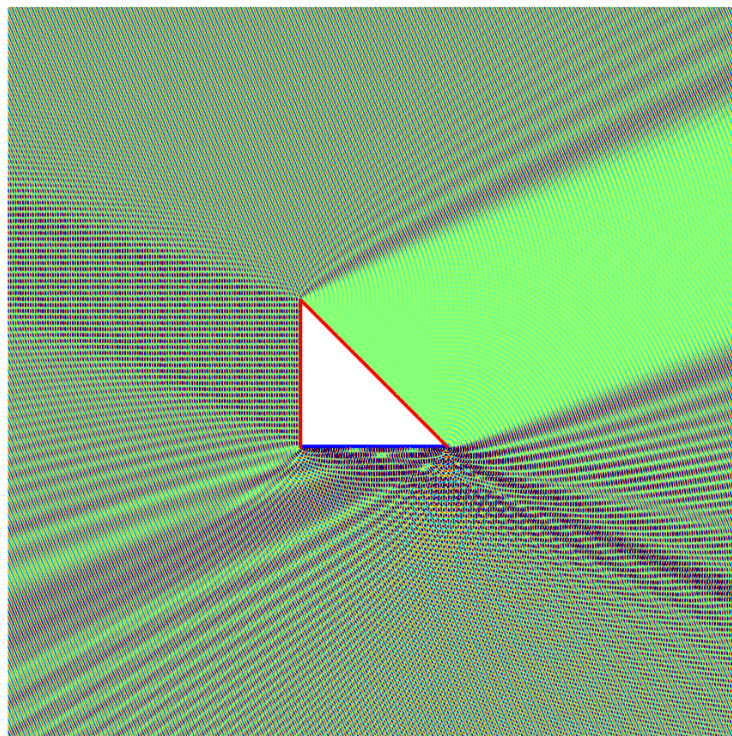
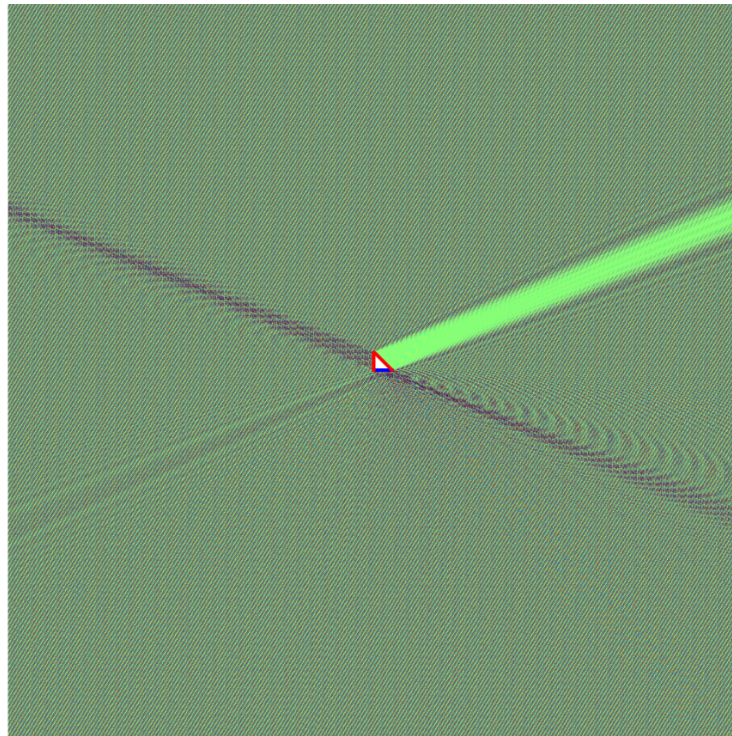


Figure 3.6: Scattering from a triangular domain under Zaremba boundary conditions. Total field.

Chapter 4

Laplace-Zaremba eigenvalue problems and novel search method

4.1 Integral formulation of the eigenvalue problem

The results in this Chapter were obtained in collaboration with professor Nilima Nigam in addition to professor Bruno, and mostly follow the contribution [2]. In this chapter we consider the eigenvalue problem

$$-\Delta u = \lambda u, \quad x \in \Omega \quad (4.1a)$$

$$u = 0, \quad x \in \Gamma_D \quad (4.1b)$$

$$\frac{\partial u}{\partial n} = 0, \quad x \in \Gamma_N. \quad (4.1c)$$

Introducing the Helmholtz Green function $G_\mu(x, y) := \frac{i}{4}H_0^1(\mu|x - y|)$ and the associated single-layer potential

$$u(x) := \int_\Gamma G_\mu(x, y)\psi(y) ds_y \quad (x \in \Omega) \quad (4.2)$$

with surface density ψ , and relying on well known expressions [33] for the values of the single layer u and its normal derivative $\frac{\partial u}{\partial n}$ on Γ , we define the operators $\mathcal{A}^{(1)} : H^{-1/2}(\Gamma) \rightarrow$

$H^{1/2}(\Gamma_D)$ and $\mathcal{A}^{(2)} : H^{-1/2}(\Gamma) \rightarrow H^{-1/2}(\Gamma_N)$ by

$$\mathcal{A}_\mu^{(1)}[\psi](x) = \int_\Gamma G_\mu(x, y)\psi(y)ds_y \quad \text{for } x \in \Gamma_D, \quad (4.3a)$$

$$\mathcal{A}_\mu^{(2)}[\psi](x) = -\frac{\psi(x)}{2} + \int_\Gamma \frac{\partial}{\partial n_x} G_\mu(x, y)\psi(y)ds_y \quad \text{for } x \in \Gamma_N, \quad (4.3b)$$

and we then define

$$\mathcal{A}_\mu =: H^{-1/2}(\Gamma) \rightarrow H^{1/2}(\Gamma_D) \times H^{-1/2}(\Gamma_N) \quad \text{by} \quad \mathcal{A}_\mu[\psi] = (\mathcal{A}_\mu^{(1)}[\psi], \mathcal{A}_\mu^{(2)}[\psi]). \quad (4.4)$$

Problem (4.1) is equivalent to the nonlinear problem of finding $\mu > 0$ for which there holds:

$$\text{“The linear system } \mathcal{A}_\mu \psi = 0 \text{ admits non-trivial solutions } \psi\text{”}. \quad (4.5)$$

To see this, let u be given by equation (4.2). Note that u does not vanish identically unless ψ does—as can be established by using uniqueness results for the Dirichlet exterior problem and the jump relations satisfied by the single layer potential and its normal derivative. Since, clearly, $-\Delta u = \mu^2 u$ throughout Ω , further, it follows that for each μ satisfying (4.5) the real number

$$\lambda = \mu^2$$

is an eigenvalue of (4.1). Further, as established in Chapter 2 (cf. also [40] for corresponding results for the pure Dirichlet problem), every eigenvalue λ equals μ^2 for some $\mu \in \mathbb{R}$ satisfying (4.5), and the solutions ψ of (4.5) are related to the corresponding eigenfunctions u of (4.1) via the relation (4.2). It follows that, as claimed, the eigenvalue problem (4.1) and problem (4.5) are equivalent.

Remark 4.1.1. *As is known [40], complex values of μ do exist for which the integral form of the eigenvalue problem admits non-trivial solutions—although, they do not correspond to eigenvalues of the Laplace operator in the bounded domain Ω . These values of μ do correspond to complex eigenvalues μ^2 (also called “scattering poles”) of the Laplace operator: they satisfy the Laplace eigenvalue equation outside Ω along with certain radiation conditions at infinity*

which allow for growth. The determination and study of these scattering poles, which is interesting in its own right [86, 98], does not fall within the scope of this thesis. A numerical method for evaluation of such poles for the Dirichlet exterior problem can be found in [115]. In fact, we suggest that the stabilization strategy proposed in Section 4.3 should be useful in the context of [115] as well.

Upon discretization of the problem (4.5) (Section 4.2) we are lead to the nonlinear problem of locating $\mu \in \mathbb{R}$ and $\mathbf{c} \in \mathbb{R}^N$ which satisfy a discrete linear system of equations of the form

$$\mathbf{A}_\mu \mathbf{c} = 0. \quad (4.6)$$

This problem is tackled in Section 4.3 by consideration of the minimum singular value $\tilde{\eta}_n(\mu)$ (and corresponding right singular vector) of a certain augmented linear system related to (4.6): the quantities μ and \mathbf{c} that satisfy (4.5) are obtained, simply, as a zero of the function $\sigma = \tilde{\eta}_n(\mu)$ and the corresponding singular vector. The vector \mathbf{c} provides a discrete approximation for the unknown density ψ ; the eigenfunction u itself can then be obtained by means of a corresponding discrete version of the representation formula (4.2).

4.2 Discrete boundary integral operator

This section presents the main algorithm for evaluation of the discrete version of the form (4.6) of the boundary operator (4.4); the discretization procedure relies on use of the high-order quadrature methods described in Sections 2.5 and 3.3.

We denote by n_q the number of discretization points used on the boundary segment Γ_q , $q = 1, \dots, Q_D + Q_N$ and we call

$$n = \sum_{q=1}^{Q_D+Q_N} n_q \quad (4.7)$$

the number of discretization points used throughout Γ . The discrete algorithms introduced in this chapter rely on use of the uniform grids

$$\sigma_q^j = (j - 1)\gamma\pi/n_q \quad , \quad j = 1, \dots, n_q \quad (4.8)$$

in the interval $0 \leq \sigma \leq \gamma\pi$, where $\gamma = 1$ for the FC-based algorithm (Section 2.5) and $\gamma = 2$ for the graded-mesh algorithm (Section 3.3). The corresponding points τ_q^j in the parameter space are given by $\tau_q^j = \xi_q(\cos(\sigma_q^j))$ in the FC-based algorithm (see equation (2.87)), and by $\tau_q^j = w_q(\sigma_q^j)$ in graded-mesh algorithm.

Remark 4.2.1. *The following procedure is suggested for determination of the values of the parameters n_q mentioned above. Given a desired meshsize $h \in \mathbb{R}$ (which should be selected so as to appropriately discretize the highest spatial oscillations under consideration) we take $n_q = \max\{n_h, n_0\}$, where n_h is the smallest integer for which the distance between any two consecutive points in Γ_q is not larger than h , and where n_0 is an integer whose role is to ensure that the number of discretization points in each boundary segment is not less than the minimum number of discretization points required by the method used (either the Fourier Continuation method, see Appendix A, or the graded-mesh algorithm, cf. equation (3.10)) to guarantee the desired convergence rate takes place.*

Remark 4.2.2. *We point out that in both the FC-based and graded-mesh algorithms (Sections 2.5 and 3.3, respectively) the approximations of the values $\mathcal{I}_{q_1, q_2}[\varphi_{q_2}](\sigma_{q_1}^j)$ used by our algorithms only depend on values of φ_{q_2} at the points $\sigma_{q_2}^j$, $j = 1, \dots, n_{q_2}$. In the smooth domain case this indeed results from the fact that an m -th order Fourier continuation f^c of a function $y = f(x)$ only depends on the values of f at the discretization points x_i (see Appendix A and take into account equations (2.100), (2.102), (2.104), and (2.106)). For the graded-mesh case, in turn, this follows from the fact that the quadrature rules (3.14), (3.15) only use values of the density φ_{q_2} at the points $\sigma_{q_2}^j$.*

In view of Remark 4.2.2 and equation (4.7) and associated text, a discrete version of the integral density ψ can be obtained in the form of an n -dimensional vector of unknowns

$$\mathbf{c} = \begin{bmatrix} \mathbf{c}_1 \\ \dots \\ \mathbf{c}_{Q_N+Q_D} \end{bmatrix}$$

where \mathbf{c}_q is a sub-vector of length n_q which contains the approximate unknown density values

at the points σ_q^j : $\mathbf{c}_q^j \sim \varphi_q(\sigma_q^j)$. An approximate boundary operator (4.6) based on either the FC method (for smooth curves Γ) or the graded mesh method (for smooth or non-smooth curves Γ) can thus be obtained in the form of a matrix

$$\mathbf{A}_\mu = \begin{bmatrix} (\mathbf{A}_\mu)_{1,1} & (\mathbf{A}_\mu)_{1,2} & \dots & (\mathbf{A}_\mu)_{1,Q_D+Q_N} \\ \dots & & & \\ (\mathbf{A}_\mu)_{Q_D+Q_N,1} & (\mathbf{A}_\mu)_{Q_D+Q_N,2} & \dots & (\mathbf{A}_\mu)_{Q_D+Q_N,Q_D+Q_N} \end{bmatrix}. \quad (4.9)$$

Here the sub-blocks $(\mathbf{A}_\mu)_{q_1,q_2}$ are discrete operators which for $q_1 = q_2 = q \in J_N$ approximate the continuous operators $-I/2 + \mathcal{I}_{q,q}$ (where I is the identity operator):

$$-\frac{\varphi_q}{2} + \mathcal{I}_{q,q}[\varphi_q](\sigma_q^j) \sim \sum_{j=1,n_q} (\mathbf{A}_\mu)_{q,q}^{i,j} \mathbf{c}_q^j, \quad i = 1, \dots, n_q, \quad (4.10)$$

and which for all other pairs of indexes $q_1, q_2 = 1, \dots, Q_D + Q_N$ approximate the continuous operators \mathcal{I}_{q_1,q_2} :

$$\mathcal{I}_{q_1,q_2}[\varphi_{q_2}](\sigma_{q_2}^j) \sim \sum_{j=1,n_{q_2}} (\mathbf{A}_\mu)_{q_1,q_2}^{i,j} \mathbf{c}_{q_2}^j, \quad i = 1, \dots, n_{q_1}.$$

In cases in which an overall FC-based method is used the blocks $(\mathbf{A}_\mu)_{q,q}$ are matrices which encapsulate the various integration methods described in Section 2.5; if the graded-mesh method is used instead then the blocks $(\mathbf{A}_\mu)_{q,q}$ collect the contributions produced by the quadrature methods presented in Section 3.3.

Details of the algorithm used to produce the blocks $(\mathbf{A}_\mu)_{q_1,q_2}$ are given in Algorithms 1 and 2 below. The input parameters in these algorithms are to be selected in accordance with Remarks 2.4.2 and 4.2.1.

4.3 Eigenvalue search

This section presents an efficient algorithm for eigenvalue search—which, in the context of the present chapter, amounts to search for values of μ in a given range $[\mu_{min}, \mu_{max}]$ for which

Algorithm 1 Construction of the matrix block $(\mathbf{A}_\mu)_{q_1, q_2}$ for the FC-based algorithm

```
1: Input  $q_1, q_2, n_{q_1}$  and  $n_{q_2}$  (Section 4.2).
2: for  $j_2 = 1 : n_{q_2}$  do
3:   Let  $c_{q_2}^{j_2} = 1$  and  $c_{q_2}^j = 0$  for  $j = 1, n_{q_2}, j \neq j_2$  (cf. Remark 4.2.2).
4:   for  $j_1 = 1 : n_{q_1}$  do
5:     With reference to Cases 1 through 3 in Section 2.5.1.1, calculate  $\phi_{q_1, q_2}^1(\sigma_{q_1}^{j_1}, \sigma_{q_2}^{j_2})$ 
     and  $\phi_{q_1, q_2}^2(\sigma_{q_1}^{j_1}, \sigma_{q_2}^{j_2})$  using eq. (2.101) in case 1, eq. (2.103) in case 2 and eq. (2.105) in
     case 3.
6:     Calculate the coefficients  $\alpha_\ell^1, \beta_\ell^1, \alpha_\ell^2, \beta_\ell^2$  of the Fourier Continuation expan-
     sions (2.100) using the FC algorithm (see Appendix A).
7:     if  $q_1 = q_2 =: q$  then
8:       Evaluate  $(\mathbf{A}_\mu)_{q, q}^{j_1, j_2}$  using the approximation in eq. (2.104).
9:       if  $q \in J_N$  and  $j_1 = j_2$  then
10:        Add the identity part corresponding to the jump of the density (eq. (4.10)).
11:       end if
12:     else
13:       if  $\tau_{q_1}^{j_1}$  is “far” from the interval  $[a_{q_2}, b_{q_2}]$  (condition (2.83)) then
14:        Evaluate  $(\mathbf{A}_\mu)_{q_1, q_2}^{j_1, j_2}$  using the approximation in eq. (2.102).
15:       else
16:        Evaluate  $(\mathbf{A}_\mu)_{q_1, q_2}^{j_1, j_2}$  using the approximation in eq. (2.106).
17:       end if
18:     end if
19:   end for
20: end for
```

the statement (4.5) is satisfied. The search algorithm presented below can be utilized in conjunction with any numerical discretization of the operator (4.4) and, indeed, it can be applied to integral formulations of more general eigenvalue problems. Naturally, however, in this chapter we apply our search algorithm in combination with the discrete version \mathbf{A}_μ of the operator \mathcal{A}_μ (cf. equations (4.4) and (4.9)) which results from suitable applications of the quadrature rules presented in Sections 2.4, 3.3, and 4.2 to the operators (2.81).

4.3.1 Discussion

In view of (4.5) and associated text, the eigenvalues λ in equation (4.1) can be approximated by the squares of the values μ for which the corresponding matrix \mathbf{A}_μ is not invertible. Thus all approximate eigenvalues $\lambda_j = \mu_j^2$ of the problem (4.1) in a given interval $[\lambda_{min}, \lambda_{max}]$ can be obtained from the values of $\mu \in [\sqrt{\lambda_{min}}, \sqrt{\lambda_{max}}]$ for which the minimum singular value

Algorithm 2 Construction of the matrix block $(\mathbf{A}_\mu)_{q_1, q_2}$ for graded-mesh algorithm

```

1: Input  $q_1, q_2, n_{q_1}$  and  $n_{q_2}$  (Section 4.2).
2: for  $j_2 = 1 : n_{q_2}$  do
3:   Let  $c_{q_2}^{j_2} = 1$  and  $c_{q_2}^j = 0$  for  $j = 1, n_{q_2}, j \neq j_2$  (cf. Remark 4.2.2).
4:   for  $j_1 = 1 : n_{q_1}$  do
5:     if  $q_1 = q_2 =: q$  then
6:       Evaluate  $(\mathbf{A}_\mu)_{q, q}^{j_1, j_2}$  using the decomposition (3.13) via combination of the logarithmic quadrature (3.14) and the trapezoidal rule (3.15).
7:       if  $q \in J_N$  and  $j_1 = j_2$  then
8:         Add the identity part corresponding to the jump of the density (eq. (4.10)).
9:       end if
10:    else
11:      Evaluate  $(\mathbf{A}_\mu)_{q_1, q_2}^{j_1, j_2}$  using the decomposition (3.11) and the trapezoidal rule (3.15).
12:    end if
13:  end for
14: end for

```

$\eta_n(\mu)$ of the matrix \mathbf{A}_μ equals zero—or is otherwise sufficiently close to zero.

Unfortunately, this approach presents significant challenges in practice—as was noted in [39, 114] in connection with applications to related Dirichlet problems for the Laplace equation (but cf. Remark 4.3.1). The difficulty is demonstrated in Figure 4.1 (solid curve) which displays the function $\eta_n(\mu)$ for values of μ in the interval $[0, 20]$ for the Zaremba eigenproblem (4.1) on a unit disc (where Dirichlet and Neumann boundary conditions are prescribed on the upper and lower halves of the disc boundary). Clearly, the function $\eta_n(\mu)$ stays at a nearly constant level except for narrow regions around minima. This makes the derivative of $\eta_n(\mu)$ nearly 0 throughout most of the search domain, and, thus, renders efficient application of root-finding methods virtually impossible.

The occurrence of this adverse characteristic of the function $\eta_n(\mu)$ can be explained easily by consideration of (4.5) and associated text. Indeed, in view of the Riemann-Lebesgue lemma, arbitrarily small values of $\mathcal{A}_\mu \psi$ can be obtained by selecting densities ψ leading to functions ϕ_{q_1, q_2}^j (equation (2.100)) which equal highly oscillatory functions of σ on the Dirichlet boundary portion Γ_D and which are close to zero on the Neumann boundary portion Γ_N ; see Figure 4.2. At the discrete level, further, for any given mesh-size n only oscillatory functions up to a certain maximal oscillation level are supported. Consequently, as n (and

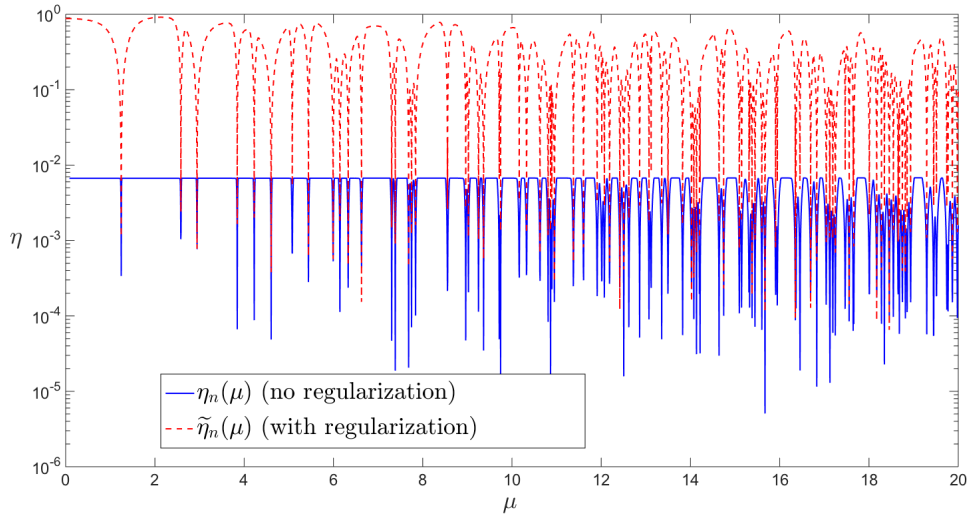


Figure 4.1: Comparison between $\eta_n(\mu)$ and $\tilde{\eta}_n(\mu)$.

therefore the maximal oscillation level) is increased, the minimum singular value $\eta_n(\mu)$ (which equals the minimum mean-square norm of $\mathbf{A}_\mu \mathbf{c}$ for \mathbf{c} in the unit sphere) itself decays like $1/n$, without significant dependence on μ —except for cases that correspond to actual eigenvalues. In order to devise a solution for this problem we note that the continuous analogue of our minimum singular value (namely, the infimum of $\|\mathcal{A}_\mu \psi\|$ over all densities ψ of unit norm) is actually equal to zero for all values of μ . But, naturally, a minimizing sequence ψ_k for which the operator values approach this infimum gives rise to single-layer potentials u_k that approach zero within Ω as well—and, thus, such sequences u_k do not approach true eigenfunctions. A solution strategy thus emerges: a normalization for the values of the single layer potential u (eq. (4.2)) *in the interior of Ω* can be used to eliminate such undesirable minimizing sequences. Details on possible implementations of this strategy are presented in the following section.

Remark 4.3.1. *From the discussion above in this section it is easy to see that difficulties associated with highly oscillatory integrands only occur in cases in which the boundary integral operator is entirely or partially of the first kind: for second-kind integral equations such complications do not arise [82, 131]. We note, however, that use of (partial or full) first-kind formulations can be highly advantageous in some cases (such as, e.g., for the problems*

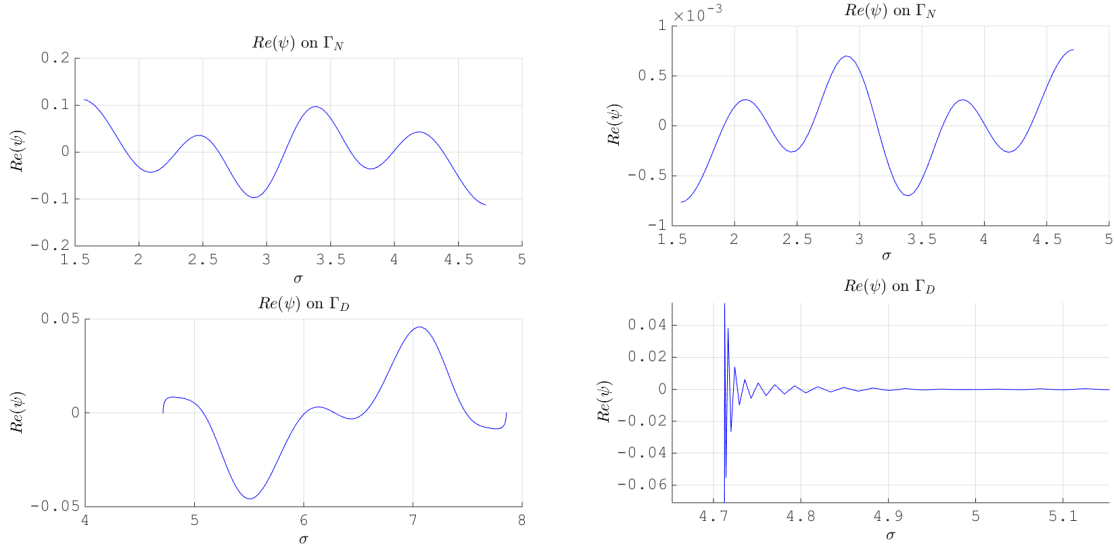


Figure 4.2: Densities (singular vectors) corresponding to smallest singular values for a formulation without regularizing interior points. Left column, μ^2 is an eigenvalue: vanishingly small values of the singular value $\eta_n(\mu)$ result for densities that are not rapidly oscillatory. Right column: μ^2 is not an eigenvalue. Note the oscillations on the Dirichlet portion of the density (lower-right image) which give rise to a small singular value $\eta_n(\mu)$ even in this case in which μ^2 is not a Dirichlet-Neumann eigenvalue.

considered in this thesis!) for which use of second-kind equations would necessarily require inclusion of hypersingular operators—which are generally significantly more challenging from a computational perspective; see e.g. [20]. The normalization techniques mentioned in Section 1 and discussed in more detail in Section 4.3.2 completely resolves the difficulty arising from use of first-kind formulations and enables successful use of numerically-well-behaved, easy-to-use first-kind equations for solution of eigenvalue problems for general domains.

4.3.2 Eigenfunction normalization.

The difficulties outlined in the previous section can be addressed by consideration of a modified discrete system of equations which, by enforcing an appropriate normalization in the domain interior, as it befits eigenfunctions of a differential operator, prevents oscillatory vectors \mathbf{c} to give rise to small values of the $\mathbf{A}_\mu \mathbf{c}$ unless μ corresponds to an actual eigenvalue; cf. Section 4.3.1.

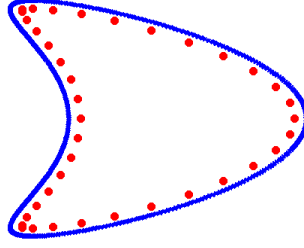


Figure 4.3: Interior curve Γ_i . An adequate discretization of Γ_i , possibly significantly coarser than the discretization on the boundary curve Γ , is used to penalize vanishingly small Laplace eigenfunctions.

To enforce such a normalization we consider equations (4.2) and (4.3), and we define an additional operator $\mathcal{A}_\mu^{(3)}$ by

$$\mathcal{A}_\mu^{(3)}[\psi](x) = \int_\Gamma G_\mu(x, y)\psi(y)ds_y \quad \text{for } x \in \Gamma_i, \quad (4.11)$$

where $\Gamma_i \subseteq \Omega$ is an adequately selected set of points in the interior of Ω . A natural choice is given by $\Gamma_i = \Omega$, in such a way that the normalization condition becomes $\int_\Omega |u|^2 dx = 1$. Other normalizations can be used, however, which lend themselves more easily to discretization. For example, letting Γ_i be a curve roughly parallel to Γ at a distance no larger than $\lambda_u/2$, cf. Figure 4.3 (where λ_u denotes the eigenfunction “wavelength” $\lambda_u = 2\pi/\mu$), one might equivalently prescribe

$$\int_{\Gamma_i} |u|^2 d\ell = 1. \quad (4.12)$$

Indeed, given that Γ_i is at a distance no larger than $\lambda_u/2$ from Γ , we expect that

$$\text{“The eigenfunction must be nonzero in a subset of } \Gamma_i \text{ of positive measure”}. \quad (4.13)$$

In the case of Dirichlet boundary conditions this statement is strongly supported by the eigenvalue bounds put forth in [15] and by the discussion in [127]. In the case of the Zaremba Dirichlet-Neumann boundary conditions we have not as yet found a corresponding theoretical discussion, but, in view of strong numerical evidence, throughout this chapter we nevertheless assume (4.13) holds.

Remark 4.3.2. *It is useful to note that, assuming (4.13), there is no non-zero density ψ for which the equations $\mathcal{A}_\mu[\psi] = 0$ and $\mathcal{A}_\mu^{(3)}[\psi] = 0$ hold simultaneously. Indeed, if these null conditions hold, (4.13) implies that the function u defined by (4.2) vanishes throughout Ω . In view of the uniqueness of solution of the Helmholtz equation in a exterior domain, further, we conclude that u vanishes throughout \mathbb{R}^2 . Taking into account the jump conditions for the normal derivative of the single layer potential this implies that $\psi = 0$, as desired.*

A discrete version of the normalization condition (4.12) can be obtained by means of a suitable, possibly equispaced discretization $\{x_j, j = 1, m\} \subseteq \Gamma_i$ together with an associated discrete operator \mathbf{B}_μ which, based on the quadrature rules for smooth integrands described in Section 4.4, approximates the values of $\mathcal{A}_\mu^{(3)}$ at the points x_j :

$$\mathbf{B}_\mu \mathbf{c} \sim [u(x_j)]. \quad (4.14)$$

Defining the rectangular matrix

$$\mathbf{C}_\mu = \begin{bmatrix} \mathbf{A}_\mu \\ \mathbf{B}_\mu \end{bmatrix}, \quad (4.15)$$

in the present discrete context (and for a sufficiently fine discretization $\{x_j, j = 1, m\} \subseteq \Gamma_i$) Remark (4.3.2) tells us that the columns of the matrix \mathbf{C}_μ ought to be linearly independent. The normalization condition can be enforced by utilizing a QR-factorization

$$\mathbf{C}_\mu = \mathbf{Q}\mathbf{R};$$

in accordance with equation (4.15), further, we express the matrix \mathbf{Q} in terms of matrices comprising of its first n rows and the remaining m rows:

$$\mathbf{Q} = \begin{bmatrix} \mathbf{Q}_A \\ \mathbf{Q}_B \end{bmatrix}. \quad (4.16)$$

(In a related but different context, a QR factorization was used in [11] to reduce or even eliminate difficulties associated with the method of particular solution for evaluation of

Laplace eigenvalues; see Remark 4.3.3 for details.)

The linearly independent columns of the matrix \mathbf{C}_μ are in fact (discrete) approximate solutions of the Helmholtz equation evaluated at the boundary points and the points on Γ_i . Therefore, so are the columns of the matrix \mathbf{Q} , since they are linear combinations of the columns of \mathbf{C}_μ . Thus, letting \mathbf{d} denote a singular vector of the matrix \mathbf{Q}_A ($\|\mathbf{d}\| = 1$) corresponding to a singular value equal to zero, $\mathbf{Q}_A \mathbf{d} = 0$ and we must necessarily have $\|\mathbf{Q}_B \mathbf{d}\| = 1$ (this follows from the orthonormality of the columns of \mathbf{Q}). Denoting $\mathbf{c} = \mathbf{R}^{-1} \mathbf{d}$, the product $\mathbf{C}_\mu \mathbf{c} = \mathbf{Q} \mathbf{d}$ is a linear combination of the columns of \mathbf{C}_μ which vanishes on Γ and for which, therefore, the mean square on Γ_i equals one. From the previous discussion in this section, the vector \mathbf{c} is a discrete version of the density ψ which yields an approximate eigenfunction of the problem (4.1) (Section 4.4) via a discrete version of the representation (4.2).

Thus, relying on the Singular Value Decomposition (SVD) of the matrix \mathbf{Q}_A for a given value of μ , and calling $\tilde{\eta}_n(\mu)$ the smallest of the corresponding singular values,

$$\tilde{\eta}_n(\mu) = \min_{\mathbf{b} \in \mathbb{R}^n, \|\mathbf{b}\|=1} \|\mathbf{Q}_A(\mu) \mathbf{b}\| = \|\mathbf{Q}_A(\mu) \mathbf{d}\|, \quad (4.17)$$

the proposed eigensolver is based on finding values of μ for which $\tilde{\eta}_n(\mu)$ is equal to zero. A pseudocode for this method is presented in Algorithm 3.

Algorithm 3 Numerical evaluation of all $\mu \in [F_{min}, F_{max}]$ for which (4.5) is satisfied.

- 1: Read input parameters h (cf. Remark 4.2.1) and N_0 (number of singular values in the wave number search range $[F_{min}, F_{max}]$ actually to be produced via SVD).
 - 2: **for** $j = 1 : N_0$ **do**
 - 3: Set $\mu := F_{min} + j \frac{F_{max} - F_{min}}{N_0}$.
 - 4: Construct the matrix of the discrete operator \mathbf{A}_μ (Algorithms 1 and 2).
 - 5: Construct the matrix of the discrete operator \mathbf{B}_μ (eq. (4.14)).
 - 6: Compute the QR-factorization of the augmented system \mathbf{C}_μ (eq. (4.15)).
 - 7: Compute the minimal singular value $\sigma_n(\mu_j)$ of \mathbf{Q}_A (cf. eq. (4.16)).
 - 8: **end for**
 - 9: Utilizing the computed values of $\sigma_n(\mu_j)$ execute the root-finding algorithm mentioned in Section 4.3.3 to produce approximate roots of the function $\sigma(\mu)$.
-

Remark 4.3.3. *As mentioned in the introduction, the method of particular solutions (MPS) relies on use of Fourier-Bessel series that match homogeneous Dirichlet boundary conditions to produce Laplace eigenvalues and eigenfunctions. A modified version of the MPS, which was introduced in reference [11], alleviates some difficulties that occur in the original version of the method by enforcing that, as is necessary in our case as well, the proposed eigenfunctions do not vanish (and, indeed, are normalized to unity) in some finite set of points in the interior of the domain. In fact, the QR-based normalization method we use is similar to that introduced in [11] and referred to as GSVD in [10]. The difficulties underlying eigenvalue search in the present integral-equation context are different from those found in the approach [11], however. Indeed, as discussed in Section 4.3.1, in the former case a phenomenon related to the Riemann-Lebesgue lemma is at work: highly oscillatory integrands of unit norm can yield small integrals. In the latter case, in contrast, the root cause lies in the fact that linear combinations of a number n of Bessel functions with coefficients of unit norm (say, in the mean square sense) can be selected which tend to zero as n grows. (Notice that, in view of the $z \rightarrow 0$ asymptotics $J_n(z) \sim \mathcal{O}(z^n)$, this fact bears connections with a well known result concerning polynomial interpolation: linear combinations of n monomials can be made to tend to zero rapidly as n grows—for example, the monic Chebyshev polynomial*

of order n tends to zero exponentially fast as $n \rightarrow \infty$.)

4.3.3 Sign changing procedure for the minimum singular value.

Consideration of Figure 4.1 clearly suggests that the function $\tilde{\eta}_n$ is a continuous but non-smooth function of μ . As is known [11, 128], however, a sign-changing methodology suffices to produce singular values as smooth (indeed analytic) functions of μ —so that high-order interpolation and root finding becomes possible. With reference to Algorithm 3, using approximate values of $\sigma_n(\mu_j)$ at points on the uniform mesh μ_j , our algorithm relies on calculation of signed singular values and subsequent polynomial interpolation to approximate the zeros of the function $\tilde{\eta}_n(\mu)$. The overall sign-changing/interpolation root-finding algorithm we use is essentially identical to that presented in [11, p. 488]. To obtain the approximate roots with prescribed error tolerance, further, we implement this procedure using nested uniform meshes around each approximate root found.

Remark 4.3.4. *The recent contribution [131] uses the Fredholm determinant to obtain a smooth function of μ that vanishes whenever μ corresponds to an eigenvalue, and it compares the efficiency of that solver to one based on consideration of singular values as a function of μ for which the singular values are merely piecewise smooth functions. The sign changing procedure described in this section, however, gives rise to smooth (analytic) dependence of the singular values as functions of μ , and thereby eliminates the potential difficulties suggested in [131].*

4.4 Eigenfunction evaluation

After the eigenvalues are obtained, the corresponding eigenfunctions can be evaluated for both FC-based and graded-mesh solvers using the representation (4.2). High-order approximate evaluation of this integral for points x sufficiently far from the boundary Γ , for which the corresponding integral kernels are smooth, is performed using the quadrature (2.102) in the case of a FC-based algorithm, and the combination of graded-mesh change of variables

and a trapezoidal rule (3.15) in the case of a graded-mesh algorithm. Methods for the evaluation of the eigenfunction in case the point x is on the boundary Γ (more precisely, on the Neumann boundary portion Γ_N , since the eigenfunctions admit zero values on the Dirichlet portion Γ_D) have already been described in detail in sections 2.4–4.2. Lastly, in case the point x is close to the boundary Γ the corresponding kernels exhibit a near-singularity. In this case an interpolation approach is used to evaluate the eigenfunction $u(x)$ at a point x : letting x_0 denote the point in Γ that is closest to x and letting L denote a straight segment passing through the points x and x_0 , the values of u at a small set of points $x_j \in L$ ($j = 0, 1, \dots$) that, except for x_0 , are sufficiently far from the boundary Γ are used to produce the value $u(x)$ by means of an interpolating polynomial. (Typically cubic or quartic polynomials were used to produce the images presented in this chapter.) To reach a prescribed tolerance it may be necessary to use increasingly fine meshes $\{x_j\}$ for which some or all elements may be closer to Γ than is required for accurate integration by means of the available boundary mesh. In such cases the Chebyshev boundary expansions that produce the solution can be oversampled (by means of zero padding of the corresponding cosine expansion) to a mesh that is sufficiently fine to produce sufficiently accurate integrals at each one of the points x_j —and the interpolation procedure then proceeds as indicated above.

4.5 Numerical results

This section presents results of numerical experiments which demonstrate the accuracy, efficiency and high-order character of the proposed eigensolver. In preparation for this discussion we note that there are only a few Zaremba eigenproblems whose spectrum is known in closed form: even for geometries such as a disc, which are separable for both the pure Dirichlet or Neumann eigenproblem, no Zaremba spectra for nontrivial selections of Γ_D and Γ_N have been evaluated explicitly. We thus first demonstrate the performance of our algorithms for a Zaremba problem for which the spectrum is available: an isosceles right triangle. We next compute the first few eigenvalues of the Zaremba problem in smooth domains (both convex and non-convex) for which no spectra have previously been put forth—either in closed form

or otherwise. As reference solutions for such problems we use results of computations we produced on the basis of well-established and validated finite element codes [63]. We emphasize that no attempt was made to optimize these finite element computations beyond the use of mesh adaptation near singular points. In addition, for certain polygonal domains with obtuse angles we compare our results with existing validated numerical simulations [89], and we then demonstrate the behavior of our algorithm in a number of challenging problems.

In all, our examples include:

- 1) A problem on a convex polygonal domain (with a Dirichlet-Neumann junction occurring at a vertex with angles of less than $\frac{\pi}{2}$; (Section 4.5.1).
- 2) An application of the FC-based solver to smooth, convex domain; (Section 4.5.2).
- 3) An application of the FC-based solver to smooth non-convex domain; (Section 4.5.3).
- 4) A problem on a polygonal domain with the Dirichlet-Neumann junction occurring at an angle greater than $\frac{\pi}{2}$. In this case, we set up the experiments to compare with corresponding theoretically-identical Laplace-Dirichlet eigenvalues of a symmetry-related domain; (Section 4.5.4).
- 5) A comparison of the performance of the FC-based and graded-mesh algorithms described in Sections 2.5 and 3.3 when both are applied to a smooth domain. (The superior performance of the FC-based algorithm dramatically improves the overall performance of the eigensolver); (Section 4.5.5).
- 6) Applications concerning high-frequency eigenvalue problems (evaluating thousands of eigenvalues and eigenfunctions, and showing, in particular, that the proposed eigensolver can successfully capture the asymptotic distribution of Zaremba eigenvalues); (Section 4.5.6).
- 7) Eigenproblems posed in multiply connected domains; (Section 4.5.7).
- 8) Applications to pure Dirichlet and pure Neumann eigenvalue problems; (Section 4.5.8).

All of the listed digits for eigenvalues produced by the various FC-based and graded-mesh eigensolvers are significant (with the last digit rounded to the nearest decimal), while in the values produced by the FEM methods a number of digits additional to the correct ones are presented (to avoid rounding the first or second decimal).

4.5.1 Convex polygonal domains

In this section the performance of the graded-mesh algorithm on simple polygonal domains is analyzed. Such domains provide instances of geometries where true eigenvalues of problem (4.1) can be computed analytically using reflection techniques. In detail, we consider the Zaremba problem on the isosceles triangle with corners $(0,0)$, $(0,1)$, and $(1,0)$. Neumann data is prescribed along one side of unit length, and Dirichlet data is prescribed along the other two sides. For this geometry the eigenvalues of (4.1) are a subset of the set of Neumann eigenvalues of a square with corners $(-1,0)$, $(1,0)$, $(1,2)$, and $(-1,2)$. More specifically, if we pick Neumann eigenfunctions of the square which have the correct symmetries, the corresponding eigenvalues are the same as those of the Zaremba problem on the described triangle. We can explicitly compute these eigenvalues on the square to be

$$\lambda_{k,\ell} = \frac{(2k+1)^2 + (2\ell+1)^2}{4} \pi^2, \quad k, \ell = 0, 1, 2, 3, \dots \quad (4.18)$$

The comparison of the approximate eigenvalues computed on the basis of 328 and 1200-point boundary meshes and the exact eigenvalues is shown in Table 4.1; corresponding eigenfunctions are depicted in Figure 4.4.

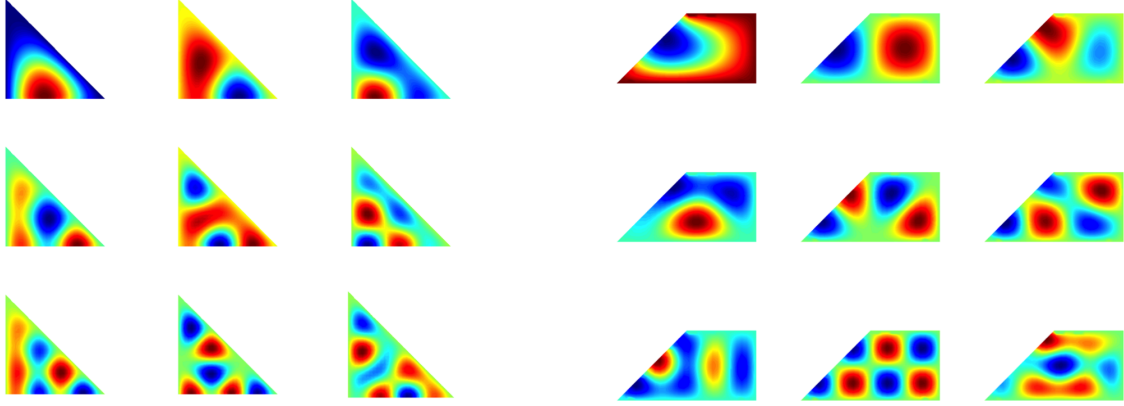


Figure 4.4: Left: Zaremba eigenfunctions for the triangular-domain eigenproblem considered in Section 4.5.1. Right: Zaremba eigenfunctions for the trapezoid-shaped-domain eigenproblem considered in Section 4.5.4.

k	ℓ	$\lambda_{k,\ell}$ exact	$\lambda_{k,\ell}$ ($n = 328$)	$\lambda_{k,\ell}$ ($n = 1200$)
0	1	24.6740110027234	24.67401100	24.6740110027234
0	2	64.1524286070808	64.15242861	64.1524286070809
1	2	83.8916374092595	83.89163742	83.8916374092596
0	3	123.3700550136170	123.3700550	123.3700550136170
1	3	143.1092638157957	143.1092638	143.1092638157957
2	3	182.5876814201531	182.5876814	182.5876814201531
0	4	202.3268902223318	202.3268902	202.3268902223319

Table 4.1: Eigenvalues $\lambda_{k,\ell}$ for the isosceles triangle considered in Section 4.5.1 produced by the proposed graded-mesh eigensolver with $n = 328$ and $n = 1200$ compared to results produced by the closed form expression (4.18).

4.5.2 Convex smooth domains

In the case of smooth domains the Dirichlet-Neumann junction takes place at a vertex with interior angle equal to π , and, thus, the corresponding eigenfunction of (4.1) is continuous but not twice continuously differentiable up to the boundary; see e.g. [122]. This fact gives rise to challenges for volumetric strategies; in particular, high-order conforming elements do

not yield high-order accuracy for this problem. Our proposed boundary integral strategy coupled with the high-accuracy FC discretization of integral operators, in turn, efficiently provides high-order convergence and highly-accurate results.

These facts are illustrated in Tables 4.2 and 4.3, which present the first Zaremba eigenvalue for the unit disc as produced by the P1 and P2 FEM algorithm [63] and the FC-based eigensolvers. Clearly the convergence resulting from the FEM methods is slow: Table 4.2 shows that, even using a mesh containing over 10,000-triangles, the FEM methods produce results with no more than 2 digits of accuracy. The FC results displayed in Table 4.3, in turn, demonstrate that the FC solver produces eigenvalues with 10 digits of accuracy using a discretization containing a mere 512 mesh points.

N_t	636	2538	10120	39662
P1	1.59	1.57	1.56	1.55
P2	1.56	1.56	1.55	1.55

Table 4.2: Convergence of first Zaremba eigenvalue on the disc. P1 and P2 FEM approaches. Here N_t is the number of triangles in the mesh.

n	64	128	256	512
λ_1	1.548549	1.54854933	1.5485493331	1.548549333189

Table 4.3: Convergence of the FC-based eigensolver: first Dirichlet-Neumann Laplace eigenvalue in the unit disc.

For reference, Table 4.4 presents corresponding results produced by P1, P2, and P1 Non-Conforming (Crouziex-Raviart) FEM methods as well as the proposed FC-algorithm for the first 10 Zaremba eigenvalues on the disc. Once again the convergence of the FEM algorithms is slow, and, using tens of thousands of unknowns, yield no more than 3 digits of accuracy. The corresponding 10 eigenvalues produced by the FC method, in turn, do contain at least a full 13 digits of accuracy.

P1	P1 NC	P2	FC eigensolver
1.55	1.54	1.55	1.548549333189
6.68	6.64	6.68	6.668097160848
8.66	8.66	8.66	8.662779904509
14.82	14.74	14.80	14.782583814100
17.86	17.83	17.85	17.848357621645
21.21	21.20	21.20	21.204559421807
25.83	25.73	25.81	25.781212572974
29.65	29.56	29.63	29.605375911651
35.93	35.90	35.92	35.914231714109
37.80	37.74	37.78	37.767236907914

Table 4.4: The first 10 Zaremba eigenvalues on the unit disc. The P1 conforming and P1 non-conforming computations are on a mesh of 40144 triangles (3 digit accuracy). The P2 conforming FEM computations are on 10136 triangles (3 digit accuracy). In contrast, 512 points suffice for the FC eigensolver (Section 2.5) to produce the eigenvalues with an accuracy of 13 digits).

4.5.3 Smooth, non-convex domains

In this experiment we consider a non-convex kite-shaped domain with smooth boundary parametrized by

$$x_1 = \cos(t) + 0.65 \cos(2t) - 0.65 \quad \text{and} \quad x_2 = 1.5 \sin(t), \quad (4.19)$$

with the Neumann and Dirichlet boundary portion Γ_N and Γ_D corresponding to $t \in [\pi/2; 3\pi/2]$ and its complement, respectively. No exact solution for this problem is available. We compare the performance of our FC-based algorithm with the performance of three finite element methods: a P1 conforming method, a P1 non-conforming (Crouziex-Raviart) method, and a P2 conforming method. The convergence of the finite element methods is once again slow: we present FEM results with three significant digits which require tens of thousands of unknowns. In contrast, the FC-based eigensolver yields 13 digits of accuracy on the basis of a mere 512 points boundary discretization. These results are detailed in Table 4.5.

In Table 4.6 we list the computational times for the FC-based solver to compute first 12 eigenvalues for the geometries considered in Sections 4.5.1 and 4.5.3. All times are given on a per-eigenvalue basis.

Crouzeix-Raviart	P1 conforming	P2 conforming	FC-based eigensolver
2.49	2.49	2.49	2.494957693616
6.24	6.26	6.25	6.253748349225
8.03	8.04	8.04	8.042440637044
12.03	12.08	12.06	12.053365383455
13.38	13.43	13.42	13.406406452033
18.04	18.06	18.05	18.047848229702
19.08	19.20	19.17	19.137393493839

Table 4.5: Numerical experiments for the kite-shaped domain. The P1 (both conforming and non-conforming) FEM methods use 40144-triangle meshes, whereas the P2 method uses a 5156-triangle mesh. The FC-based eigensolver uses 512 boundary points.

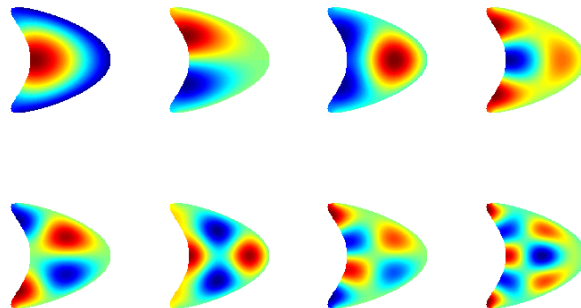


Figure 4.5: Zaremba eigenfunctions for the kite-shaped-domain eigenproblem described in Section 4.5.3.

4.5.4 Polygonal domains with obtuse Dirichlet-Neumann junctions

The L-shaped domain provides an important test case. In reference [89] a set of validated numerical experiments is presented for the Dirichlet eigenvalue problem on an L-shaped domain (a square of side length two with a unit square removed). These numerical results were produced by means of finite element discretizations. For the first Dirichlet eigenvalue, a *provable* interval [9.5585, 9.6699] which brackets the true eigenvalue is provided.

Using symmetry arguments it can be easily seen that some of the Zaremba eigenvalues for the trapezoid that results by cutting the L-shaped domain along a symmetry line coincide with certain Dirichlet eigenvalues on the L-shaped domain. The graded-mesh algo-

Domain	Time (err. 10^{-5})	Time (err. 10^{-10})
Disc	0.09 s	1.13 s
Kite	0.18 s	1.88 s

Table 4.6: FC-based eigensolver. Computational times per-eigenvalue for the first 12 eigenvalues.

i	Lower bound	Upper bound	λ_i (graded-mesh eigensolver)
1	9.55	9.66	9.639723844021955
3	19.32	19.78	19.739208802178748
5	30.86	32.05	31.912635957137709

Table 4.7: Eigenvalues corresponding to the symmetric eigenfunctions for the L-shaped domain. Comparison with table 5.5 in [89]. Eigenvalues produced by means of the graded-mesh eigensolver are computed with at least 13 digits of accuracy (by convergence analysis).

rithm introduced in this thesis produces the approximation 9.639723844021955 for the first eigenvalue—clearly within the guaranteed interval—and several other eigenvalues are computed without difficulty (see Figure 4.4). Table 4.7 displays the eigenvalue bounds resulting from use of the FEM algorithm from reference [89, Table 5.5] as well as those produced by means of the graded-mesh algorithm presented in this thesis. Figure 4.4 (right) presents depictions of several Zaremba eigenfunctions on the trapezoid mentioned above. In Table 4.8 we list the computational times for the graded-mesh solver to compute first 12 eigenvalues for the geometries considered in Sections 4.5.2 and 4.5.4. All times are given on a per-eigenvalue basis.

Domain	Time (err. 10^{-5})	Time (err. 10^{-10})
Triangle	0.07 s	1.19 s
Trapezoid	0.18 s	1.89 s

Table 4.8: Graded-mesh eigensolver. Computational times per-eigenvalue for the first 12 eigenvalues.

4.5.5 Comparison of FC-based and graded-mesh approaches

Sections 2.5 and 3.3 describe FC-based and graded-mesh eigensolvers for high-order evaluation of Zaremba eigenvalues on smooth and Lipschitz geometries, respectively. As indicated in Remark 2.5.3, however, the graded-mesh algorithm can also be applied to smooth geometries. Figure 4.6 compares the convergence history for both of these algorithms as they are used to obtain the Zaremba eigenvalue $\lambda_{18} = 73.1661817902$ for the unit disc (where Dirichlet and Neumann boundary conditions are prescribed on the upper and lower halves of the disc boundary). This figure demonstrates a general fact: for smooth geometries the FC-based approach significantly outperforms the (more generally applicable) graded-mesh algorithm. The somewhat slower convergence of the graded-mesh solver relates, in part, to the relatively large value $\alpha = 1$ associated with the 180° angle that occurs at Dirichlet-Neumann junctions on smooth curves; cf. Remark 3.3.3.

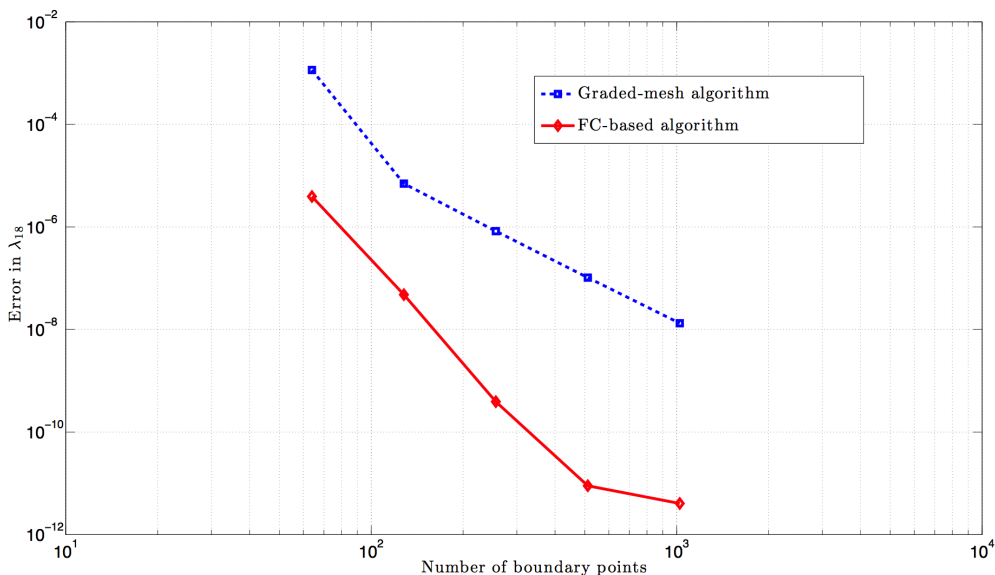


Figure 4.6: Sample convergence history resulting from the FC-based eigensolver and the graded-mesh eigensolver for the eighteenth Zaremba eigenvalue λ_{18} discussed in Section 4.5.4. The computational times required for evaluation each one of the eigenvalue approximations by means of the FC solver and the graded-mesh solver are as follows. FC-solver times: 0.23s, 0.67s, 2.82s, 19.19s, 119.7s. Graded-mesh solver: 0.09s, 0.60s, 1.93s, 16.11s, 112.90s. We note, for example, that an error of 10^{-7} results from the FC-solver in this case in a computational time of 0.67 seconds; for the same accuracy, the computing time required by the graded mesh solver is 16.11 seconds.

4.5.6 High-frequency wave numbers

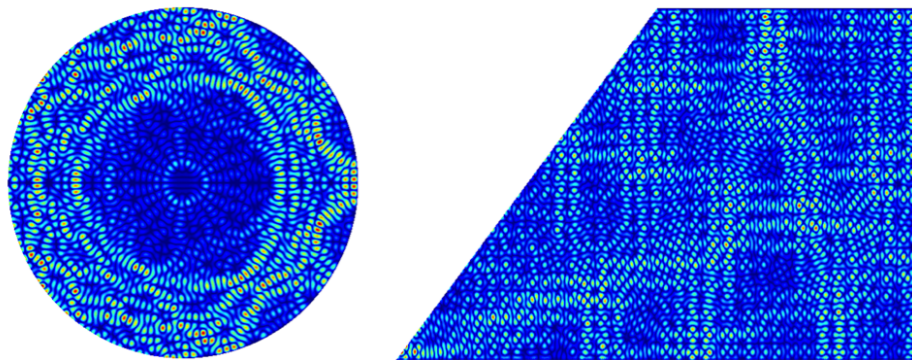


Figure 4.7: High frequency eigenfunctions mentioned in Section 4.5.6.

The high-order convergence of the algorithms presented in this thesis enables evaluation of eigenvalues and eigenfunctions in very wide frequency ranges. For example, we have used our solver to produce the first 3668 eigenvalues and eigenfunctions for the eigenproblem mentioned in Section 4.5.4 with a full 13 digits of accuracy (the eigenvalues are displayed in Figure 4.8 (left)). The single-core computational time required for evaluation of the first 9 eigenvalues was 17 seconds, while for the last 9 eigenvalues (that correspond to higher values of λ , and, therefore, finer discretization meshes required for a given accuracy) the computational time was 189 minutes. In another example, Figure 4.7 shows an eigenfunction for a unit disc corresponding to the eigenvalue $\lambda = 10005.97294969$ (left) and an eigenfunction for a trapezoid (that also corresponds to symmetric Laplace-Dirichlet eigenfunction for L-shaped domain (cf. Section 4.5.4) corresponding to the eigenvalue $\lambda = 40013.2312203$ (right)).

Our next experiment concerns the number $N(x)$ of Dirichlet-Neumann eigenvalues λ satisfying $0 < \lambda \leq x$. Since, as is known, Zaremba eigenvalues lie between corresponding Dirichlet and Neumann eigenvalues, the Zaremba eigenvalues must obey the Weyl asymptotic relation [100, 118, 123, 124]

$$\lim_{x \rightarrow \infty} \frac{N(x)}{x|\Omega|} = C_d. \quad (4.20)$$

Here $|\Omega|$ is the volume of the domain $\Omega \subset \mathbb{R}^d$ and, letting ω_d equal the volume of the

unit ball in d dimensions, $C_d = (2\pi)^{-d}\omega_d$ denotes the Weyl constant. The right portion of Figure 4.8 displays the ratio $N(x)/(x|\Omega|)$ as a function of x for the Zaremba case, and for all of the geometries considered earlier in this Section: a triangle (Section 4.5.1), the unit disc (Section 4.5.2), a kite-shaped domain (Section 4.5.3), and a trapezoid (Section 4.5.4). This figure clearly shows that the numerical solutions satisfies the asymptotic relation (4.20).

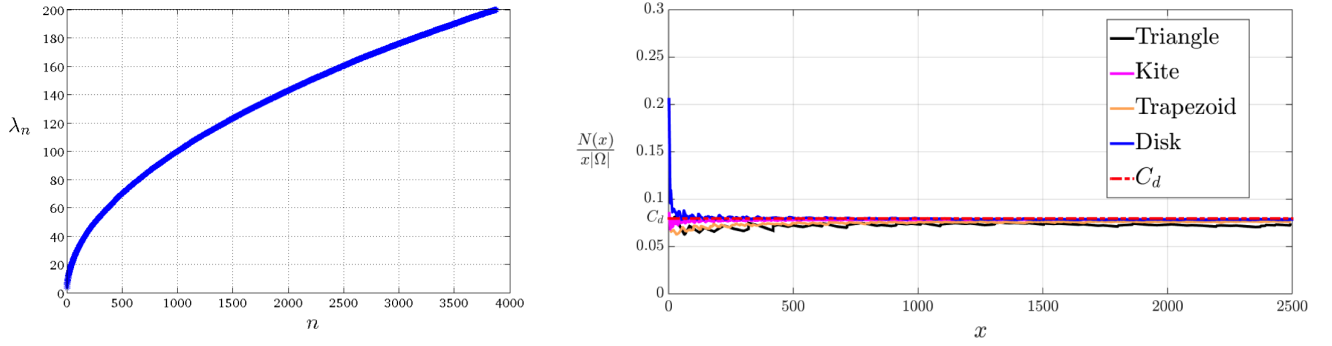


Figure 4.8: Left: First 3668 Zaremba eigenvalues for the trapezoidal domain eigenproblem considered in Section 4.5.4. Right: Ratio $\frac{N(x)}{x|\Omega|}$ (eq. (4.20)) for Zaremba eigenvalue problems on various domains and, in red, the Weyl constant C_d .

4.5.7 Multiply connected domains

This section discusses application of the proposed eigensolver methodologies to multiply connected domains—for which integral eigensolvers generally produce spurious resonances that result from eigenvalues of the domains interior to inner boundaries [27, 28], as demonstrated by the right image in Figure 4.9. We have found that by enforcing an additional condition based on use of interior points in a manner related to that considered in Section 4.3—which, in the present case, is designed to ensure that the function u in equation (4.2) vanishes in the set Ω_i consisting of all the bounded components of the complement of Ω —a new version of the function $\tilde{\eta}_n(\mu)$, denoted by $\hat{\eta}_n(\mu)$ in what follows, is obtained that equals zero only at the true eigenvalues of the given multiply connected domain. In order to ensure vanishing throughout Ω_i the algorithm utilizes a sufficiently fine set of points interior to Ω_i arranged on a curve that is roughly parallel to the boundary of Ω_i at a distance no larger than $\lambda_u/2$ from that boundary. An argument analogous to the one presented in Section 4.3.2 shows

that, indeed, a prospective eigenfunction must vanish throughout Ω_i provided it vanishes on such a set of interior points.

In detail, the algorithm utilizes a certain matrix D_μ which, based on the quadrature rules for smooth integrands described in Section 4.4, approximates the values of the single-layer potential (4.2) at the aforementioned set of interior points. Clearly, D_μ is uniquely defined for each given set of interior points in Ω_i and for each given set of boundary discretization points. Letting n_i and n denote the numbers of interior points and boundary discretization points, respectively, we note that the first n_i columns (resp. the last $n - n_i$ columns) of the matrix $V = [v_1, \dots, v_n]$ in the SVD

$$D_\mu = U\Sigma V^T \quad (4.21)$$

of the matrix D_μ correspond to nonzero singular values (resp. zero singular values) of D_μ , and thus, in particular, the last $n - n_i$ columns of V span the kernel of the matrix D_μ . Defining the matrix $V_1 = [v_{n_i+1}, \dots, v_n]$ whose columns equal the last $n - n_i$ columns of V , the matrix C_μ (equation (4.15)) can be restricted to the kernel of D_μ via multiplication on the right by the matrix V_1 . The resulting matrix $\widehat{C}_\mu = C_\mu \cdot V_1$ can then be treated by means of the approach described in Section 4.3.2: considering the QR-decomposition

$$\widehat{C}_\mu = \widehat{Q}\widehat{R}, \quad (4.22)$$

the algorithm finds the desired eigenvalues by seeking the zeros of the function $\widehat{\eta}_n(\mu)$ which is defined as the smallest singular value of the matrix \widehat{Q}_A consisting of the first n rows of \widehat{Q} .

To demonstrate the multiply-connected domain methodology, we consider a domain consisting of the polygon determined by the set of exterior vertices $(0, 0)$, $(0, 3)$, $(2, 4)$, $(3, 2)$, $(3, 0)$ and the set of interior vertices $(1, 1)$, $(1, 2)$, $(2, 3)$ with Dirichlet boundary conditions on all sides. Figure 4.9 depicts true and spurious eigenfunction for this domain corresponding to the eigenvalues $\lambda = 76.619031$ and $\lambda = 77.663162$, respectively. As can be seen in Figure 4.10, the procedure effectively screens out the spurious eigenvalue $\lambda = 77.663162$.

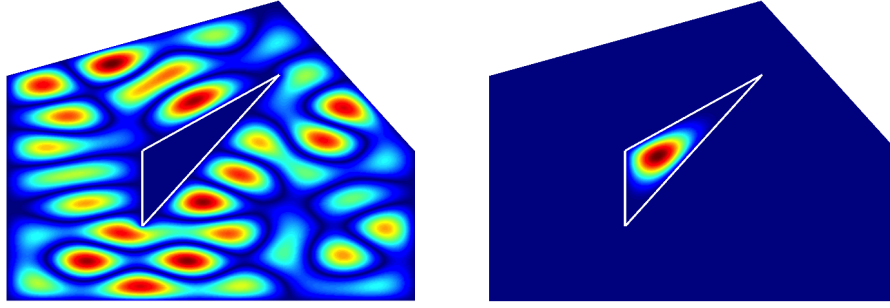


Figure 4.9: True and spurious eigenfunction for multiply connected domain. Left: true eigenfunction corresponding to $\lambda = 76.619031$. Right: spurious eigenfunction corresponding to $\lambda = 77.663162$.

4.5.8 Pure Dirichlet and Pure Neumann eigenfunctions

As mentioned in the introduction, the methods described in this thesis can be applied to a variety of eigenvalue problems (see Remark 4.3.1 for a discussion in these regards). In particular, Laplace eigenfunctions for pure Dirichlet or pure Neumann boundary conditions can be computed using the proposed eigensolver: both problems can be treated as particular cases of the more general Zaremba problem (for which $\Gamma_D = \emptyset$ or $\Gamma_N = \emptyset$, respectively). Sample eigenfunctions produced by our methods under pure Dirichlet and pure Neumann boundary conditions are presented in Figure 4.11.

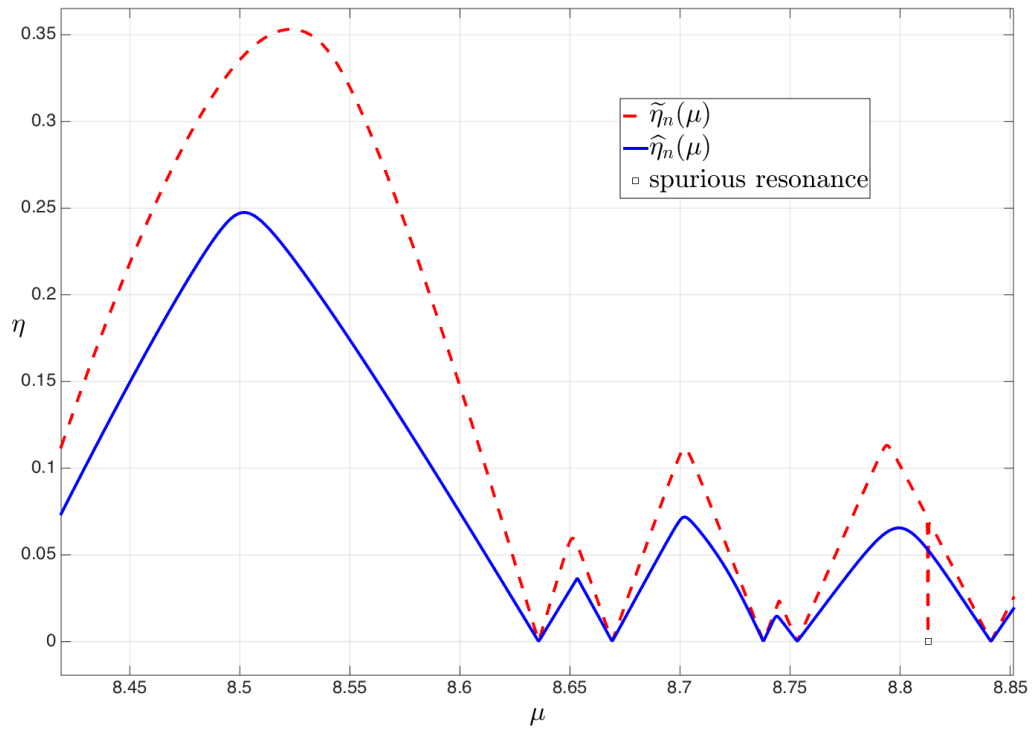


Figure 4.10: Filtering of spurious eigenvalue. Dashed curve: function $\tilde{\eta}_n(\mu)$; solid curve: $\hat{\eta}_n(\mu)$.

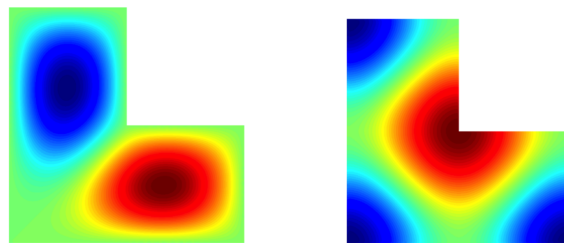


Figure 4.11: Eigenfunctions for L-shaped domain with Dirichlet (left) and Neumann (right) boundary conditions.

Chapter 5

Steklov eigenvalue solver

The results in this Chapter were obtained in collaboration with professor Nilima Nigam in addition to professor Oscar Bruno and Nurbek Tazhimbetov.

5.1 Preliminaries

We consider the eigenvalue problem

$$\begin{aligned}\Delta u_m &= 0 & x \in \Omega \\ \frac{\partial u_m}{\partial n} &= 0 & x \in \Gamma_N \\ \frac{\partial u_m}{\partial n} &= \lambda_m u_m & x \in \Gamma_S\end{aligned}\tag{5.1}$$

for eigenvalues λ_m and eigenfunction u_m , where $\Omega \subset \mathbb{R}^2$ is a bounded domain with a Lipschitz piecewise-smooth boundary Γ and where Γ_N and Γ_S are the Neumann and Steklov boundary portions, $\Gamma = \bar{\Gamma}_N \cup \bar{\Gamma}_S$, which are disjoint relatively-open subsets of Γ (see Figure 5.1). Of course problems containing a Dirichlet portion Γ_D are also important, but for conciseness here we only consider cases where $\Gamma_D = \emptyset$. In the case in which additionally $\Gamma_N = \emptyset$ the problem (5.1) is referred to as the Steklov eigenvalue problem and λ_m and u_m are called Steklov eigenvalues and eigenfunctions. If Γ_N is nonempty, problem (5.1) is called the sloshing eigenvalue problem—since (5.1) is the eigenfunction equation associated with small oscillations of the free surface of an ideal fluid subject to gravity [48, 69]—and λ_m and u_m are called the sloshing eigenvalues and eigenfunctions. Clearly, the Steklov problem coincides

with the eigenproblem for the Dirichlet-to-Neumann operator $\Lambda: H^{\frac{1}{2}}(\Gamma) \rightarrow H^{-\frac{1}{2}}(\Gamma)$, given by $\Lambda u = \partial_n(\mathcal{H}u)$, where $\mathcal{H}u$ denotes the unique harmonic extension of $u \in H^{\frac{1}{2}}(\Gamma)$ to Ω .

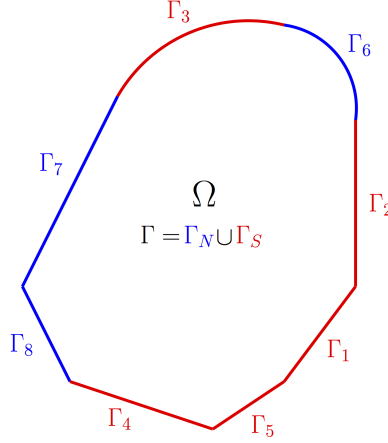


Figure 5.1: Boundary decomposition illustration. Red line: Steklov boundary. Blue line: Neumann boundary.

In what follows we assume the piecewise-smooth boundary Γ is expressed in the form

$$\Gamma = \bigcup_{q=1}^{Q_N+Q_S} \Gamma_q, \quad (5.2)$$

where Q_N and Q_S denote the numbers of smooth Neumann and Steklov boundary portions, and where for $1 \leq q \leq Q_N$ (resp. $Q_N + 1 \leq q \leq Q_N + Q_S$) Γ_q denotes a *smooth* Neumann (resp. Steklov) segment of the boundary curve Γ . Clearly, letting

$$J_N = \{1, \dots, Q_N\} \quad \text{and} \quad J_S = \{Q_N + 1, \dots, Q_N + Q_S\}$$

we see that

$$\overline{\Gamma}_N = \bigcup_{q \in J_N} \Gamma_q \quad \text{and} \quad \overline{\Gamma}_S = \bigcup_{q \in J_S} \Gamma_q$$

are the (piecewise smooth) portions of Γ upon which Neumann and Steklov boundary conditions are enforced, respectively. Throughout this chapter it is assumed that both Neumann-Steklov junctions and non-smooth points in Γ necessarily occur at a common endpoint of two segments Γ_{q_1} and Γ_{q_2} ($1 \leq q_1, q_2 \leq Q_N + Q_S$). (Note that consecutive values of the index q do not necessarily correspond to consecutive boundary segments; see e.g. Figure 5.1.) Without

loss of generality we assume that the boundary curve Γ possesses a (possibly non-smooth) 2π -periodic counterclockwise parametric representation of the form

$$x(t) = (x_1(t), x_2(t)), \quad 0 \leq t \leq 2\pi. \quad (5.3)$$

Parametrizations of the boundary portions Γ_q for each $q \in J_N \cup J_S$ are then given by the restriction of the function $x(t)$ to the interval $[a_q, b_q]$; in what follows it is assumed that $x(t)$ satisfies the regularity condition $[x'_1(t)]^2 + [x'_2(t)]^2 > 0$ for all $t \in [a_q, b_q]$ and for each $q \in J_N \cup J_S$. Clearly, $[0, 2\pi] = \cup_{q=1}^{Q_N+Q_S} [a_q, b_q]$ where the intersection of any subintervals in this union is either the empty set or a set containing a single point.

As is well known, the eigenvalues for both the Steklov and the sloshing problems form a discrete set; as is common practice these are enumerated in increasing order:

$$0 = \lambda_1(\Omega) \leq \lambda_2(\Omega) \leq \lambda_3(\Omega) \leq \dots \quad (5.4)$$

Note that for any domain Ω we have $\lambda_1(\Omega) = 0$ and u_1 is a constant function. Steklov eigenvalues are also characterized by the min-max formula

$$\lambda_k(\Omega) = \min \left\{ \frac{\int_{\Omega} |\nabla v|^2 dx}{\int_{\Gamma} v^2 ds} : v \in H^1(\Omega), \int_{\Gamma} v u_j = 0, j = 1, \dots, k-1 \right\}. \quad (5.5)$$

5.2 Integral equation formulation

Since for both Steklov and sloshing problem the eigenvalue condition $\frac{\partial u_m}{\partial n} = \lambda_m u_m$ concerns only the boundary values of the solution and its normal derivative, use of integral equation methods for problem (5.1) lead directly upon discretization, to a matrix eigenvalue problem. In fact, such approaches are used in [30, 68]. In order to avoid the inclusion of hypersingular operators (which are generally significantly more challenging from a computational perspective; see e.g. [20]) we use eigenfunction representations based on single layer

potential. Unfortunately, the simple representation

$$u(x) = S[\varphi] = \int_{\Gamma} \Phi(x - y)\varphi(y)ds(y) \quad (5.6)$$

(where $\Phi(x) = -\frac{1}{2\pi} \log |x|$ is a fundamental solution of two-dimensional Laplace equation) presents some difficulties: the single layer operator S restricted to the boundary may not be injective. (It is injective only provided the domain Ω satisfies the following condition: there exists a point $z_0 \in \Omega$ such that $|x - z_0| \neq 1$ for all $x \in \Gamma$ (see [80, Theorem 7.38].) A modified formulation

$$u(x) = \int_{\Gamma} \Phi(x - y)(\varphi(y) - M[\varphi])ds(y) + M[\varphi] \quad (5.7)$$

based on the averaging operator

$$M[\varphi] = \frac{1}{|\Gamma|} \int_{\Gamma} \varphi(y)ds(y) \quad (5.8)$$

is suggested in [80, Equation 7.58] that successfully eliminates the non-invertibility problem: as shown in [80, Theorem 7.41] the corresponding boundary operator is bijective. The proposed Steklov and sloshing eigensolvers for (5.1) are therefore based on use of the representation (5.7). Taking into account well known expressions (see e.g. [80]) for the jump of the single layer potential and its normal derivative across Γ , the eigenvalue problem (5.6) is reduced to a system of integral equations

$$\begin{aligned} & \int_{\Gamma} \frac{\partial \Phi(x - y)}{\partial n(x)} (\varphi(y) - M[\varphi])ds(y) + \frac{1}{2}(\varphi(x) - M[\varphi]) = \\ & = \lambda \left(\int_{\Gamma} \Phi(x - y)(\varphi(y) - M[\varphi])ds(y) + M[\varphi] \right) \quad x \in \Gamma_S \\ & \int_{\Gamma} \frac{\partial \Phi(x - y)}{\partial n(x)} (\varphi(y) - M[\varphi])ds(y) + \frac{1}{2}(\varphi(x) - M[\varphi]) = 0 \quad x \in \Gamma_N \end{aligned} \quad (5.9)$$

for λ and ϕ .

5.3 Nystrom method for Steklov eigenvalue problem on smooth domains

In cases in which the boundary Γ is smooth and $\Gamma_N = \emptyset$, the Steklov eigenfunctions u_m and the corresponding densities φ are smooth functions [76]. These problems can thus be treated by highly effective spectrally-accurate methods [34, 80], which, like those used in Chapters 2 and 3, are based on explicit resolution of logarithmic singularities on the bases of Fourier analysis. In order to construct a spectral method for approximation of the integral operators in equation (5.9) we first use the parametrization (5.3) to evaluate the point values of these operators at a point $x = (x_1(t), x_2(t))$ ($0 \leq t \leq 2\pi$) by means of the parametrization $y = (x_1(\tau), x_2(\tau))$ of the integration curve: using the notations $\psi(\tau) = \varphi(x_1(\tau), x_2(\tau))$ ($0 \leq \tau \leq 2\pi$) and letting $r(t, \tau) = \sqrt{(x_1(t) - x_1(\tau))^2 + (x_2(t) - x_2(\tau))^2}$, the system (5.9) of integral equations is thus re-expressed in the form

$$\begin{aligned} & \int_0^{2\pi} L(t, \tau)(\psi(\tau) - M[\varphi])d\tau + \frac{1}{2}(\psi(t) - M[\varphi]) = \\ & = \lambda \left(\int_{\Gamma} K(t, \tau)(\psi(\tau) - M[\varphi])d\tau + M[\varphi] \right) \quad t \in [a_q, b_q], q \in J_S \quad (5.10) \\ & \int_0^{2\pi} L(t, \tau)(\psi(\tau) - M[\varphi])d\tau + \frac{1}{2}(\psi(t) - M[\varphi]) = 0 \quad t \in [a_q, b_q], q \in J_N, \end{aligned}$$

where

$$\begin{aligned} L(t, \tau) &= \frac{1}{2\pi} \frac{(x'_2(t)[x_1(t) - x_1(\tau)] - x'_1(t)[x_2(t) - x_2(\tau)])}{r^2(t, \tau)} \sqrt{[x'_1(\tau)]^2 + [x'_2(\tau)]^2}, \\ K(t, \tau) &= \frac{1}{2\pi} \log [r(t, \tau)] \sqrt{[x'_1(\tau)]^2 + [x'_2(\tau)]^2}, \quad \text{and} \\ M[\varphi] &= \frac{\int_0^{2\pi} (\psi(\tau)) \sqrt{[x'_1(\tau)]^2 + [x'_2(\tau)]^2} d\tau}{\int_0^{2\pi} \sqrt{[x'_1(\tau)]^2 + [x'_2(\tau)]^2} d\tau}. \end{aligned} \quad (5.11)$$

In view of this expression for the integral operators, in which some things are periodic,

we employ the quadrature rule

$$\int_0^{2\pi} \log \left(4 \sin \frac{t - \tau}{2} \right) f(\tau) d\tau \approx \sum_{j=0}^{2n-1} R_j^{(n)}(t) f(t_j), \quad 0 \leq t \leq 2\pi, \quad (5.12)$$

with the quadrature weights given by

$$R_j^{(n)} := -\frac{2\pi}{n} \sum_{m=1}^{n-1} \frac{1}{n} \cos m(t - t_j) - \frac{\pi}{n^2} \cos n(t - t_j), \quad j = 0, \dots, 2n-1, \quad (5.13)$$

which result from certain explicit integrations [34] along with the trapezoidal rule

$$\int_0^{2\pi} f(\tau) d\tau \approx \frac{\pi}{n} \sum_{j=0}^{2n-1} f(t_j) \quad (5.14)$$

to approximate the integrals in (5.10). The resulting approximation of the integral equation system yields a generalized matrix eigenvalue problem of the form

$$\mathbf{A}\mathbf{X} = \mathbf{B}\mathbf{X} \quad (5.15)$$

which approximates spectrally the continuous eigenproblem, and which can be solved numerically by means of the QZ-algorithm (see [56]).

5.4 Graded-mesh algorithm for sloshing problem and Steklov problem on non-smooth domains

As soon as either the boundary Γ contains geometric singularities or Γ_N is nonempty the corresponding Steklov or sloshing eigenfunctions may (typically do) exhibit singularities near the corner points or Steklov-Neumann junctions [76]. In order to enable high-order solution

of the integral equations (5.9) we rely on the decomposition

$$\begin{aligned} \int_{\Gamma} \frac{\partial \Phi(x-y)}{\partial n(x)} (\varphi(y) - M[\varphi]) ds(y) &= \sum_{q=1}^{Q_N+Q_S} \int_{\Gamma_q} \frac{\partial \Phi(x-y)}{\partial n(x)} (\varphi(y) - M[\varphi]) ds_y \\ \lambda \int_{\Gamma} \Phi(x-y) (\varphi(y) - M[\varphi]) ds(y) &= \sum_{q=1}^{Q_N+Q_S} \int_{\Gamma_q} \frac{\partial}{\partial n_x} \Phi(x-y) (\varphi(y) - M[\varphi]) ds_y \end{aligned} \quad (5.16)$$

for the corresponding integral operators and we approximate each one of the integrals on the right-hand sides of (5.16) the integrals in (5.16) over each of the portions Γ_q using the change of variables of the form (3.10) (Section 3.3.1) that alleviates the singularities in the integral densities, and use the quadrature rules described in detail in Section 3.3.2.

5.5 Numerical results

In this section we present the results of several numerical experiments for the smooth domain and graded-mesh algorithms for Steklov and sloshing eigenvalue problems. Figure 5.2 depicts the spectral convergence of our eigensolver as it is used to calculate the first 32 Steklov eigenvalues of the kite-shaped domain (see equation 2.111).

The right portion of Figure 5.3 depicts sample Steklov eigenfunction for the star-shaped domain given by parametrization $x(t) = (1 + 0.3 \cos(5t)) \cos(t)$, $y(t) = (1 + 0.3 \cos(5t)) \sin(t)$ and the left portion depicts sample Steklov eigenfunction for the kite-shaped domain.

In the next experiment we demonstrate in Figure 5.4 the high-frequency Steklov eigenfunctions for the unit disc and the kite-shaped domain. Note that since the value of the Steklov eigenfunctions decays exponentially fast with the distance of the evaluation point to the boundary (see e.g. [54]), the absolute value of the high-frequency eigenfunction for the unit disc on Figure 5.4 is equal to the machine epsilon for the most of the domain interior.

In the next two experiments we demonstrate the capabilities of the Steklov eigensolver when it is applied to multiply connected domains. Weinstock [121] proved that for simply-connected planar domains the inequality

$$\sigma_1(\Omega) |\partial\Omega| \leq 2\pi \quad (5.17)$$

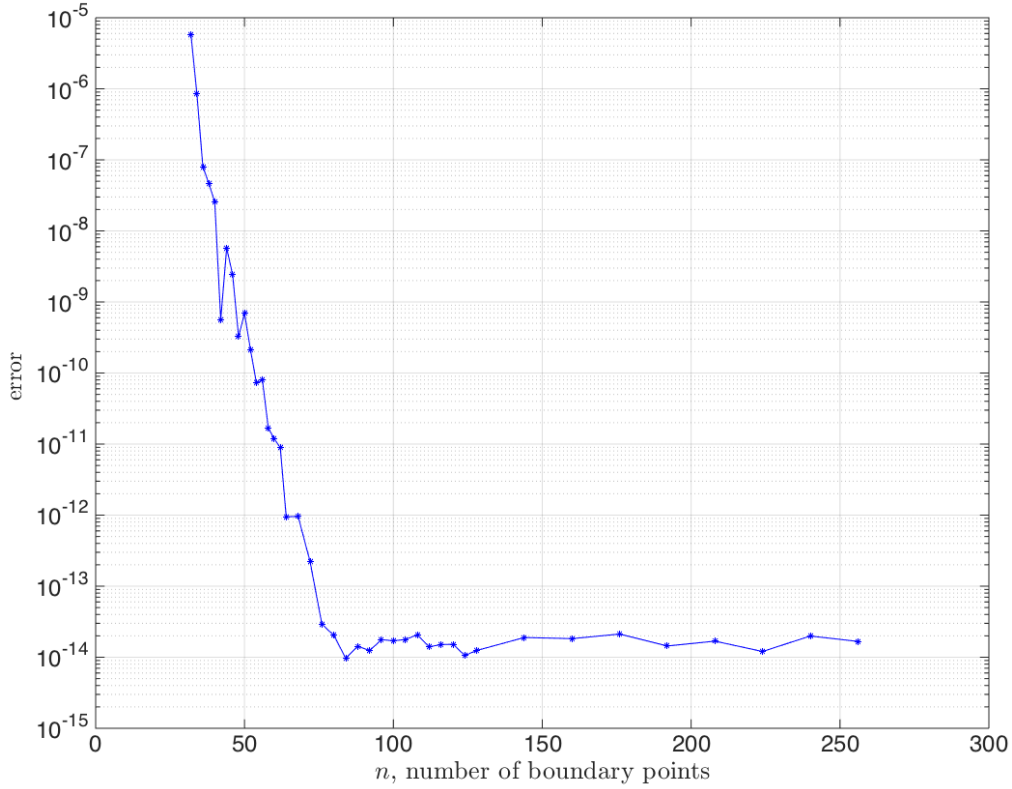


Figure 5.2: Maximum errors for the first 32 Steklov eigenvalues of a kite-shaped domain.

holds (cf. equation (1.4) and associated text). Reference [54] provides an example of the failure of this inequality for multiply connected domain (an annulus). Figure 5.5 (bottom) depicts the value $\sigma_1(\Omega)|\partial\Omega| - 2\pi$ for a family of annuli $\Omega = \epsilon \leq r \leq 1$ as a function of ϵ . Numerical experiments confirm that for $0 \leq \epsilon \leq \frac{\sqrt{17}-3}{4}$ the inequality (5.17) does not hold. This value can also be obtained using implicit relations for the Steklov eigenvalues of the annuli (see [54, Section 4.2]). Figure 5.5 (top) provides a comparison of the values $\sigma_1(\Omega)|\partial\Omega| - 2\pi$ for the annuli as well as domains with an exterior boundary given by a unit circle and interior boundary given by a circle of radius ϵ centered at point $(0.4, 0)$.

Figure 5.6 depicts a sample Steklov eigenfunction for a multiply connected domain containing 49 interior holes of randomly distributed radii. Figure 5.7, finally, displays a sample sloshing eigenfunction for a half-ellipse shaped domain obtained with our graded-mesh eigen-solver.

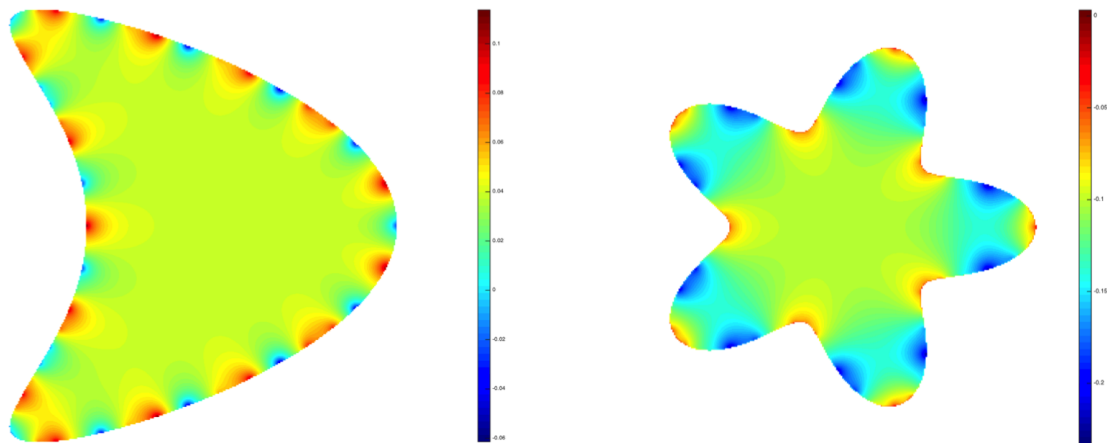


Figure 5.3: Steklov Eigenfunction for the kite-shaped domain (left) and the star-shaped domain (right).

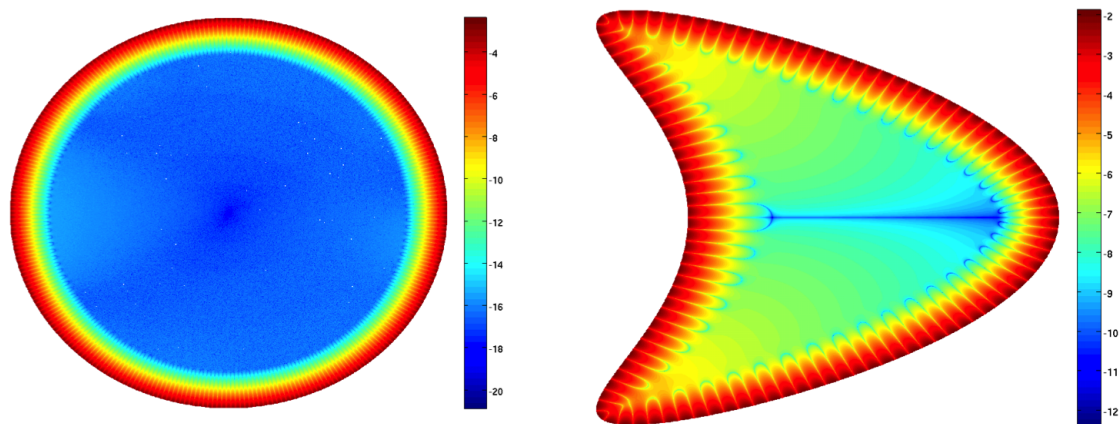


Figure 5.4: High-frequency Steklov eigenfunctions.

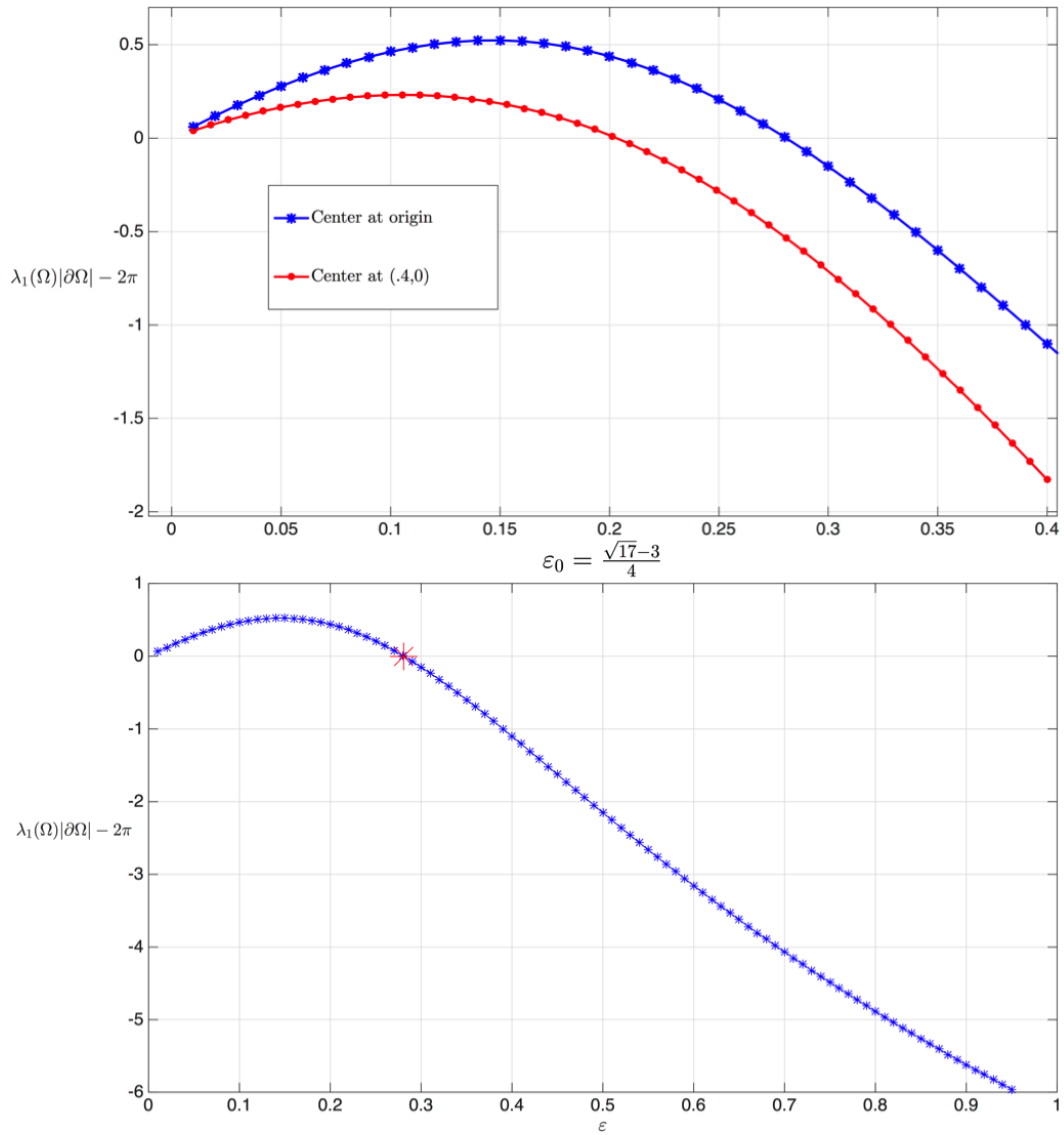


Figure 5.5: Failure of Weinstock inequality for multiply connected domains.

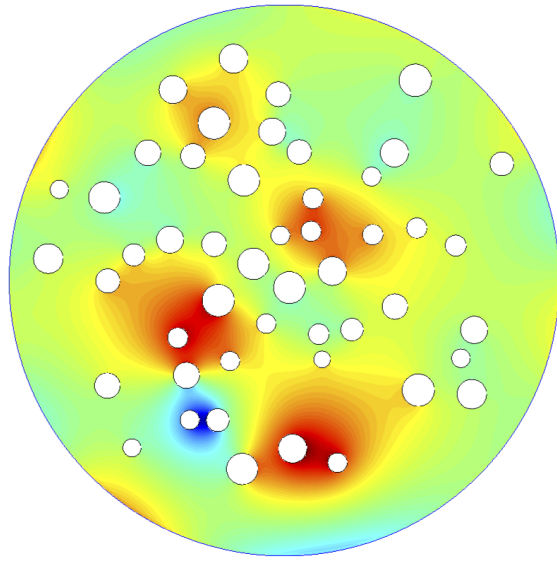


Figure 5.6: Steklov eigenfunction for a multiply connected domain.

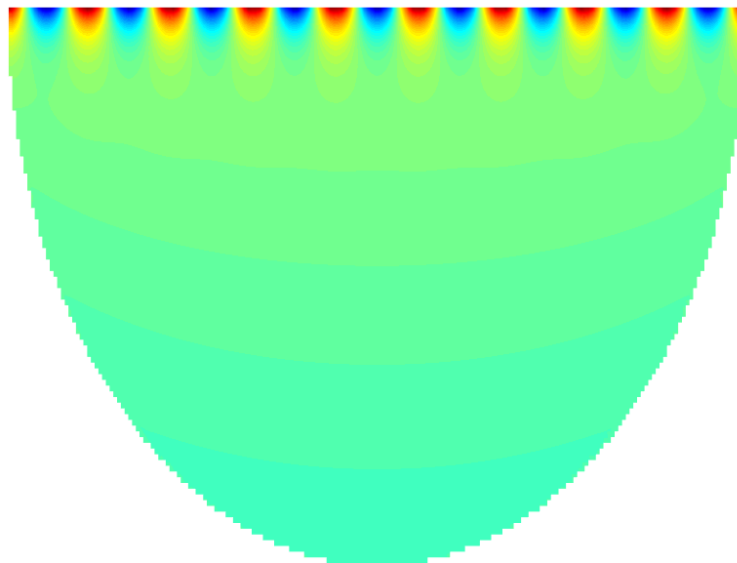


Figure 5.7: Sloshing eigenfunction.

Chapter 6

Conclusions and future work

6.1 Conclusions

This thesis has introduced a novel integral-equation methodology for solution of boundary value problems and Laplace and Steklov eigenproblems under a range of challenging boundary conditions. By precisely accounting for the singularities of the boundary densities and kernels, the relevant boundary integral operators are discretized with accuracies of very high order. Methods are presented for smooth domains where singularities arise from mismatch in boundary conditions (based on Fourier Continuation techniques) and for Lipschitz domains (based on use of graded meshes). A stabilization technique is used to obtain a robust non-local eigenvalue-search method. The resulting solvers allow for highly accurate and efficient approximation of scattering solutions, eigenvalues and eigenfunctions, even for cases that involve strongly singular solutions/eigenfunctions and/or very high frequencies; they can tackle a variety of elliptic problems under general boundary conditions; and they can generate eigenfunction expansions suitable for use in the solution of time-domain parabolic and hyperbolic problems in non-separable spatial domains.

6.2 Future work

In this section we describe a number of natural continuations of the present contributions which, we believe, provide a broad and enriching research program in both theoretical and computational aspects of scattering theory, spectral theory, and their applications in science and engineering.

6.2.1 Applications to antenna problems

This section contains a brief description of the application of the eigensolvers for various cross-sectional geometries of Quadruple Ridged Flared Horn (QRFH) antenna. The antenna is depicted in Figure 6.1; note the presence of multiple corners in each cross-section of the antenna structure; a typical cross-section is displayed on the left portion of Figure 6.2.

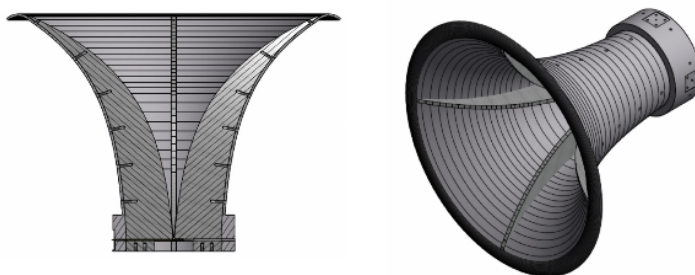


Figure 6.1: QRFH antenna.

The cross sections of the antenna are determined by two geometric parameters: thickness and gap values; see Figure 6.2 (left). From antenna theory, TE and TM modes (or Dirichlet and Neumann eigenvalues) of these cross sections are of particular practical significance.

Relying on integral direct and indirect formulations for Neumann and Dirichlet problems, respectively, Nystrom discretizations on graded meshes are used for each edge of the piecewise-smooth boundary. Figure 6.2 (right) displays a sample eigenmode obtained by the approaches under consideration (eigenvalue $\mu = 11.92174$ for a geometry with gap 1.86 and thickness value 0.05) (with radius normalized to one). A comparison with results provided by

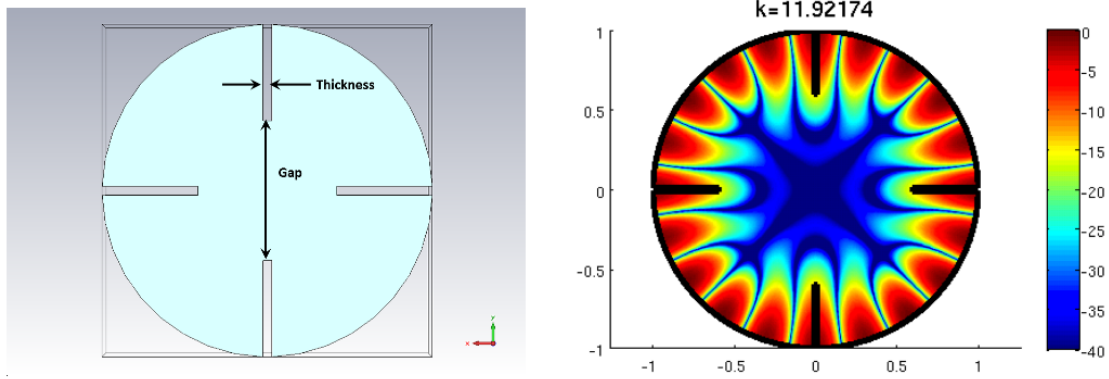


Figure 6.2: Left: QRFH antenna cross section. Right: sample TM mode.

a commercial EM software package is provided in Figure 4.1 as a function of the gap parameter and for thickness parameter equal to .02. The left portion of the figure demonstrates that the modes obtained by the proposed solver (star-shaped markers) generally coincide with the modes obtained by the commercial EM solver (circular markers). The right figure presents a zoom-in of a portion of the left figure, which emphasizes the fact that, in view of its limited accuracy, the commercial software does not correctly track individual eigenvalues, as antenna parameters are varied in such a way that eigenvalue branches approach each other. As can be seen in this figure, the present solver can be used to track eigenvalue branches effectively.

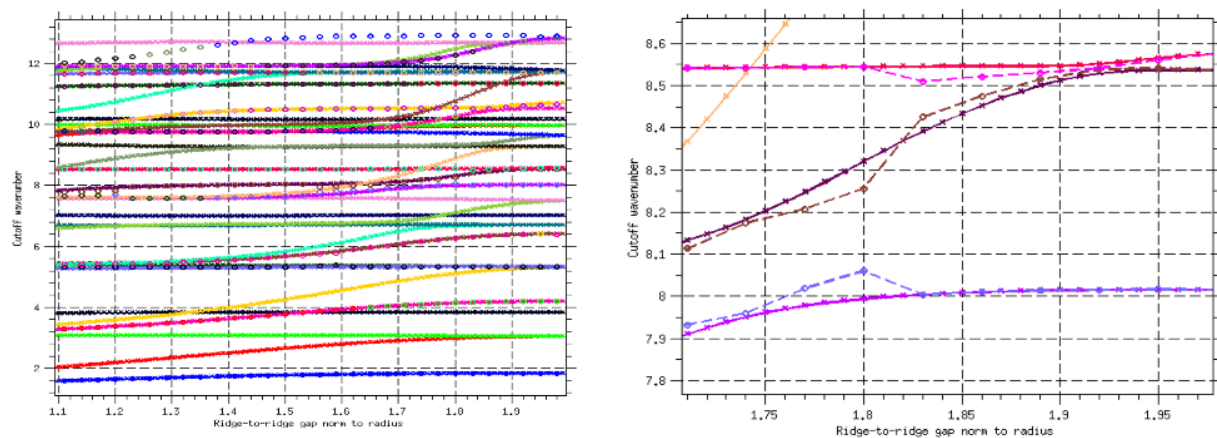


Figure 6.3: Mode tracking. Comparison with commercial solver.

6.2.2 Fully iterative solvers for eigenvalue problems.

In Chapter 4 eigenvalue searches for the Laplace eigenvalue problems are carried out by examining the minimum singular value $\sigma_n(\mu)$ of an appropriate discretized operator. If the number of discretization points is large, which is the case for two- and three-dimensional problems with high values of wavenumber μ , the direct SVD computation can become expensive. For such problems an alternative evaluation of $\sigma_n(\mu)$ based on accelerated operator implementations and fully-iterative algorithms is currently under development.

6.2.3 Solution of Zaremba problems for electromagnetic Maxwell equations.

As indicated in Chapter 1 the Zaremba problem also serves as a natural stepping stone for treatment of full electromagnetic problems with mixed transmission/perfect-conductor boundary conditions, such as those that are found in printed circuit boards, reflectarray antennas, etc. The schematic in Figure 6.4 shows a single conducting element “printed” on the surface of a dielectric substrate. Current work suggests that some of the main methodologies introduced in this thesis can be successfully extended to the more general dielectric/perfect-conductor electromagnetic context.

6.2.4 Transmission eigenvalues

Consider a simply connected domain Ω with boundary $\partial\Omega = \Gamma$. In the transmission eigenvalue problem, which arises as fundamental element in the solution of inverse scattering problem by means of the linear sampling method [23, 31], “transmission eigenvalues” k , $0 \leq \arg k \leq \pi/2$ are sought along with and a non-vanishing pair of functions

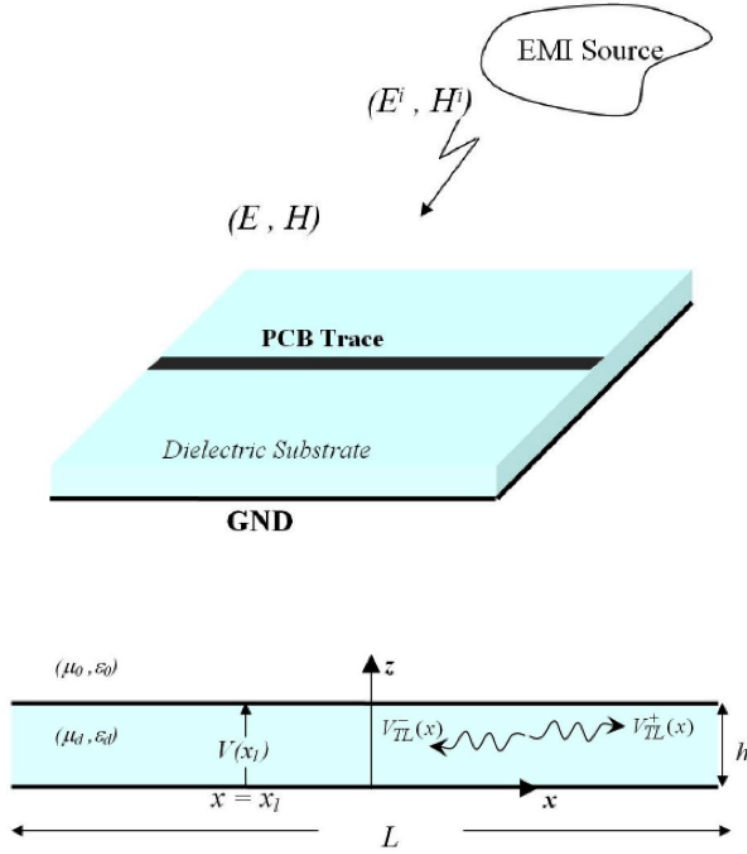


Figure 6.4: Mixed boundary-value problem arising in simulation of electromagnetic fields in and around printed circuit boards [74].

$(u, v) \in H^1(\Omega) \times H^1(\Omega)$ satisfying

$$\Delta w + nk^2 w = 0 \quad \text{in } \Omega, \quad (6.1a)$$

$$\Delta v + k^2 v = 0 \quad \text{in } \Omega, \quad (6.1b)$$

$$w = v \quad \text{on } \Gamma, \quad (6.1c)$$

$$\frac{\partial w}{\partial n} = \frac{\partial v}{\partial n} \quad \text{on } \Gamma, \quad (6.1d)$$

where $w, v \in L^2(\Omega)$, $w - v \in H_0^2(\Omega) = \{u \in H^2(\Omega) : u = \frac{\partial u}{\partial n} = 0 \text{ on } \partial\Omega = \Gamma\}$, and the refracting index $n > 1$ is assumed constant in Ω .

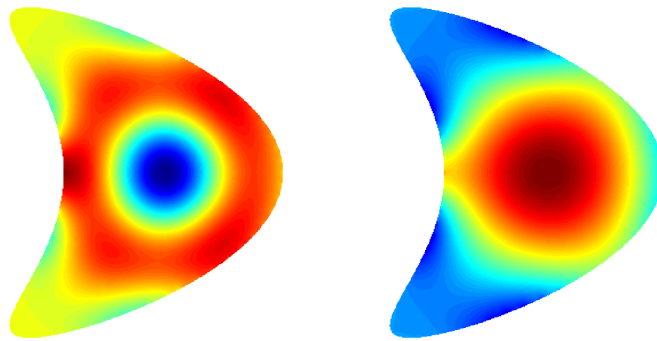
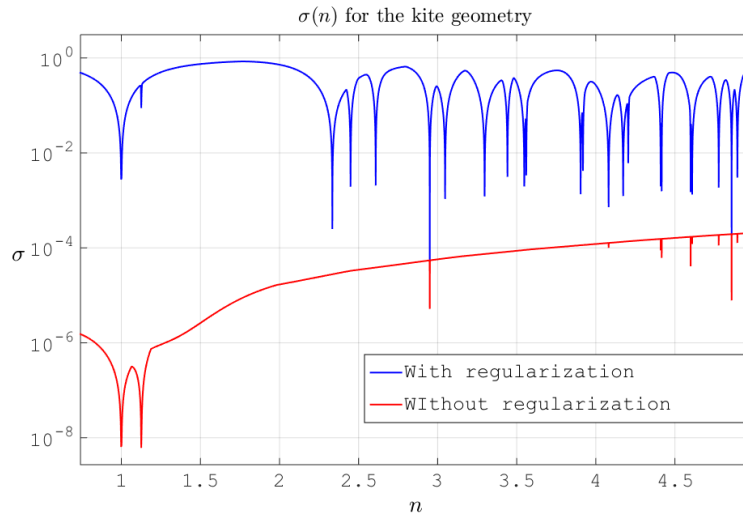


Figure 6.5: Upper portion: Regularization of the $\sigma(n)$ function for the transmission eigenvalue problem. Lower portion: Sample transmission eigenfunctions for the kite geometry.

The values of $k > 0$ for which the homogeneous interior transmission problem (6.1) admits a non-zero solution $(v, w) \in (L^2(\Omega))^2$ with $w - v \in H_0^2(\Omega)$, are called transmission eigenvalues. In reference [23], it is shown that for $n > 1$ there exists an infinite number of transmission eigenvalues which can only accumulate at ∞ .

The upper portion of Figure 6.5 demonstrates results of an application of the transmission eigensolver, including the regularization technique described in Chapter 4, to the transmission eigenvalue problem (6.1) for the kite-shaped geometry. The lower portion of the Figure 6.5 displays a sample pair (v, w) of eigenfunctions.

6.2.5 Time explicit PDE solver using eigenfunction expansion and separation of variables.

Dissipation and dispersion errors give rise to significant difficulties in numerical solutions of time-dependent PDEs. For second-order linear equations associated with an elliptic spatial operator L , a spectral time-domain solution based on use of eigenvalues and eigenfunctions can be obtained numerically, even for non-separable geometries, provided the linear spatial operator L possesses a complete set of eigenfunctions, and provided sufficiently many eigenvalues and eigenfunctions can be effectively computed numerically: the time-dependent solution can then be produced on the basis of explicit solutions of a decoupled set of ODEs.

The following example demonstrates the character of such solvers for a simple wave equation of the form

$$\begin{aligned}u_{tt}(t, x) - \Delta u(t, x) &= 0 \quad x \in \Omega, \\u(0, x) &= h(x).\end{aligned}\tag{6.2}$$

Approximating the initial data $u_0(x)$ by means of a finite sum of the Laplace-Dirichlet eigenfunctions

$$h(x) \approx \sum_{i=1}^N c_i u_i(x),\tag{6.3}$$

where each eigenfunction u_i satisfies the Laplace eigenvalue problem with the corresponding eigenvalue μ_i^2 , the approximately solution, which yields bounded errors for infinitely long times, is given by formula

$$u(x, t) = \sum_{i=1}^N c_i \cos \mu_i t u_i(x).\tag{6.4}$$

The only unknowns in this expression are the coefficient c_i —which equal, of course, the Fourier coefficients of the initial data h (equation 6.3). The full PDE problem thus reduces to the problem of evaluating the Fourier coefficients of the initial data function h .

Assuming the eigenfunctions u_i are normalized, the coefficients c_i in the expansion (6.4) are given by

$$c_i = \int_{\Omega} h(x) u_i(x) dx.\tag{6.5}$$

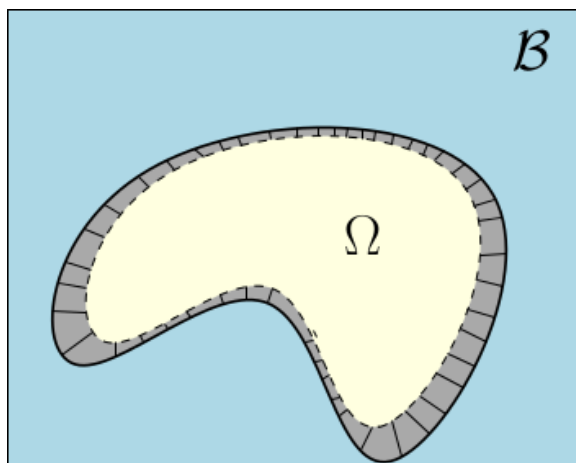


Figure 6.6: Integration using partition of unity.

In what follows we present an effective numerical approach for evaluation of the integrals (6.5). The algorithm is based on use of an infinitely smooth windowing function η that blends the value 1 for all points in Ω at a distance bigger than or equal to a certain value δ to the boundary $\partial\Omega$, to the value 0 at and outside the boundary $\partial\Omega$ (see Figure 6.6).

Using such a function the integration problem can be reduced to cases which can be treated with high accuracy by means of tensor-product integration methods. Indeed, say that we wish to evaluate the integral

$$\int_{\Omega} f(x, y) dx dy = \int_{\Omega} f(x, y) \eta(x, y) dx dy + \int_{\Omega} f(x, y) (1 - \eta(x, y)) dx dy \quad (6.6)$$

for a given function $f = f(x, y)$ defined in the set Ω depicted in Figure 6.6. Denoting by $\tilde{f}(x, y)$ the continuation by 0 of the product $f(x, y)\eta(x, y)$ to the rectangular domain \mathcal{B} (see Figure 6.6), the first integral can be reexpressed in the form

$$\int_{\Omega} f(x, y) \eta(x, y) dx dy = \int_{\mathcal{B}} \tilde{f}(x, y) dx dy \quad (6.7)$$

and evaluated numerically with super-algebraic accuracy by means of the trapezoidal rule.

In order to evaluate the second integral on the right hand side of equation (6.6), and assuming for simplicity of exposition that $\partial\Omega$ is a smooth curve, let $(x_b(\theta), y_b(\theta))$ ($0 \leq \theta \leq 2\pi$) denote a corresponding smooth parametrization of $\partial\Omega$, and let $\mathbf{n} = [n_x(\theta), n_y(\theta)]$ denote the

corresponding inner normal vector. Then, the change of variables

$$\begin{aligned}x(\theta, s) &= x_b(\theta) - sn_x(\theta) \\y(\theta, s) &= y_b(\theta) - sn_y(\theta)\end{aligned}\tag{6.8}$$

can be used to reexpress the integral in the form

$$\int_{\Omega} f(x, y)(1 - \eta(x, y)) dx dy = \int_0^{2\pi} d\theta \int_0^{\delta} f(\theta, s)(1 - \eta(\theta, s)) J(\theta, s) ds,\tag{6.9}$$

that is, an integral along the direction normal to the curve for a small distance δ followed by integration around the curve. For the Jacobian we have

$$J(\theta, s) = \begin{vmatrix} -n_x(\theta) & x'_b(\theta) - sn'_x(\theta) \\ -n_y(\theta) & y'_b(\theta) - sn'_y(\theta) \end{vmatrix}.\tag{6.10}$$

The integral on the right hand side of equation (6.9) can then be approximated with superalgebraic accuracy by means of the trapezoidal rule in the θ variable and Chebyshev integration in the s variable.

Figure 6.7 demonstrates the solution obtained using equation (6.4) on the basis of the first $N = 150$ Laplace-Dirichlet eigenfunctions for the wave equation on the kite-shaped domain with Dirichlet boundary conditions for a set of times $t = 1000000$, $t = 1000001$, $t = 1000002$ and $t = 1000003$ s. The initial data h is given by a symmetric mollifier-function supported in the interior of the domain. The accuracy of the solution does not ever deteriorate with time. Or, more precisely, all truncations of an eigenfunction expansion give rise to errors that are bounded, for all time, by a constant which tends to zero as the expansion truncation levels are increased.

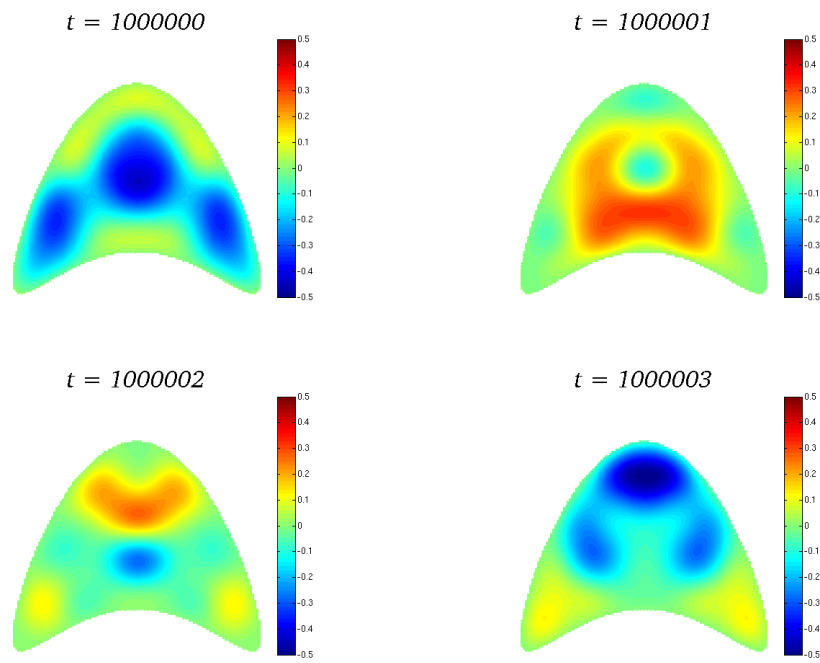


Figure 6.7: Solution of the wave equation (6.2) for the kite-shaped geometry.

Appendix A

Appendix: The Fourier Continuation method (FC)

Given N point values $f(x_i)$ ($x_i = \frac{i\pi}{N-1}$, $i = 0, \dots, N-1$) of a smooth function $f(x)$ defined in the interval $[0, \pi]$, the Fourier Continuation algorithm produces rapidly convergent periodic approximations f^c of f to an interval of length larger than π . In view of the closed-form integrals (2.107)-(2.108) used in Section 2.5.1.2, which lie at the basis of our FC-based quadrature method, in the context of the present thesis the needed periodicity length is 2π —so that the Fourier continuation of the function f takes the form

$$f^c(x) = \sum_{k=-F}^F a_k e^{ikx} \quad (\text{A.1})$$

for some value of F . (The form (A.1) applies to expansions with an odd number $2F + 1$ of terms, but obvious alternative forms may be used to include expansions containing an even number of terms.) In this thesis we use the “blending-to-zero” version of the algorithm, which was introduced in [3], together with small additional adjustments to enable use of the long continuation intervals required in the present thesis. For additional details, including convergence studies of FC approximations, we refer to [3, 21, 91].

The extended periodicity interval is used in the FC method to eliminate discontinuities that arise in a period- π extension of the function f , and thus, to eliminate the difficulties arising from the Gibbs phenomenon. The FC representation (A.1) is based on use of a preliminary discrete extension of f to the interval $[\pi - L, L]$ ($L > \pi$) which contains $[0, \pi]$

in its interior. This discrete extension is obtained by appending to the original N function values an additional $C > 0$ function values that provide a smooth transition from f_{N-1} to 0 in the interval $[\pi, L]$, as well as C function values that provide a smooth transition from f_0 to zero in the interval $[\pi - L, 0]$. Here $L = \pi(N + C)/(N - 1)$ with C small enough so that $L < 3\pi/2$.

To obtain the function values in the extension domains $[\pi - L, 0]$ and $[\pi, L]$ we use a certain FC(Gram) algorithm [21] which is briefly described in what follows. The FC(Gram) method constructs, at first, a polynomial approximant to f in each one of the intervals $[x_0, x_{d-1}]$ and $[x_{N-d}, x_{N-1}]$ (for some small integer number d independent of N) on the basis of the given function values at the discretization points x_0, x_1, \dots, x_{d-1} and $x_{N-d}, x_{N-d+1}, \dots, x_{N-1}$, respectively; see Figure A.1. Following [21], in this thesis these interpolants are obtained as projections onto a certain basis of orthogonal polynomials: the Gram polynomial basis of order m . The FC(Gram) algorithm then utilizes a precomputed smooth function for each member of the Gram basis which smoothly blends the basis polynomial to the zero function over the distance $L - \pi$; see [3, 21, 91] for details.

In view of the large continuation intervals required in this thesis, the function values on the interval $[\pi - L, L]$ produced as indicated above are subsequently padded by an appropriate number of zero values to produce values of a 2π -periodic smooth function (see Figure A.1). The algorithm is completed via an application of the Fast Fourier Transform (FFT) to the 2π periodic extended discrete function—to produce the coefficients a_k of the Fourier continuation f^c shown in (A.1). Throughout this thesis we have used the parameter values $C = 27$, $d = 6$, and $m = 5$.

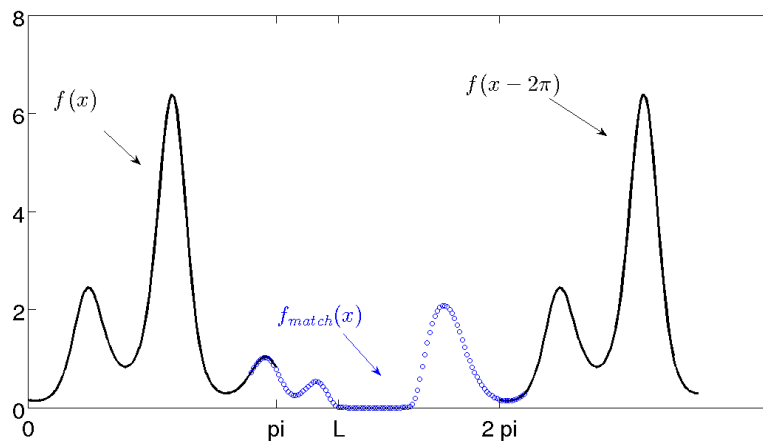


Figure A.1: Demonstration of the blending-to-zero FC algorithm.

Appendix B

Solution at interior resonances

In this section we describe an algorithm for evaluation of the solution of the problem (2.1) for an exterior domain Ω , and for a value of k^2 that either equals or is close to an interior Dirichlet eigenvalue of the Laplace operator in the bounded set $\mathbb{R}^2 \setminus \Omega$. As mentioned in Section 2.2 in this case the system of integral equations (2.4) does not have a unique solution. However, the solution of the PDE is uniquely solvable for any value of k .

The non-invertibility of the aforementioned continuous systems of integral equations at a wavenumber $k = k^*$ manifests itself at the discrete level in non-invertibility or ill-conditioning of the system matrix $\mathcal{A} := \mathcal{A}(k)$ for values of k close to k^* . Therefore, for k near k^* the numerical solution of the Zaremba problems under consideration (which in what follows will be denoted by $\tilde{u} := \tilde{u}_k(x)$ to make explicit the solution dependence on the parameter k) cannot be obtained via direct solution the linear system $\mathcal{A}(k)\eta = f$. As is known, however, the solutions $u = u_k$ of the continuous boundary value problem are analytic functions of k for all real values of k —including, in particular, for k equal to any one of the spurious resonances mentioned above—and therefore, the approximate values $\tilde{u}_k(x)$ for k sufficiently far from k^* can be used, via analytic continuation, to obtain corresponding approximations around $k = k^*$ and even at a spurious resonance $k = k^*$.

In order to implement this strategy for a given value of $k = k_0$ it is necessary for our algorithm to possess a capability to perform two steps:

1. To determine whether k_0 is “sufficiently far” from any one of the spurious resonances k^* .
- 2a. If k_0 is “sufficiently far” then simply invert the linear system by means of either an LU

decomposition or the usually already available Singular Value Decomposition (which is used to determine the “distance from resonance”).

- 2b. If k_0 is not “sufficiently far” from one of the spurious resonances k^* , then obtain the PDE solution at k_0 by analytic continuation from solutions for values of k in a neighborhood of k_0 which are “sufficiently far” from k^* .

Here the terms “sufficiently far” are defined to basically mean that, at the given frequency k , the linear system can be inverted without significant error amplifications. It has been noticed in practice [102] that the regions within which inversion is not possible are very small indeed, in such a way that analytic continuation from “sufficiently far” can be performed to the singular or nearly singular frequency k_0 with any desired accuracy. For full details in these regards see [102].

The numerical results confirming highly accurate evaluation of the PDE solution even for resonant frequencies are presented in Figure B.1 for the case of the FC-based solver applied to the Zaremba boundary value problem on the unit disc. The convergence rates are compared for two frequencies: $k = 11$ (where the solutions are obtained using an LU decomposition) and the resonant frequency $k = 11.791534439014281$ (with solutions obtained by means of analytic continuation).

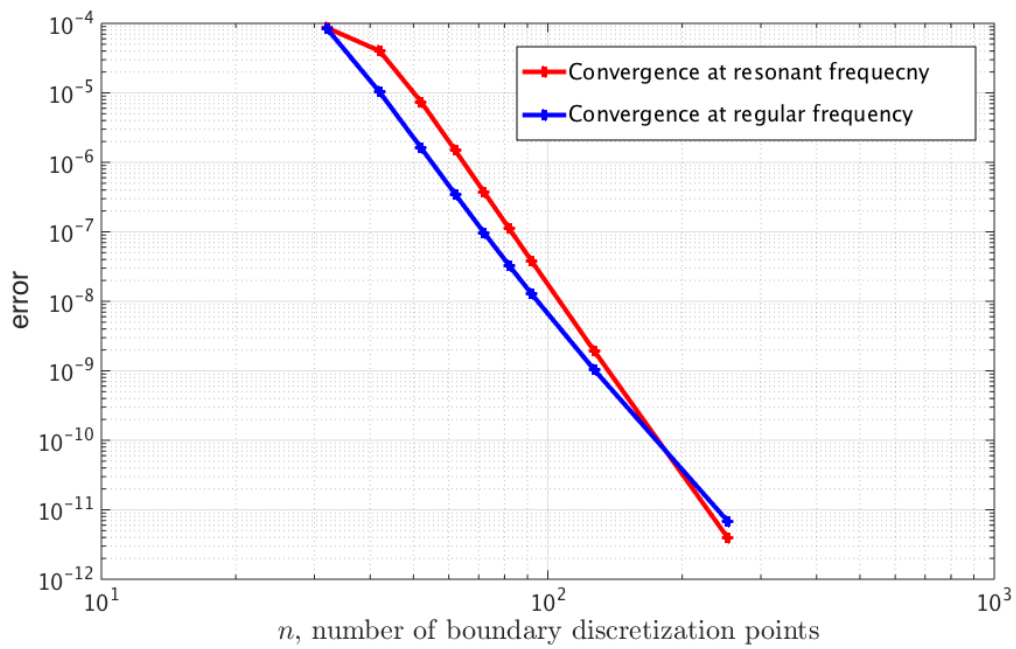


Figure B.1: Convergence comparison at a regular and a resonant frequency.

Appendix C

Closed form expressions for integrals with a logarithmic kernel

In this appendix we present certain closed-form expressions for integrals of trigonometric functions multiplied by a logarithmic kernel. The results in this appendix were obtained in collaboration with professor Fernando Reitich in addition to professor Oscar Bruno.

We consider the following integrals:

$$\int_0^\pi \log(|z - \cos(\theta)|) \cos(n\theta) d\theta, \quad (\text{C.1})$$

$$\int_0^\pi \log(|z - \cos(\theta)|) \sin(n\theta) d\theta, \quad (\text{C.2})$$

where z is a real number. If $|z| < 1$ equation (C.1) is related to eigenvalues of Symm's operator [111] and can be evaluated directly:

$$\int_0^\pi \log(|z - \cos(\theta)|) \cos(n\theta) d\theta = \lambda_n. \quad (\text{C.3})$$

Here $\lambda_n = \frac{1}{2n}$ for $n \neq 0$ and $\frac{\log(2)}{2}$ for $n = 0$. To obtain the values of both integrals (C.1), (C.2) for all values of z , we consider the operator

$$A_n(z) = \int_0^\pi \log(z - \cos(\theta)) e^{in\theta} d\theta. \quad (\text{C.4})$$

Clearly

$$\int_0^\pi \log(z - \cos(\theta)) \cos(n\theta) d\theta = \operatorname{Re}(A_n(z)), \quad (\text{C.5})$$

$$\int_0^\pi \log(z - \cos(\theta)) \sin(n\theta) d\theta = \operatorname{Im}(A_n(z)). \quad (\text{C.6})$$

We consider the following cases:

1. Case $n = 0$

In this case

$$A_0(z) = \int_0^\pi \log|z - \cos(\theta)| d\theta \quad (\text{C.7})$$

$$A'_0(z) = \int_0^\pi \frac{1}{z - \cos(\theta)} d\theta = \frac{\pi}{\sqrt{z^2 - 1}}. \quad (\text{C.8})$$

Hence,

$$A_0(z) = \pi \log\left(z + \sqrt{z^2 - 1}\right) + C = \pi \operatorname{Acosh}|z| + C. \quad (\text{C.9})$$

If $z \rightarrow \infty$, $A_0(z) \simeq \pi \log(z)$, $\Rightarrow C = -\pi \log(2)$, and

$$A_0(z) = \pi \operatorname{Acosh}(z) - \pi \log(2). \quad (\text{C.10})$$

2. Case $z \geq 1$, $n \geq 1$

Let Γ denote the arc $|z| = 1$, $\operatorname{Im}(z) > 0$ (see figure C.1). Then

$$\begin{aligned} A_n(z) &= \int_\Gamma \log\left(z - \frac{\omega + \frac{1}{\omega}}{2}\right) \omega^{n(-i)} \frac{d\omega}{\omega} = \\ &= (-i) \int_\Gamma [\log(2\omega z - \omega^2 - 1) - \log(2\omega)] \omega^{n-1} d\omega. \end{aligned} \quad (\text{C.11})$$

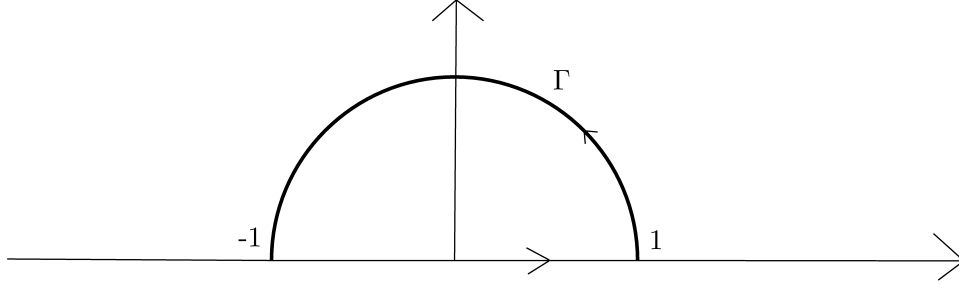


Figure C.1: Integration contour.

Let ω_1 and ω_2 denote the roots of quadratic polynomial

$$2\omega z - \omega^2 - 1 = -(\omega - \omega_1)(\omega - \omega_2). \quad (\text{C.12})$$

It is easy to check that

$$\omega_1 = z + \sqrt{z^2 - 1} \geq 1, \quad \omega_2 = z - \sqrt{z^2 - 1} = \frac{1}{\omega_1} \leq 1, \quad (\text{C.13})$$

and

$$A_n(z) = (-i) \int_{\Gamma} [\log(\omega_1 - \omega) + \log(\omega - \omega_2) - \log(2\omega)] \omega^{n-1} d\omega. \quad (\text{C.14})$$

Applying the Cauchy residue theorem to each integral on the right-hand side of equation (C.14) we obtain

$$\begin{aligned} \int_{\Gamma} \log(\omega) \omega^{n-1} d\omega &= - \int_{-1}^1 \log(x) x^{n-1} dx = \\ &- \int_{-1}^1 \log|x| x^{n-1} dx - i\pi \int_{-1}^0 x^{n-1} dx = \frac{1}{n^2} [1 - (-1)^n] + i\pi \frac{(-1)^n}{n}, \end{aligned} \quad (\text{C.15})$$

and

$$\begin{aligned} \int_{\Gamma} \log(\omega - \omega_2) \omega^{n-1} d\omega &= - \int_{-1}^1 \log(x - \omega_2) x^{n-1} dx = \\ &- \int_{-1}^1 \log|x - \omega_2| x^{n-1} dx - \int_{-1}^{\omega_2} i\pi x^{n-1} dx. \end{aligned} \quad (\text{C.16})$$

Using integration by parts for the functions $u = \log|x - \omega_2|$ and $v = \frac{x^n - \omega_2^n}{n}$, the first integral on the right hand side of equation (C.16) is given by

$$\begin{aligned}
\int_{-1}^1 \log|x - \omega_2| x^{n-1} dx &= \left(\frac{x^n - \omega_2^n}{n} \log|x - \omega_2| \right) \Big|_{-1}^1 - \int_{-1}^1 \frac{x^n - \omega_2^n}{n} \frac{1}{x - \omega_2} dx = \\
&= \frac{1 - \omega_2^n}{n} \log|1 - \omega_2| - \frac{(-1)^n - \omega_2^n}{n} \log|1 + \omega_2| - \\
&\quad - \int_{-1}^1 \frac{1}{n} (x^{n-1} + x^{n-2}\omega_2 + \dots + x\omega_2^{n-2} + \omega_2^{n-1}) dx = \\
&= \frac{1 - \omega_2^n}{n} \log|1 - \omega_2| - \frac{(-1)^n - \omega_2^n}{n} \log|1 + \omega_2| - \frac{1}{n} \sum_{j=0}^{n-1} \omega_2^j \frac{(1 - (-1)^{n-j})}{n-j}.
\end{aligned} \tag{C.17}$$

Then the expression (C.16) can be rewritten as

$$\begin{aligned}
\int_{\Gamma} \log(\omega - \omega_2) \omega^{n-1} d\omega &= -\frac{1 - \omega_2^n}{n} \log|1 - \omega_2| + \frac{(-1)^n - \omega_2^n}{n} \log|1 + \omega_2| + \\
&\quad + \frac{1}{n} \sum_{j=0}^{n-1} \omega_2^j \frac{(1 - (-1)^{n-j})}{n-j} - i\pi \frac{\omega_2^n - (-1)^n}{n}.
\end{aligned} \tag{C.18}$$

Similarly

$$\begin{aligned}
\int_{\Gamma} \log(\omega_1 - \omega) \omega^{n-1} d\omega &= - \int_{-1}^1 \log|\omega_1 - x| x^{n-1} dx = \\
&= -\frac{1 - \omega_1^n}{n} \log|1 - \omega_1| + \frac{(-1)^n - \omega_1^n}{n} \log|1 + \omega_1| + \frac{1}{n} \sum_{j=0}^{n-1} \omega_1^j \frac{(1 - (-1)^{n-j})}{n-j}
\end{aligned} \tag{C.19}$$

and equations (C.15), (C.16), and (C.19) yield

$$\begin{aligned}
A_n(z) &= \int_0^\pi \log(z - \cos(\theta)) e^{in\theta} d\theta = \\
&(-i) \int_\Gamma [\log(\omega_1 - \omega) + \log(\omega - \omega_2) - \log(2\omega)] \omega^{n-1} d\omega = \\
&= (-i) \left[-\frac{1 - \omega_1^n}{n} \log|1 - \omega_1| + \frac{(-1)^n - \omega_1^n}{n} \log|1 + \omega_1| \right. \\
&+ \frac{1}{n} \sum_{j=0}^{n-1} \omega_1^j \frac{(1 - (-1)^{n-j})}{n-j} - \frac{1 - \omega_2^n}{n} \log|1 - \omega_2| \\
&+ \frac{(-1)^n - \omega_2^n}{n} \log|1 + \omega_2| + \frac{1}{n} \sum_{j=0}^{n-1} \omega_2^j \frac{(1 - (-1)^{n-j})}{n-j} - i\pi \frac{\omega_2^n - (-1)^n}{n} \\
&\left. - \frac{1}{n^2} [1 - (-1)^n] - i\pi \frac{(-1)^n}{n} + \log(2) \frac{1 - (-1)^n}{n} \right] \\
&= (-i) \left[-\frac{1 - \omega_1^n}{n} \log|1 - \omega_1| + \frac{(-1)^n - \omega_1^n}{n} \log|1 + \omega_1| \right. \\
&+ \frac{1}{n} \sum_{j=0}^{n-1} (\omega_1^j + \omega_2^j) \frac{(1 - (-1)^{n-j})}{n-j} - \frac{1 - \omega_2^n}{n} \log|1 - \omega_2| \\
&\left. + \frac{(-1)^n - \omega_2^n}{n} \log|1 + \omega_2| - i\pi \frac{\omega_2^n}{n} - \frac{1}{n^2} [1 - (-1)^n] + \log(2) \frac{1 - (-1)^n}{n} \right]. \tag{C.20}
\end{aligned}$$

3. Case $0 < z < 1$, $n \geq 1$

In this case it is easy to see that in this case ω_1 and ω_2 are both complex, but the formula (C.20) still holds.

4. Case $z < 0$, $n \geq 1$

In this case it is easy to see that

$$\begin{aligned}
A_n(-z) &= \int_0^\pi \log(|-z - \cos(\theta)|) e^{in\theta} d\theta = \\
&= |\theta' = \pi - \theta| = \int_0^\pi \log(|z - \cos(\theta')|) e^{i(n\pi - n\theta')} d\theta' = (-1)^n A_n(z). \tag{C.21}
\end{aligned}$$

Equations (C.10), (C.20), and (C.21) provide the necessary expressions.

From a computational perspective, evaluating sum of the terms that contain $(\omega_1)^n$, for

$\omega_1 > 1$ in equation (C.20) may result in loss of accuracy due to cancellation errors, since, as can be seen from equation (C.20), the resulting sum is bounded. Instead we use the following expressions:

$$\begin{aligned} \frac{1}{n} \sum_{j=0}^{n-1} \omega_1^j \frac{(1 - (-1)^{n-j})}{n-j} &= |k = n-j| = \frac{1}{n} \sum_{k=1}^n \frac{\omega_1^n (1 - (-1)^k)}{\omega_1^k k} \\ &= \frac{\omega_1^n}{n} \sum_{k=1}^n \omega_2^k \frac{(1 - (-1)^k)}{k} = \frac{2\omega_1^n}{n} \left(\omega_2 + \frac{\omega_2^3}{3} + \frac{\omega_2^5}{5} + \dots + \frac{\omega_2^{n^*}}{n^*} \right), \end{aligned} \quad (\text{C.22})$$

where $n^* = n$ if n is odd and $n^* = n - 1$ if n is even. Then

$$\begin{aligned} \text{Im}(A_n(z)) &= \frac{1 - \omega_1^n}{n} \log |1 - \omega_1| - \frac{(-1)^n - \omega_1^n}{n} \log |1 + \omega_1| \\ &- \frac{1}{n} \sum_{j=0}^{n-1} (\omega_1^j + \omega_2^j) \frac{(1 - (-1)^{n-j})}{n-j} + \frac{1 - \omega_2^n}{n} \log |1 - \omega_2| - \frac{(-1)^n - \omega_2^n}{n} \log |1 + \omega_2| \\ &+ \frac{1}{n^2} [1 - (-1)^n] - \log(2) \frac{1 - (-1)^n}{n} = \frac{\log |1 - \omega_1|}{n} - \frac{(-1)^n \log |1 + \omega_1|}{n} \\ &+ \frac{1 - \omega_2^n}{n} \log |1 - \omega_2| - \frac{(-1)^n - \omega_2^n}{n} \log |1 + \omega_2| + \frac{1}{n^2} [1 - (-1)^n] \\ &- \log(2) \frac{1 - (-1)^n}{n} - \frac{1}{n} \sum_{j=0}^{n-1} \omega_2^j \frac{(1 - (-1)^{n-j})}{n-j} \\ &+ \frac{\omega_1^n}{n} \left(\log \frac{|1 + \omega_1|}{|1 - \omega_1|} - 2 \left(\omega_2 + \frac{\omega_2^3}{3} + \frac{\omega_2^5}{5} + \frac{\omega_2^{n^*}}{n^*} \right) \right). \end{aligned} \quad (\text{C.23})$$

The last line in equation (C.23) still represents a challenge from the computational point of view. However, using the fact that $\omega_2 < 1$ and the Taylor expansion of $\log \frac{|1 + \omega_1|}{|1 - \omega_1|}$ near $\omega_1 = 0$, we obtain

$$\frac{\omega_1^n}{n} \left(\log \frac{|1 + \omega_1|}{|1 - \omega_1|} - 2 \left(\omega_2 + \frac{\omega_2^3}{3} + \frac{\omega_2^5}{5} + \dots + \frac{\omega_2^{n^*}}{n^*} \right) \right) = \frac{2\omega_1^n}{n} \sum_{k=1}^{\infty} \frac{\omega_2^{n^*+2k}}{n^*+2k}. \quad (\text{C.24})$$

Expression (C.24) is then substituted in (C.20) to obtain

$$\begin{aligned}
\int_0^\pi \log(r - \cos(\sigma)) e^{in\sigma} d\sigma = & (-i) \left[-\frac{1 - \omega_1^n}{n} \log|1 - \omega_1| + \frac{(-1)^n - \omega_1^n}{n} \log|1 + \omega_1| \right. \\
& + \frac{1}{n} \sum_{j=0}^{n-1} (\omega_1^j + \omega_2^j) \frac{(1 - (-1)^{n-j})}{n-j} - \frac{1 - \omega_2^n}{n} \log|1 - \omega_2| \\
& \left. + \frac{(-1)^n - \omega_2^n}{n} \log|1 + \omega_2| - i\pi \frac{\omega_2^n}{n} - \frac{1}{n^2} [1 - (-1)^n] + \log(2) \frac{1 - (-1)^n}{n} \right].
\end{aligned} \tag{C.25}$$

Bibliography

- [1] AIRY, G. B. Tides and waves. *Encyclopedia metropolitana* (1841).
- [2] AKHMETGALIYEV, E., BRUNO, O., AND NIGAM, N. A boundary integral algorithm for the laplace dirichletneumann mixed eigenvalue problem. *Journal of Computational Physics* 298 (2015), 1–28.
- [3] ALBIN, N., AND BRUNO, O. A spectral FC solver for the compressible Navier-Stokes equations in general domains I: Explicit time-stepping. *Journal of Computational Physics* 230 (2011), 6248–6270.
- [4] ALESSANDRINI, G., AND MAGNANINI, R. Elliptic equations in divergence form, geometric critical points of solutions, and stekloff eigenfunctions. *SIAM Journal on Mathematical Analysis* 25, 5 (1994), 1259–1268.
- [5] ANTONIETTI, P. F., BUFFA, A., AND PERUGIA, I. Discontinuous galerkin approximation of the laplace eigenproblem. *Computer methods in applied mechanics and engineering* 195, 25 (2006), 3483–3503.
- [6] BANGERTH, W., HARTMANN, R., AND KANSCHAT, G. deal. iia general-purpose object-oriented finite element library. *ACM Transactions on Mathematical Software (TOMS)* 33, 4 (2007), 24.
- [7] BANUELOS, R., KULCZYCKI, T., POLTEROVICH, I., AND SIUDEJA, B. Eigenvalue inequalities for mixed steklov problems. *Operator theory and its applications, Amer. Math. Soc. Transl. Ser 2* (2010), 19–34.

- [8] BARNETT, A. H., AND BETCKE, T. Quantum mushroom billiards. *Chaos: An Interdisciplinary Journal of Nonlinear Science* 17, 4 (2007), 043125.
- [9] BELLOVA, K., AND LIN, F.-H. Nodal sets of steklov eigenfunctions. *Calculus of Variations and Partial Differential Equations* (2014), 1–30.
- [10] BETCKE, T. The generalized singular value decomposition and the method of particular solutions. *SIAM Journal on Scientific Computing* 30, 3 (2008), 1278–1295.
- [11] BETCKE, T., AND TREFETHEN, L. Reviving the method of particular solutions. *SIAM Review* 47-3 (2005), 469–491.
- [12] BI, H., AND YANG, Y. Multiscale discretization scheme based on the rayleigh quotient iterative method for the steklov eigenvalue problem. *Mathematical Problems in Engineering* 2012 (2012).
- [13] BLESZYNSKI, E., BLESZYNSKI, M., AND JAROSZEWICZ, T. Aim: Adaptive integral method for solving large-scale electromagnetic scattering and radiation problems. *Radio Science* 31, 5 (1996), 1225–1251.
- [14] BOFFI, D. Finite element approximation of eigenvalue problems. *Acta Numer* 19, 01 (2010), 1–120.
- [15] BORISOV, D., AND FREITAS, P. Asymptotics of dirichlet eigenvalues and eigenfunctions of the laplacian on thin domains in \mathbb{R}^d . *Journal of Functional Analysis* 258, 3 (2010), 893–912.
- [16] BRITT, D., TSYNKOV, S., AND TURKEL, E. A high-order numerical method for the helmholtz equation with nonstandard boundary conditions. *SIAM Journal on Scientific Computing* 35, 5 (2013), A2255–A2292.
- [17] BRUNO, O. P., AND HASLAM, M. C. Regularity theory and superalgebraic solvers for wire antenna problems. *SIAM Journal on Scientific Computing* 29, 4 (2007), 1375–1402.

- [18] BRUNO, O. P., AND KUNYANSKY, L. A. A fast, high-order algorithm for the solution of surface scattering problems: basic implementation, tests, and applications. *Journal of Computational Physics* 169, 1 (2001), 80–110.
- [19] BRUNO, O. P., AND LINTNER, S. K. Second-kind integral solvers for TE and TM problems of diffraction by open arcs. *Radio Science* 47, 6 (2012).
- [20] BRUNO, O. P., AND LINTNER, S. K. A high-order integral solver for scalar problems of diffraction by screens and apertures in three-dimensional space. *Journal of Computational Physics* 252 (2013), 250–274.
- [21] BRUNO, O. P., AND LYON, M. High-order unconditionally stable FC-AD solvers for general smooth domains I. Basic elements. *Journal of Computational Physics* 229 (2009), 2009–2033.
- [22] BRUNO, O. P., OVAL, J. S., AND TURC, C. A high-order integral algorithm for highly singular PDE solutions in Lipschitz domains. *Computing* 84, 3-4 (2009), 149–181.
- [23] CAKONI, F., GINTIDES, D., AND HADDAR, H. The existence of an infinite discrete set of transmission eigenvalues. *SIAM Journal on Mathematical Analysis* 42, 1 (2010), 237–255.
- [24] CAKONI, F., HSIAO, G. C., AND WENDLAND, W. L. On the boundary integral equation method for a mixed boundary value problem of the biharmonic equation. *Complex Variables, Theory and Application: An International Journal* 50, 7-11 (2005), 681–696.
- [25] CAO, L.-Q., AND LUO, J.-L. Multiscale numerical algorithm for the elliptic eigenvalue problem with the mixed boundary in perforated domains. *Applied Numerical Mathematics* 58, 9 (2008), 1349–1374.

- [26] CHANG, D.-C., HABAL, N., AND SCHULZE, B.-W. The edge algebra structure of the zarembo problem. *Journal of Pseudo-Differential Operators and Applications* 5, 1 (2014), 69–155.
- [27] CHEN, J., LIN, J., KUO, S., AND CHYUAN, S. Boundary element analysis for the helmholtz eigenvalue problems with a multiply connected domain. *Proceedings of the Royal Society of London. Series A: Mathematical, Physical and Engineering Sciences* 457, 2014 (2001), 2521–2546.
- [28] CHEN, J., LIU, L., AND HONG, H.-K. Spurious and true eigensolutions of helmholtz bies and bems for a multiply connected problem. *Proceedings of the Royal Society of London. Series A: Mathematical, Physical and Engineering Sciences* 459, 2036 (2003), 1891–1924.
- [29] CHEN, J. T., LIN, S. Y., CHEN, I. L., AND LEE, Y. T. Mathematical analysis and numerical study to free vibrations of annular plates using BIEM and BEM. *Internat. J. Numer. Methods Engrg.* 65, 2 (2006), 236–263.
- [30] CHENG, P., HUANG, J., AND WANG, Z. Nyström methods and extrapolation for solving steklov eigensolutions and its application in elasticity. *Numerical Methods for Partial Differential Equations* 28, 6 (2012), 2021–2040.
- [31] COLTON, D., AND KIRSCH, A. A simple method for solving inverse scattering problems in the resonance region. *Inverse problems* 12, 4 (1996), 383.
- [32] COLTON, D., AND KRESS, R. *Inverse Acoustic and Electromagnetic Scattering Theory*. Springer, 1984.
- [33] COLTON, D. L., AND KRESS, R. *Integral Equation Methods in Scattering Theory*, first ed. Pure and Applied Mathematics. John Wiley & Sons Inc., New York, 1983.
- [34] COLTON, D. L., AND KRESS, R. *Inverse Acoustic and Electromagnetic Scattering Theory*. Springer, 1998.

- [35] COSTABEL, M., AND STEPHAN, E. A direct boundary integral equation method for transmission problems. *Journal of mathematical analysis and applications* 106, 2 (1985), 367–413.
- [36] DENZLER, J. Bounds for the heat diffusion through windows of given area. *Journal of mathematical analysis and applications* 217, 2 (1998), 405–422.
- [37] DUDUCHAVA, R., AND TSAAVA, M. Mixed boundary value problems for the helmholtz equation in arbitrary 2d-sectors. *Georgian Mathematical Journal* 20, 3 (2013), 439–467.
- [38] DUDUCHAVA, R., AND TSAAVA, M. Mixed boundary value problems for the laplace-beltrami equations. *arXiv preprint arXiv:1503.04578* (2015).
- [39] DURÁN, M., MIGUEZ, M., AND NÉDÉLEC, J.-C. Numerical stability in the calculation of eigenfrequencies using integral equations. *Journal of computational and applied mathematics* 130, 1 (2001), 323–336.
- [40] E.TAYLOR, M. *Partial Differential Equations: Qualitative studies of linear equations*. No. v. 2 in Applied Mathematical Sciences. Springer, 1997.
- [41] FABER, G. *Beweis, dass unter allen homogenen Membranen von gleicher Fläche und gleicher Spannung die kreisförmige den tiefsten Grundton gibt*. Verlagd. Bayer. Akad. d. Wiss., 1923.
- [42] FABRIKANT, V. *Mixed boundary value problems of potential theory and their applications in engineering*, vol. 68. Kluwer Academic Pub, 1991.
- [43] FALTINSEN, O. M., AND TIMOKHA, A. N. Analytically approximate natural sloshing modes for a spherical tank shape. *Journal of Fluid Mechanics* 703 (2012), 391–401.
- [44] FICHERA, G. Analisi esistenziale per le soluzioni dei problemi al contorno misti, relativi all’equazione e ai sistemi di equazioni del secondo ordine di tipo ellittico, autoaggiunti. *Annali della Scuola Normale Superiore di Pisa-Classe di Scienze* 1, 1-4 (1949), 75–100.

- [45] FICHERA, G. Sul problema della derivata obliqua e sul problema misto per l'equazione di laplace. *Bollettino dell'Unione Matematica Italiana* 7, 4 (1952), 367–377.
- [46] FOKAS, A. S. *Complex variables: introduction and applications*. Cambridge University Press, 2003.
- [47] FOLLAND, G. B. *Introduction to partial differential equations. 2nd edition*. Princeton University Press, 1995.
- [48] FOX, D. W., AND KUTTLER, J. R. Sloshing frequencies. *Zeitschrift für angewandte Mathematik und Physik ZAMP* 34, 5 (1983), 668–696.
- [49] FOX, L., HENRICI, P., AND MOLER, C. Approximations and bounds for eigenvalues of elliptic operators. *SIAM Journal on Numerical Analysis* 4 (1967), 89–102.
- [50] GILBARG, D., AND TRUDINGER, N. S. *Elliptic Partial Differential Equations of Second Order*, vol. 224. Springer Science & Business Media, 2001.
- [51] GIRAUD, G. *Problèmes mixtes et Problèmes sur des variétés closes, relativement aux équations linéaires du type elliptique*. Imprimerie de l'Université, 1934.
- [52] GIROUARD, A., AND POLTEROVICH, I. On the Hersch-Payne-Schiffer inequalities for Steklov eigenvalues. *Functional Analysis and its Applications* 44, 2 (2010), 106–117.
- [53] GIROUARD, A., AND POLTEROVICH, I. Shape optimization for low neumann and steklov eigenvalues. *Mathematical Methods in the Applied Sciences* 33, 4 (2010), 501–516.
- [54] GIROUARD, A., AND POLTEROVICH, I. Spectral geometry of the steklov problem. *arXiv preprint arXiv:1411.6567* (2014).
- [55] GISSER, D., ISAACSON, D., AND NEWELL, J. Electric current computed tomography and eigenvalues. *SIAM Journal on Applied Mathematics* 50, 6 (1990), 1623–1634.
- [56] GOLUB, G. H., AND VAN LOAN, C. F. *Matrix computations*, vol. 3. JHU Press, 2012.

- [57] GREBENKOV, D. S. Laplacian eigenfunctions in nmr. i. a numerical tool. *Concepts in Magnetic Resonance Part A* 32, 4 (2008), 277.
- [58] GREEN, G. Note on the motion of waves in canals. *Transactions of the Cambridge Philosophical Society* 7 (1848), 87.
- [59] GREEN, G., ET AL. On the motion of waves in a variable canal of small depth and width. *Transactions of the Cambridge Philosophical Society* 6 (1838), 457.
- [60] GREENGARD, L., AND ROKHLIN, V. A fast algorithm for particle simulations. *Journal of computational physics* 73, 2 (1987), 325–348.
- [61] GREENHILL, A.-G. Wave motion in hydrodynamics. *American Journal of Mathematics* (1886), 62–96.
- [62] HADAMARD, J. Sur les ondes liquides. *Rend. Acad. Lincei* 5, 25 (1916), 716–719.
- [63] HECHT, F. New development in freefem++. *J. Numer. Math.* 20, 3-4 (2012), 251–265.
- [64] HELSING, J. Integral equation methods for elliptic problems with boundary conditions of mixed type. *Journal of Computational Physics* 228:23 (2009), 8892–8907.
- [65] HELSING, J. Solving integral equations on piecewise smooth boundaries using the recip method: a tutorial. In *Abstract and Applied Analysis* (2013), vol. 2013, Hindawi Publishing Corporation.
- [66] HERSCH, J., PAYNE, L. E., AND SCHIFFER, M. M. Some inequalities for stekloff eigenvalues. *Archive for Rational Mechanics and Analysis* 57, 2 (1974), 99–114.
- [67] HESTHAVEN, J. S., AND WARBURTON, T. High-order nodal discontinuous galerkin methods for the maxwell eigenvalue problem. *Philosophical Transactions of the Royal Society of London A: Mathematical, Physical and Engineering Sciences* 362, 1816 (2004), 493–524.

- [68] HUANG, J., AND LÜ, T. The mechanical quadrature methods and their extrapolation for solving bie of steklov eigenvalue problems. *Journal of Computational Mathematics* 22, 5 (2004).
- [69] IBRAHIM, R. A. *Liquid sloshing dynamics: theory and applications*. Cambridge University Press, 2005.
- [70] KAC, M. Can one hear the shape of a drum? *American Mathematical Monthly* (1966), 1–23.
- [71] KAMIYA, N., ANDOH, E., AND NOGAE, K. Eigenvalue analysis by the boundary element method: New developments. *Engineering Analysis with Boundary Elements* 12 (1993), 151–162.
- [72] KARAMANOS, S. A., PAPAPROKOPIOU, D., AND PLATYRRACHOS, M. A. Finite element analysis of externally-induced sloshing in horizontal-cylindrical and axisymmetric liquid vessels. *Journal of Pressure Vessel Technology* 131, 5 (2009), 051301.
- [73] KELLAND, P. Xxvi.on the theory of waves. part i. *Transactions of the Royal Society of Edinburgh* 14, 02 (1840), 497–545.
- [74] KHAN, Z. A. *EMI/EMC analysis of electronic systems subject to near zone illuminations*. PhD thesis, The Ohio State University, 2007.
- [75] KIRCHHOFF, G. Über stehende schwingungen einer schweren flüssigkeit. *Annalen der Physik* 246, 5 (1880), 34–46.
- [76] KOMARENKO, A. Asymptotic expansion of eigenfunctions of a problem with a parameter in the boundary conditions in a neighborhood of angular boundary points. *Ukrainian Mathematical Journal* 32, 5 (1980), 433–437.
- [77] KOZLOV, V., KUZNETSOV, N., AND MOTYGIN, O. On the two-dimensional sloshing problem. In *Proceedings of the Royal Society of London A: Mathematical, Physical and Engineering Sciences* (2004), vol. 460, The Royal Society, pp. 2587–2603.

- [78] KRAHN, E. Über eine von rayleigh formulierte minimaleigenschaft des kreises. *Mathematische Annalen* 94, 1 (1925), 97–100.
- [79] KRESS, R. A Nystrom method for boundary integral equations in domains with corners. *Numer. Math.* 58 (1990), 145–161.
- [80] KRESS, R. *Linear integral equations*, vol. 82. Springer, 1999.
- [81] KULCZYCKI, T., KWASNICKI, M., AND SIUDEJA, B. Spilling from a cognac glass. *arXiv preprint arXiv:1311.7296* (2013).
- [82] KUO, S., YEIH, W., AND WU, Y. Applications of the generalized singular-value decomposition method on the eigenproblem using the incomplete boundary element formulation. *Journal of Sound and Vibration* 235, 5 (2000), 813–845.
- [83] KUSSMAUL, R. Ein numerisches Verfahren zur Lösung des Neumannschen Aussenraumproblems für die Helmholtzsche Schwingungsgleichung. *Computing (Arch. Elektron. Rechnen)* 4 (1969), 246–273.
- [84] KUZNETSOV, N., KULCZYCKI, T., KWAŚNICKI, M., NAZAROV, A., POBORCHI, S., POLTEROVICH, I., AND SIUDEJA, B. The legacy of vladimir andreevich steklov. *Notices of the AMS* 61, 1 (2014).
- [85] LAMB, H. *Hydrodynamics*. Cambridge university press, 1932.
- [86] LENOIR, M., VULLIERME-LEDARD, M., AND HAZARD, C. Variational formulations for the determination of resonant states in scattering problems. *SIAM J. Math. Anal.* 23, 3 (1992), 579–608.
- [87] LI, M., LIN, Q., AND ZHANG, S. Extrapolation and superconvergence of the Steklov eigenvalue problem. *Advances in Computational Mathematics* 33, 1 (2010), 25–44.
- [88] LI, Y., AND WANG, Z. An approximate analytical solution of sloshing frequencies for a liquid in various shape aqueducts. *Shock and Vibration* 2014 (2014).

- [89] LIU, X., AND OISHI, S. Verified eigenvalue evaluation for the laplacian over polygonal domains of arbitrary shape. *SIAM J. Numer. Anal.* 51 (2013), 634–1654.
- [90] LORENZI, A. A mixed boundary value problem for the laplace equation in an angle (1st part). *Rendiconti del Seminario Matematico della Università di Padova* 54 (1975), 147–183.
- [91] LYON, M., AND BRUNO, O. P. High-order unconditionally stable FC-AD solvers for general smooth domains II. elliptic, parabolic and hyperbolic PDEs; theoretical considerations. *Journal of Computational Physics* 229, 9 (2010), 3358–3381.
- [92] MACDONALD, H. Waves in canals. *Proceedings of the London Mathematical Society* 1, 1 (1893), 101–113.
- [93] MACDONALD, H. Waves in canals and on a sloping bank. *Proceedings of the London Mathematical Society* 1, 1 (1895), 622–634.
- [94] MAGENES, E. Sui problemi di derivata obliqua regolare per le equazioni lineari del secondo ordine di tipo ellittico. *Annali di Matematica Pura ed Applicata* 40, 1 (1955), 143–160.
- [95] MARTENSEN, E. Über eine Methode zum räumlichen Neumannschen Problem mit einer Anwendung für torusartige Berandungen. *Acta Math.* 109 (1963), 75–135.
- [96] MASON, J. C., AND HANDSCOMB, D. C. Chebyshev polynomials. *Chapman&Hall, London* (2003).
- [97] MCLEAN, W. C. H. *Strongly elliptic systems and boundary integral equations*. Cambridge university press, 2000.
- [98] MOISEYEV, N. Quantum theory of resonances: Calculating energies, widths and cross-sections by complex scaling. *Physics Reports* 302 (1998), 221–293.
- [99] MOLER, C. Accurate bounds for the eigenvalues of the laplacian and applications to rhombical domains. Tech. Rep. CS-TR-69-121, Department of Computer Science, Stanford University, 1969.

- [100] NETRUSOV, Y., AND SAFAROV, Y. Weyl asymptotic formula for the laplacian on domains with rough boundaries. *Communications in mathematical physics* 253, 2 (2005), 481–509.
- [101] OSTROGRADSKY, M. A. *Mémoire sur la propagation des ondes dans un bassin cylindrique*, vol. 3. Mem. des Sav. Etrang, 1826.
- [102] PÉREZ-ARANCIBIA, C., AND BRUNO, O. P. High-order integral equation methods for problems of scattering by bumps and cavities on half-planes. *JOSA A* 31, 8 (2014), 1738–1746.
- [103] POINCARÉ, H. *Leçons de mécanique céleste professées à la Sorbonne.....: Théorie des marées*, vol. 3. Gauthier-Villars, 1905.
- [104] POISSON, S. Sur les petites oscillations de l'eau contenue dans un cylindre. *Ann De Gergonne* (1828).
- [105] POISSON, S.-D. *Mémoire sur l'équilibre et mouvement des corps élastiques*. L'Académie des sciences, 1828.
- [106] RAYLEIGH, J. W. S. B. *The theory of sound*, vol. 2. Macmillan, 1896.
- [107] RAYLEIGH, L. On waves. *Phil. Mag* 1, 5 (1876), 257–279.
- [108] SAG, T. W., AND SZEKERES, G. Numerical evaluation of high-dimensional integrals. *Math. Comput* 18 (1964), 245–253.
- [109] (SANKT-PETERBURG), I. A. N. *Novi commentarii Academiae Scientiarum Imperialis Petropolitanae*, vol. 3. Acad. Scient., 1750.
- [110] SANTOSA, F., VOGELIUS, M., AND XU, J.-M. An effective nonlinear boundary condition for a corroding surface. identification of the damage based on steady state electric data. *Zeitschrift für angewandte Mathematik und Physik ZAMP* 49, 4 (1998), 656–679.

- [111] SARANEN, J., AND VAINIKKO, G. *Periodic Integral and Pseudodifferential Equations with Numerical Approximation*. Springer-Verlag, 2002.
- [112] SIGNORINI, A. Sopra un problema al contorno nella teoria delle funzioni di variabile complessa. *Annali di Matematica Pura ed Applicata (1898-1922)* 25, 1 (1916), 253–273.
- [113] SIMON, B. The neumann laplacian of a jelly roll. *Proceedings of the American Mathematical Society* 114, 3 (1992), 783–785.
- [114] STEINBACH, O., AND UNGER, G. A boundary element method for the Dirichlet eigenvalue problem of the Laplace operator. *Numer. Math.* 113, 2 (2009), 281–298.
- [115] STEINBACH, O., AND UNGER, G. Convergence analysis of a Galerkin boundary element method for the Dirichlet Laplacian eigenvalue problem. *SIAM J. Numer. Anal.* 50, 2 (2012), 710–728.
- [116] STEKLOFF, W. Sur les problemes fondamentaux de la physique mathématique (suite et fin). In *Annales scientifiques de l'École Normale Supérieure* (1902), vol. 19, pp. 455–490.
- [117] STOKES, G. G. Report on recent researches in hydrodynamics. *British Association Report 1* (1846).
- [118] STRAUSS, W. A. *Partial differential equations: An introduction*. Wiley, 2008.
- [119] WARSCHAWSKI, S. On differentiability at the boundary in conformal mapping. *Proceedings of the American Mathematical Society* 12, 4 (1961), 614–620.
- [120] WARSCHAWSKI, S. E. On the higher derivatives at the boundary in conformal mapping. *Transactions of the American Mathematical Society* 38, 2 (1935), 310–340.
- [121] WEINSTOCK, R. Inequalities for a classical eigenvalue problem. *Journal of Rational Mechanics and Analysis* 3, 6 (1954), 745–753.

- [122] WENDLAND, W. L., STEPHAN, E., HSIAO, G. C., AND MEISTER, E. On the integral equation method for the plane mixed boundary value problem of the laplacian. *Mathematical Methods in the Applied Sciences* 1, 3 (1979), 265–321.
- [123] WEYL, H. Über die asymptotische verteilung der eigenwerte. *Nachrichten von der Gesellschaft der Wissenschaften zu Göttingen, Mathematisch-Physikalische Klasse* 1911 (1911), 110–117.
- [124] WEYL, H. Das asymptotische verteilungsgesetz der eigenwerte linearer partieller differentialgleichungen (mit einer anwendung auf die theorie der hohlraumstrahlung). *Mathematische Annalen* 71, 4 (1912), 441–479.
- [125] WIGLEY, N. M. Asymptotic expansions at a corner of solutions of mixed boundary value problems. *Journal of Mathematics and Mechanics* 13 (1964), 549–576.
- [126] WIGLEY, N. M. Mixed boundary value problems in plane domains with corners. *Mathematische Zeitschrift* 115, 1 (1970), 33–52.
- [127] WOODWORTH, M. B., AND YAGHJIAN, A. D. Derivation, application and conjugate gradient solution of dual-surface integral equations for three-dimensional, multi-wavelength perfect conductors. *Progress In Electromagnetics Research* 5 (1991), 103–129.
- [128] WRIGHT, K. Differential equations for the analytic singular value decomposition of a matrix. *Numerische Mathematik* 63, 1 (1992), 283–295.
- [129] YAN, Y., SLOAN, I. H., ET AL. *On integral equations of the first kind with logarithmic kernels*. University of NSW, 1988.
- [130] ZAREMBA, S. Sur un probleme mixte relatifa léquation de laplace. *Bulletin de l'Académie des sciences de Cracovie, Classe des sciences mathématiques et naturelles, série A* (1910), 313–344.

- [131] ZHAO, L., AND BARNETT, A. Robust and efficient solution of the drum problem via nostrum approximation of the fredholm determinant. *arXiv preprint arXiv:1406.5252* (2014).